

ISTANBUL TECHNICAL UNIVERSITY ★ GRADUATE SCHOOL OF SCIENCE
ENGINEERING AND TECHNOLOGY

**NUMERICAL AND EXPERIMENTAL INVESTIGATION OF THE EFFECT
OF REFRIGERANT MIXTURES ON THE REFRIGERATION SYSTEM**

Ph.D. THESIS

Mustafa ÖZSİPAHI

Department of Mechanical Engineering

Mechanical Engineering Programme

JANUARY 2020

**NUMERICAL AND EXPERIMENTAL INVESTIGATION OF THE EFFECT
OF REFRIGERANT MIXTURES ON THE REFRIGERATION SYSTEM**

Ph.D. THESIS

Mustafa ÖZSİPAHI
(503132021)

Department of Mechanical Engineering

Mechanical Engineering Programme

Thesis Advisor: Prof. Dr. Hasan GÜNEŞ

JANUARY 2020

İSTANBUL TEKNİK ÜNİVERSİTESİ ★ FEN BİLİMLERİ ENSTİTÜSÜ

**SOĞUTKAN KARIŞIMLARININ SOĞUTMA SİSTEMİ ÜZERİNDEKİ
ETKİSİNİN SAYISAL VE DENEYSEL İNCELENMESİ**

DOKTORA TEZİ

**Mustafa ÖZSİPAHİ
(503132021)**

Makina Mühendisliği Anabilim Dalı

Makina Mühendisliği Programı

Tez Danışmanı: Prof. Dr. Hasan GÜNEŞ

OCAK 2020

Mustafa ÖZSİPAHİ, a Ph.D. student of ITU Graduate School of Science Engineering and Technology 503132021 successfully defended the thesis entitled “NUMERICAL AND EXPERIMENTAL INVESTIGATION OF THE EFFECT OF REFRIGERANT MIXTURES ON THE REFRIGERATION SYSTEM”, which he prepared after fulfilling the requirements specified in the associated legislations, before the jury whose signatures are below.

Thesis Advisor : **Prof. Dr. Hasan GÜNEŞ**
Istanbul Technical University

Jury Members : **Dr. Hüsnü KERPIÇÇİ**
Arcelik A.Ş.

Assist. Prof. Dr. Sertaç ÇADIRCI
Istanbul Technical University

Prof. Dr. Yakup Erhan BÖKE
Istanbul Technical University

Prof. Dr. Hakan DEMİR
Yildiz Technical University

Date of Submission : 31 December 2019

Date of Defense : 29 January 2020





To my wife and family,



FOREWORD

I would like to express my gratitude and appreciation to my supervisor, Prof.Dr. Hasan GÜNEŞ, whose support I have always felt in difficult times, who shared his profound knowledge and experiences over the years.

I would like to thank my committee members Dr. Hüsni KERPIÇÇİ who provided his support and knowledge during the projects realized with Arçelik A.Ş. and Asst.Prof. Sertaç ÇADIRCI for his support.

I wish to express special thanks to my colleagues Res.Asst Umut Can COŞKUN and Asst.Prof. Abdussamet SUBAŞI for their teamwork and friendship over the years. Additionally, I wish to thank Assoc.Prof. Erkan GÜNPINAR for his friendship and guidance. I would like to thank Haluk Anıl KÖSE for his support during the project. I wish also to thank Res.Asst. İbrahim Hakkı TONYALI and to the technicians Eyüp ATASEVEN, Mehmet Ziya KUMCU, Erdal DİNÇ for their efforts.

I would also like to thank Prof.Dr.-Ing. Ullrich HESSE, who provided me with a working environment during my stay at TU Dresden and to the staff of Bitzer-Chair of Refrigeration, Cryogenics and Compressor Technology who did not spare their friendship.

I would like to extend my appreciation to my jury members, Prof.Dr. Yakup Erhan BÖKE and Prof.Dr. Hakan DEMİR, for their constructive comments and suggestions.

I would like to gratefully and sincerely thank the Scientific and Technological Research Council of Turkey (TÜBİTAK) for the financial support provided through project number 215M873.

Finally, I would like to express my honest gratitude to my family for their continuous support and to my wife who has added joy to my life.

January 2020

Mustafa ÖZSİPAHI
Mechanical Engineer, M.Sc.



TABLE OF CONTENTS

	<u>Page</u>
FOREWORD	ix
TABLE OF CONTENTS	xi
ABBREVIATIONS	xiii
LIST OF TABLES	xv
LIST OF FIGURES	xvii
SUMMARY	xxi
ÖZET	xxiii
1. INTRODUCTION	1
1.1 Vapor Compression Refrigeration Cycle.....	2
1.2 Environmental Aspect of Refrigerants	4
1.3 Lubricants	9
1.4 Compressors	10
1.5 Literature Survey	11
1.6 Aim of this thesis.....	28
1.7 Framework.....	29
2. EXPERIMENTAL STUDIES	31
2.1 The Effect of Refrigerant Mixtures on the Household Refrigeration System	32
2.1.1 Refrigerant mixtures test stand (REFMIX)	33
2.1.1.1 Leakage tests.....	37
2.1.1.2 Start-up behavior of the system	38
2.1.1.3 Sensor fluctuations during the experiments	40
2.1.1.4 Results.....	42
2.1.2 Calorimeter test stand	51
2.1.3 Small refrigeration compressor power test stand	54
2.1.4 The compatibility of the refrigerant with oil	57
2.2 Lubrication System of the Compact Inverter Compressor	58
2.2.1 Problem description.....	59
2.2.2 Oil mass flow rate measurements	60
2.2.3 Results	61
2.2.4 Flow visualizations	65
2.3 Concluding Remarks	67
3. NUMERICAL STUDIES	71
3.1 Numerical Investigation of the Lubrication System	71
3.2 Sliding Mesh Method	72
3.2.1 Computational model	73
3.2.2 Governing equations.....	74
3.2.3 Convergence tests	75

3.2.4 Effect of rotational speed.....	77
3.2.5 Effect of viscosity.....	78
3.2.6 Instantaneous flow fields	79
3.2.7 Effect of electrical motor acceleration.....	82
3.2.8 Effect of refrigerant	83
3.3 Moving Reference Frame Method.....	83
3.3.1 Computational model	84
3.3.2 Governing equations.....	85
3.3.3 Convergence tests	85
3.3.4 Effect of rotational speed	87
3.3.5 Effect of viscosity.....	88
3.3.6 Effect of refrigerant dissolving in the oil.....	89
3.3.7 Instantaneous flow fields	90
3.3.8 Effect of electrical motor acceleration.....	90
3.4 Concluding Remarks	91
4. CONCLUSIONS.....	95
REFERENCES.....	99
APPENDICES.....	107
APPENDIX A.1	109
APPENDIX A.2	111
CURRICULUM VITAE.....	117

ABBREVIATIONS

AC	: Alternating Current
ASHRAE	: American Society of Heating, Refrigerating and Air-Conditioning Engineers
CFC	: Chlorofluorocarbon
CFD	: Computational Fluid Dynamics
CFL	: Courant-Friedrichs-Lewy Condition
CIC	: Compact Inverter Compressor
COP	: Coefficient of Performance
DC	: Direct Current
DIN	: Deutsches Institut für Normung
EU	: European Union
GWP	: Global Warming Potential
HC	: Hydrocarbon
HCFC	: Hydrochlorofluorocarbon
HFC	: Hydrofluorocarbon
HFO	: Hydrofluoro-Olefin
HVAC	: Heating, Ventilating and Air Conditioning
MRF	: Moving Reference Frame
ODP	: Ozone Depletion Potential
ODS	: Ozone-Depleting Substance
PISO	: Pressure-Implicit with Splitting Operators
RTD	: Resistance Temperature Detector
SIMPLE	: Semi-Implicit Method for Pressure Linked Equations
SM	: Sliding Mesh
SST	: Shear Stress Transport
UDF	: User Defined Function
VoF	: Volume of Fluid



LIST OF TABLES

	<u>Page</u>
Table 2.1 : List of instruments.....	34
Table 2.2 : List of the sensors.....	35
Table 2.3 : Summary of investigated cases for R600a.	43
Table 2.4 : Detailed results for R600a tested at ASHRAE standards.	44
Table 2.5 : Detailed results for R600a/R290 (40%/60% by weight) refrigerant mixture tested at ASHRAE standards.....	46
Table 2.6 : Effect of condensation temperature on the COP, tested with R600a/R290 (40%/60% by weight).....	48
Table 2.7 : Detailed results for R600a/R290 (60%/40% by weight) refrigerant mixture tested at ASHRAE standards.....	49
Table 2.8 : Results of calorimeter tests for R600a/R290 (40%/60% by weight) refrigerant mixture at ASHRAE standards.	52
Table 2.9 : Temperature readings of experiments at 3000 rpm.	56
Table 2.10 : The details of the compressor model.....	59
Table 2.11 : The instrumentation list of the test stand.	61
Table 2.12 : Standard deviation values of the experiments.	63
Table 3.1 : Mesh independence tests for SM method.	76
Table 3.2 : Properties of investigated refrigerants.....	83
Table 3.3 : Mesh independence tests for MRF method.....	85
Table 3.4 : Properties of RENISO WF10 A.....	89
Table A.1 : Measured temperature values of RTD probes.	110
Table A.2 : Measured temperature values of RTD probes.	110
Table A.3 : Pressure readings of the pressure sensors.	110



LIST OF FIGURES

	<u>Page</u>
Figure 1.1 : Schematic and T-s diagram for the ideal vapor-compression refrigeration cycle [3].	2
Figure 1.2 : Schematic and T-s diagram for the actual vapor-compression refrigeration cycle [4].	4
Figure 1.3 : Time line for refrigerants [7].	5
Figure 1.4 : Flow diagram of ODSs phase-out process [8].	6
Figure 1.5 : The transition in global consumption from CFCs to HCFCs and to HFCs [8]......	7
Figure 1.6 : Scenarios of HFC emissions and global average surface-temperature response [10, 11].	8
Figure 1.7 : Approximate range of capacity covered by various compressor types [7].	10
Figure 1.8 : Test results for various refrigerants [22].	13
Figure 1.9 : Refrigerant progression [26].	14
Figure 1.10 : Temperature profiles of refrigerant and HTF in condenser and evaporator: a) pure refrigerant b) zeotropic refrigerant mixture [28].	15
Figure 1.11 : Layout of flow circuits in test facility [44].	19
Figure 1.12 : Schematic diagram of the oil heat transfer model geometry [53]......	21
Figure 1.13 : Detailed appearance of the hermetic reciprocating compressor [55]..	22
Figure 1.14 : Two different fluid flow models in the crankshaft a) rotating crankshaft and stationary screw pump b) rotating crankshaft with screw flights and stationary cylindrical apparatus [56]......	23
Figure 1.15 : Schematic representation of the hermetic reciprocating compressor with thermocouple positions [70].	26
Figure 2.1 : Temperature profiles in evaporator a) different b) constant temperature slope.	32
Figure 2.2 : Simplified scheme of glide concept [5].	33
Figure 2.3 : Schematic view of the test stand.	34
Figure 2.4 : Detailed view of REFMIX.	36
Figure 2.5 : Cycle process for single component refrigerants and zeotropic refrigerant mixtures [79].	37
Figure 2.6 : High pressure leakage test.	38
Figure 2.7 : Low pressure leakage test (Negative values indicate the vacuum medium).	38
Figure 2.8 : Temperature variations after the compressor start-up.	39
Figure 2.9 : Pressure variations after the compressor start-up.	39
Figure 2.10 : Time-dependent change of suction pressure during the experiment...	40
Figure 2.11 : Time-dependent change of discharge pressure during the experiment.	40

Figure 2.12: Time-dependent change of suction temperature during the experiment.....	41
Figure 2.13: Time-dependent change of refrigerant mass flow rate during the experiment.....	41
Figure 2.14: Pressure-enthalpy diagram of R600a plotted at ASHRAE standards.	42
Figure 2.15: Effect of compressor speed on the COP and input power, tested with refrigerant R600a.	44
Figure 2.16: Effect of evaporator temperature at different compressor speeds on the COP, tested with refrigerant R600a.....	45
Figure 2.17: Effect of compressor speed on the COP and input power, tested with R600a/R290 (40%/60% by weight).....	46
Figure 2.18: Effect of evaporator temperature on the COP, tested with R600a/R290 (40%/60% by weight).....	47
Figure 2.19: Effect of compressor speed on the COP and power consumption, tested with R600a/R290 (60%/40% by weight).....	48
Figure 2.20: Effect of evaporator temperature on the COP, tested with R600a/R290 (60%/40% by weight).....	49
Figure 2.21: COP values obtained from REFMIX at ASHRAE standards for various refrigerant mixtures.	50
Figure 2.22: Temperature-controlled vessel room [80].	51
Figure 2.23: Calorimeter test set up.	52
Figure 2.24: Comparison of results for R600a and R600a/R290 (40%/60% by weight) refrigerant mixture.	53
Figure 2.25: Increase in COP relative to R600a results.	54
Figure 2.26: Layout of the compressor power test stand.....	55
Figure 2.27: Pressure enthalpy diagram.	55
Figure 2.28: Experimental results of the compressor power test stand tested at DIN EN 13771-1.....	56
Figure 2.29: Kinematic viscosity of RENISO WF5 A-R600a mixture.....	57
Figure 2.30: Kinematic viscosity of RENISO WF10 A-R600a mixture.....	57
Figure 2.31: Compact Inverter Compressor (CIC).	58
Figure 2.32: Crankshaft of the CIC.	59
Figure 2.33: Instruments of the experimental set up: 1. CIC 2. Pre-heated oil sump 3. Control panel 4. PID controller 5. Direct current relay 6. Frequency generator 7. Precision balance 8. Beakers	60
Figure 2.34: Thermocouple positions in the pre-heated oil sump and compressor case.....	61
Figure 2.35: Temperature fluctuations during measurement.	62
Figure 2.36: Standard deviation of the oil mass flow rates at 3000 rpm, 5 cSt.	63
Figure 2.37: The oil mass flow rate results for 3,5 and 10 cSt.	64
Figure 2.38: The effect of viscosity on the oil mass flow rate at 3000 rpm.	65
Figure 2.39: Flow visualization test bench.....	65
Figure 2.40: Instantaneous snapshots of the CIC at 3000 rpm, high speed camera at 1000 fps.	66
Figure 3.1 : CAD data of the CIC.....	72
Figure 3.2 : Simplified domain used in SM method: red part: crankshaft, grey part on the top and bottom of the crankshaft: interface.	73

Figure 3.3 : Generated mesh zones a) solid and b) fluid domain.	74
Figure 3.4 : Time step size test carried out with SM method.	77
Figure 3.5 : Time dependent change of oil mass flow rate for various rotational speeds.	78
Figure 3.6 : Effect of oil viscosity on the oil mass flow rate a) 3000 rpm b) 4500 rpm.	79
Figure 3.7 : Instantaneous oil phase fields with SM model at t= 0.02, 0.04, 0.06, 0.14 and 0.4 s. Oil volume fractions are colored from 0 (blue) to 1 (red).	80
Figure 3.8 : Instantaneous isosurfaces of the oil volume fraction at 3000 rpm from the top-view of the CIC.	81
Figure 3.9 : Oil mass flow rate variation during CIC start-up.	82
Figure 3.10 : Effect of refrigerant on the oil mass flow rate.	83
Figure 3.11 : Computational model of the MRF method.	84
Figure 3.12 : a) Effect of flow solver b) Mass flow rate variations with respect to time.	86
Figure 3.13 : Effect of rotational speed on the oil mass flow rate.	87
Figure 3.14 : Effect of viscosity on the oil mass flow rate.	88
Figure 3.15 : Effect of refrigerant dissolving in the oil on the oil mass flow rate.	89
Figure 3.16 : Instantaneous oil phase fields with MRF model at t=0.05, 0.1, 0.2, 0.3, 0.4 and 2 s. Oil volume fractions are colored from 0 (blue) to 1 (red).	90
Figure 3.17 : Oil mass flow rate variation during CIC start-up with the MRF method.	91
Figure 3.18 : Comparison of CFD results with experiments.	92
Figure A.1 : Temperature calibration with calibration bath.	109
Figure A.2 : Pressure calibration with dead-weight pressure tester.	110
Figure A.3 : Effect of compressor speed a) R600a b) R600a/R290 mixture	111
Figure A.4 : Effect of evaporation pressure a) 1500 rpm b) 2100 rpm	112
Figure A.5 : Effect of evaporation pressure a) 3000 rpm b) 4500 rpm	113



NUMERICAL AND EXPERIMENTAL INVESTIGATION OF THE EFFECT OF REFRIGERANT MIXTURES ON THE REFRIGERATION SYSTEM

SUMMARY

Increasing energy costs urge not only developing but also developed countries to have new regulations on energy prevention and recovery. Several protocols have already applied to reduce global warming and ozone depletion potential. These protocols force producers and suppliers to work with less harmful refrigerants in the refrigeration and air conditioning sector. Besides using environment-friendly refrigerants, it is also demanded to increase the energy efficiency of such devices to compete with the rivals of the global market.

Reciprocating compressors in the refrigeration systems such as refrigerators and freezers are the main components in the household appliances. Moreover, the largest part of the electric consumption related to refrigerators is caused by compressors. Due to the increasing demands on new refrigerants considering their efficiency and the regulations for the protection of the environment, the natural refrigerants or refrigerant blends are widely used. Within the study, the effect of refrigerant mixtures on the household refrigeration system is studied. In addition to the refrigerant mixtures, the optimum lubricant is investigated for the reciprocating compressors.

In the first chapter, a brief introduction to the vapor compression refrigeration systems is given. Lubricants and compressors used in vapor compression refrigeration systems are mentioned and a comprehensive literature survey is presented in this chapter.

In the second chapter, experimental studies are discussed. This chapter divided into two parts. In the first part, the effect of refrigerant mixtures on the household refrigeration is studied. In this context, in house refrigerant mixtures test stand is constructed. The performance evaluation of the three different refrigerant mixtures of R600a/R290 is compared with R600a. The performance results of the test stand are compared with calorimeter tests carried out by Arcelik A.S. and the results of both test stands are showed that increase in energy efficiency is possible by using R600a/R290 refrigerant mixture. In the second part, the lubrication system of the hermetic reciprocating compressor is investigated in detail. Oil management and lubrication mechanism in journal bearings may change drastically between compressor maximum and minimum speeds. Nevertheless, sufficient lubrication should be provided to the bearings and all moving parts to avoid any mechanical damage on the compressor. In this context, in house lubrication test bench is built using various instruments. Experiments are conducted to investigate the effect of viscosity and compressor speed on the oil mass flow rate of the compressor. In addition to the oil mass flow rate measurements, flow visualization is performed and flow patterns inside the compressor are given for start-up and steady-state operating conditions.

In the third chapter, numerical investigations are presented in detail. This chapter is divided into two sections. Firstly, the numerical modeling of the lubrication system of a compact inverter compressor (CIC) is presented. In the numerical modeling, a finite volume-based ANSYS-FLUENT package is used to model two-phase (air-oil) flow inside the compressor using the Volume of Fluid Method (VoF) method. Transient behavior of the oil flow under laminar flow conditions is both simulated by imposing Sliding Mesh (SM) and the Moving Reference Frame (MRF) methods at various crankshaft speeds varying between 1200 and 4500 rpm. The measurements are used to compare/validate CFD results obtained from SM and MRF methods. Moreover, the start-up behavior of the compressor is studied and the instantaneous flow field is given for both methods. Advantage and disadvantage of the methods are mentioned in the study.



SOĞUTKAN KARIŞIMLARININ SOĞUTMA SİSTEMİ ÜZERİNDEKİ ETKİSİNİN SAYISAL VE DENEYSEL İNCELENMESİ

ÖZET

Artan enerji maliyetleri, sadece gelişmekte olan ülkeleri değil, aynı zamanda gelişmiş ülkeleri de enerji kısıtlama ve iyileştirme konusunda yeni düzenlemelere sahip olmaya teşvik etmektedir. Küresel ısınma ve ozon tabakasının incelmeye potansiyelini azaltmak için halihazırda çeşitli protokoller uygulanmıştır. Bu protokoller üreticileri ve tedarikçileri soğutma ve iklimlendirme sektöründe daha az zararlı soğutucu akışkanlarla çalışmaya zorlar. Çevre dostu soğutucuların kullanılmasının yanı sıra, küresel pazarın rakipleriyle rekabet etmek için bu tür cihazların enerji verimliliğinin artırılması da talep edilmektedir.

Daha verimli ürünler geliştirmek ile birlikte, dünyanın karşılaştığı bir diğer sorun olan küresel ısınmanın azaltılmasına ilişkin soğutma sistemleri üzerinde birçok kısıtlama vardır. Soğutma sektörü küresel sera gazı emisyonlarının % 7.8'ini oluşturmaktadır. HFC'lerin üretimini ve tüketimini aşamalı olarak azaltmayı amaçlayan 2016 yılında onaylanan Montreal Protokolü'ndeki Kigali Değişikliği, 65 ülke tarafından onaylandıktan sonra 1 Ocak 2019'da yürürlüğe girdi. Değişikliğin amacı 2047 yılına kadar HFC kullanımını % 80 oranında azaltmak ve 2100 yılına kadar gerçekleşmesi beklenen 0.1 °C ile 0.3 °C arasındaki küresel sıcaklık artışından kaçınmaktır.

Dünya genelinde kullanılan toplam soğutma, klima ve ısı pompası sistemi sayısı 3 milyar civarındadır ve soğutma sektörü dünya çapında kullanılan toplam elektriğin yaklaşık % 17'sini tüketmektedir. Buzdolapları ve dondurucular gibi soğutma sistemlerinde pistonlu kompresörler ve çamaşır kurutucularında kullanılan ısı pompaları için dönel kompresörler bu ev aletlerinin ana bileşenleridir. Buzdolapları ve kurutucularla ilgili elektrik tüketiminin en büyük kısmı kompresörlerden kaynaklanmaktadır. Bu çalışma kapsamında, soğutucu karışımlarının soğutma sistemleri üzerindeki etkisi incelenmiştir. Soğutucu karışımlarına uygun yağlar kullanılması kompresör ömrü açısından son derece önemlidir. Bu bağlamda, tez kapsamında çeşitli nümerik ve deneysel çalışmalara yer verilmiştir.

Tezin birinci bölümünde, buhar sıkıştırımlı soğutma çevrimi kısaca tanıtılmıştır. Soğutucu akışkanların tarihi ve çevresel etkileri kısaca açıklanmış ve buhar sıkıştırımlı soğutma çevrimlerinde kullanılan kompresörler ve yağlara değinilerek, konu ile ilgili detaylı bir literatür çalışması verilmiştir.

Tez kapsamında yapılan deneysel çalışmalar ikinci bölümde verilmiştir. Bu bölüm iki kısma ayrılarak incelenmiştir. Birinci kısımda soğutkan karışımlarının soğutma çevrimi üzerindeki etkisi incelenmiştir. Bu bağlamda, kurum içi soğutkan karışımları test düzeneği kurulmuştur. Test düzeneği oluşturan bileşenlerin listesi verilmiş ve ilgili cihazların ölçme hassasiyetleri belirtilmiştir. Test sisteminin sızdırmazlığı,

yüksek basınç ve vakum ortamında gösterilmiştir. Kompresör çalışmasından sistemin kararlı hale gelene kadar geçen sürede basınç ve sıcaklık değişimleri gösterilmiş ve deney süresince emme ve basma basıncı, emme sıcaklığı ve debimetredeki ölçüm dalgalanmaları çizdirilmiştir. Bu çalkantı aralıklarının $\pm 1\%$ bandında gerçekleştiği gözlemlenmiştir. Soğutkan karışımları test sisteminde öncelikle R600a gazının COP değerleri ASHRAE koşulları için elde edilmiş, daha sonra buharlaşma sıcaklığının kompresör performansına etkisine değinilmiştir. Daha sonra R600a/R290 karışımı ağırlıkça üç farklı oranda %40/%60, %60/%40 ve %30/%70 basılarak deneyler tekrar edilmiştir. Soğutkan karışımları kullanılarak elde edilen bağıl COP artışları verilmiştir. Ayrıca elde edilen sonuçlar Arçelik A.Ş. tarafından yapılmış kalorimetre testleri ile kıyaslanmıştır. Her iki sistemden elde edilen sonuçlara göre R600a/R290 soğutkan karışımı kullanarak enerji tasarrufu mümkün olmaktadır. Bir sonraki bölümde ise TU Dresden Üniversitesi'nde bulunan küçük kompresörler için güç tüketimi test kurulumu verilmiş ve kurulan sistem ile temel farklılıklarına değinilmiştir. Sonuç olarak R600a/R290 (ağırlıkça %40 ve %60) kullanarak %15 oranında COP artışı gözlemlenmiştir. İkinci kısımda, temel olarak hermetik inverter kompresörün yağlama sistemi ele alınmıştır. Yağ kütleli debisinin elde edilebilmesi için kurum içi deneysel yağ ölçüm sistemi çeşitli komponentler kullanılarak oluşturulmuştur. Kompresör hızının kütleli yağ debisine etkisi, kompresör çalışma aralığı olan 1200-4500 devir/dak. arasında, detaylı bir şekilde taranarak incelenmiştir. Bunun yanında, yağ viskozitesinin etkisi üç farklı kinematik viskozite değeri 3, 5 ve 10 cSt kullanılarak incelenmiştir. Kompresör yağlama sisteminde temel olarak etkili olan dönel ve viskoz kuvvetlerin etkili olduğu bölgelere bağıl olarak sonuçlar yorumlanmıştır. Ayrıca, hızlı kamera kullanılarak akış görselleştirme yapılmış, kompresör içerisindeki yağ dağılımı deneysel olarak görselleştirilmiştir. Akış görselleştirme deneyleri, kompresörün kalkış anı ve daimi rejime ulaşma anında yapılmıştır. Motor kalkış verisi bu görsellerin işlenmesi ile elde edilerek bir sonraki bölümde kullanılmıştır

Üçüncü bölümde ise tez kapsamında gerçekleştirilen nümerik çalışmalara yer verilmiştir. Bu bölüm kapsamınca yağlama sistemi sayısal olarak modellenmiştir. Kompresör yağlama sistemindeki krank milinin hareketi birinci kısımda Kayan Çözüm Ağı (SM) ikinci kısımda ise Hareketli Referans Çerçevesi (MRF) metodları kullanılarak modellenmiştir. SM metodu, sayısal alandaki sınırların ve çözüm ağlarının katı cisim hareketinde birlikte hareket ettiği özel bir dinamik çözüm ağı hareketi türüdür. SM metodu çözüm ağının zamanla hareketinden dolayı doğal olarak zamana bağımlıdır. Hesaplama alanındaki çözüm ağları herhangi bir deformasyona uğramaz ve yönetici denklemler MRF metodundan farklıdır. SM metodu, çoklu referans çerçevesindeki akışları modellemenmesi için en doğru yöntem olarak tanımlanır. Bu metod, aynı zamanda uzun hesaplama süresi gerektirir. MRF metodunda ise hareketli bölgenin bağıl hareketi hesaba katılmaz, başka bir deyişle çözüm ağı sabitlenir. Bu hermetik pistonlu bir kompresörün krank milinin hareketinin sabit bir pozisyonda dondurulması ve anlık akış alanlarının bu pozisyon üzerinden hesaplanması anlamına gelir. Akış alanında dönen bir parçanın bulunduğu birçok mühendislik uygulamasında, nümerik metod olarak MRF yaygın olarak tercih edilir. Bunun bazı örnekleri zayıf rotor-stator etkileşimli turbomakina uygulamaları, rüzgar türbinleri ve karıştırma tanklarıdır. Simülasyonlar sonlu hacimler tabanlı ANSYS-FLUENT yazılımı kullanılarak gerçekleştirilmiştir. Her bir metod için sayısal çözüm alanı, yönetici denklemler, çözüm ağı ve zaman adımından bağımsızlık testleri verilmiştir. Her bir model için kompresör hızının etkisi geniş bir bant

aralığında taranmış ve deneysel olarak elde edilen sonuçlarla valide edilmiştir. SM metodu tahminlerinin 2800 d/dak. ve üzerinde, deney sonuçlara daha yaklaştığı görülmektedir. Ayrıca SM metodu ile kompresör içerisindeki anlık yağ hareketi görselleştirilmiştir. Bu metod ile krank milinin farklı konumlarındaki pozisyonu nümerik olarak modellenilebilmektedir. Ek olarak, viskozite etkisi ve soğutkanın yağ içinde çözünmesi sayısal olarak incelenmiştir. SM ve MRF metodu ile yapılan analizlerde viskozite azaldıkça yağ kütleli debisi arttığı görülmüştür. Buna ek olarak, kullanılan soğutkan/yağ karışımı için, soğutkanın yağ içerisindeki çözünme oranına göre karışımın viskozite değişimini veren Daniel eğrileri ile, üç farklı çözünme orandaki viskozite değerleri elde edilmiştir. Böylece soğutkanın yağ içerisindeki çözünme oranının artmasıyla viskozitenin azaldığı ve bunun da kütleli yağ debisini arttırdığı görülmüştür. Bu çalışmalara ek olarak, elektrik motorunun kalkışı Kullanıcı Tanımlı Fonksiyon (UDF) kullanılarak modellenmiş ve yağ tırmanma zamanı iki farklı metod için hesaplanmıştır.





1. INTRODUCTION

Increasing energy costs urge not only developing but also developed countries to have new regulations on energy prevention and recovery. Moreover, several countries in the EU announce some incentives to increase the usage of more energy-efficient products. For example, the refrigerators in the market having an energy index lower than A are replaced with the A+++ refrigerators, energy-saving reaches the annual electrical energy production of the Keban Dam in Turkey. Therefore design and production of energy-efficient products with appropriate costs are a very crucial issue for manufacturers.

The total number of refrigeration, air conditioning and heat pump systems in use worldwide are around 3 billion, and the refrigeration sector consumes nearly 17% of the overall electricity used worldwide [1]. Reciprocating compressors in the refrigeration systems such as refrigerators and freezers and rotary compressors for heat pumps used in the laundry dryers are the main components in these household appliances. The largest part of the electric consumption related to refrigerators and dryers is caused by compressors.

In addition to improving more-efficient products, there are many restrictions on cooling systems related to reducing global warming, which is another problem the world is facing. The refrigeration sector accounted for 7.8% of global greenhouse gas emissions. The Kigali Amendment to the Montreal Protocol approved in 2016, aimed to progressively reduce the production and consumption of HFCs, should allow avoiding an increase in average temperatures between 0.1 °C and 0.3 °C by 2100 [2].

Due to the increasing demands on new refrigerants considering their efficiency and the regulations for the protection of the environment, the natural refrigerants or refrigerant blends are widely used. By the application of these new working media, the demands on compressor manufacturers as well as on the suppliers of lubricants increase. Considering the background of the Kigali Amendment and EU-regulation 517/2014,

new fluids and fluid mixtures need to be developed as substitutes for non-permissible refrigerants and also for more efficient operation.

In this study, the effects of zeotropic refrigerant mixtures are investigated to increase the energy efficiency of the refrigeration system by using new refrigerant blends with appropriate lubricants and additives which are less harmless and more environment-friendly compared to conventional refrigerants.

1.1 Vapor Compression Refrigeration Cycle

The ideal vapor compression cycle is the most widely used cycle for refrigerators, air-conditioning systems, heat pumps and it is shown schematically on a T-s diagram in Figure 1.1. It consists of four major thermal processes.

- 1-2 Isentropic compression in compressor.
- 2-3 Constant pressure heat reduction in condenser.
- 3-4 Throttling in an expansion device.
- 4-1 Constant pressure heat absorption in an evaporator.

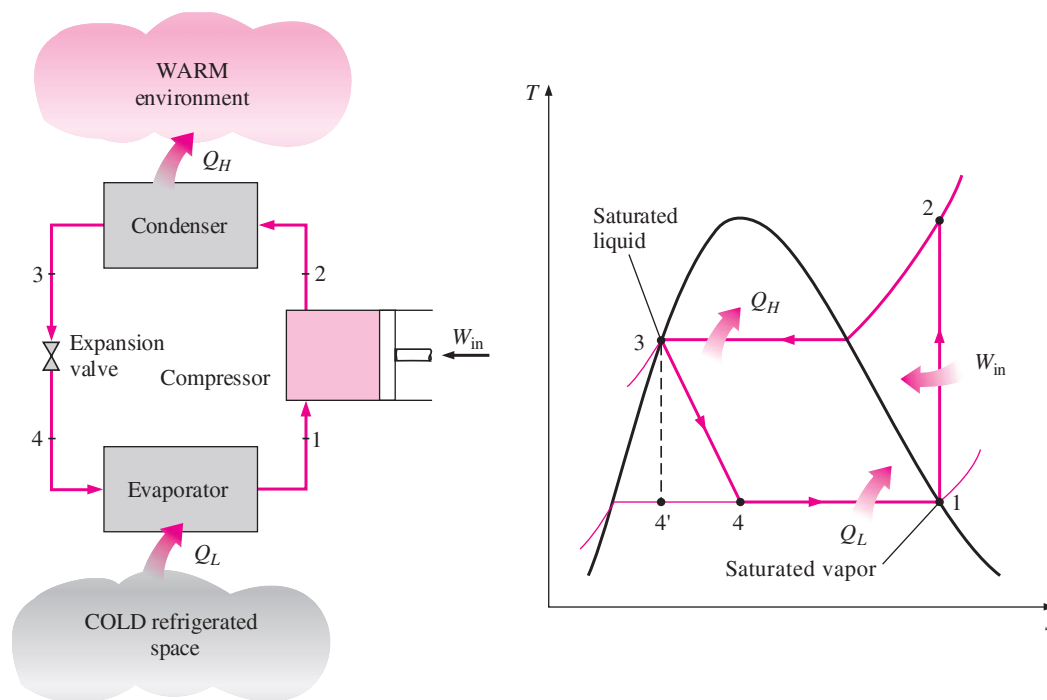


Figure 1.1 : Schematic and T-s diagram for the ideal vapor-compression refrigeration cycle [3].

In an ideal vapor compression cycle, the refrigerant enters the compressor as saturated vapor and is compressed isentropically to the condenser pressure. During the compression process, the temperature of the refrigerant rises above the surrounding medium temperature. Then the refrigerant enters the condenser, whose purpose is to provide a heat transfer surface through which heat dissipates from the refrigerant to the condensing medium and leaves as saturated liquid. The saturated liquid refrigerant enters a throttling device whose function is to reduce the pressure of the liquid refrigerant entering the evaporator so that the liquid refrigerant will vaporize in the evaporator at the desired low temperature. The refrigerant enters the evaporator as a low-quality saturated mixture and it completely evaporates by absorbing heat from the refrigerated space. The refrigerant leaves the evaporator as saturated vapor and reenters the compressor, completing the cycle.

The condenser and evaporator do not involve any work, and the compressor can be assumed as adiabatic. Then the COPs of the refrigerators and heat pumps operating on the vapor compression refrigeration cycle are given below [3].

$$COP_R = \frac{q_L}{w_{net,in}} = \frac{h_1 - h_4}{h_2 - h_1} \quad (1.1)$$

$$COP_{HP} = \frac{q_H}{w_{net,in}} = \frac{h_2 - h_3}{h_2 - h_1} \quad (1.2)$$

The actual vapor compression cycle is shown in Figure 1.2. There are some clear differences between the ideal and actual cycle mainly because of the pressure and temperature drops associated with the refrigerant flow and heat transfer to or from the surroundings. Superheating (referring to superheating of the refrigerant vapor leaving evaporator) and subcooling (referring to subcooling of the refrigerant liquid leaving the condenser) are apparently two significant processes in actual vapor compression cycles and are applied to provide better efficiency (COP) and to avoid some technical problems. Additionally, depending on the temperatures of the refrigerant and surroundings entropy may increase or decrease in the compression process. Ideally, the refrigerant is assumed to leave the condenser as a saturated liquid at the condenser pressure however, it is unavoidable to have some pressure drop in the condenser and line through the condenser to throttling device. There is also some pressure drop occurs in the evaporator and the line between the evaporator and compressor.

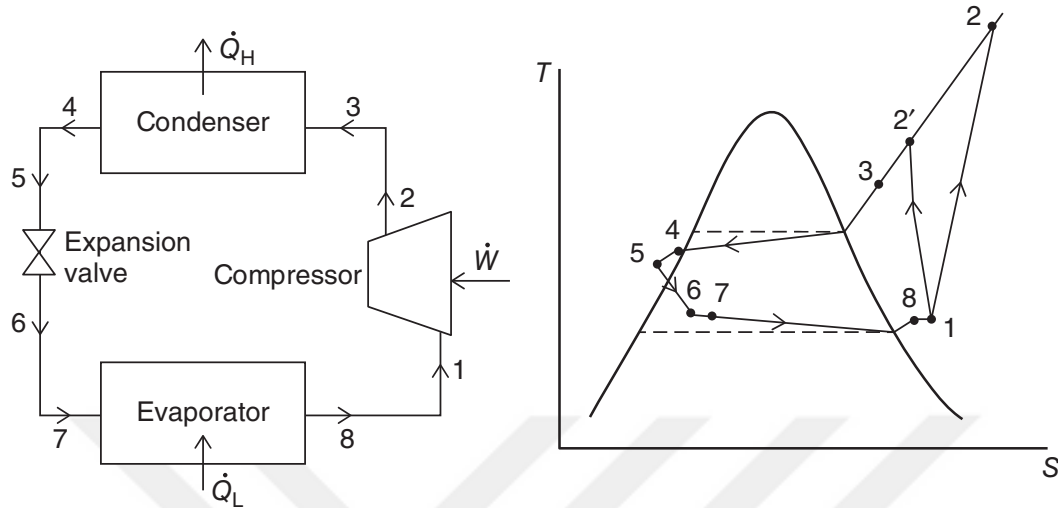


Figure 1.2 : Schematic and T-s diagram for the actual vapor-compression refrigeration cycle [4].

1.2 Environmental Aspect of Refrigerants

International Institute of Refrigeration defines refrigerant as working fluid in a refrigerating system absorbing heat at low pressure/temperature and rejecting it at a higher pressure/temperature. Concerning the vapor compression cycle, the refrigerant is the working fluid of the cycle which vaporizes in the evaporator and condenses in the condenser by transferring heat to the surrounding medium.

The ethyl ether (R610) was the first fluid known with outstanding thermodynamic properties that makes it a remarkable refrigerant. This characteristic was noticeable when a little amount is spilled on the hand. The almost instantaneous evaporative effect causes a cooling feeling in the skin, while a portion of the substance is evaporated by absorbing heat from hand [5]. In this context, ethyl ether was first proposed refrigerant in a closed cycle to freeze water into ice by Oliver Evans in 1805 and it is used as a refrigerant in the first patented refrigeration machine with the capacity to operate continuously was built by Jacob Perkins in 1834 [6]. Ethyl ether followed by ammonia (R717), carbon dioxide (R744), methyl chloride (R40), sulfur dioxide (R764), butane (R600), ethane (R170), propane (R290), isobutane (R600a), gasoline and chlorofluorocarbons (CFCs), among others. Three of these refrigerants

became very popular, ammonia and sulfur dioxide for refrigerators and carbon dioxide preferably for ships' refrigeration [3,4].

With advancing of the usage of the refrigeration systems, there were some incidents with the refrigerants resulted in serious illness and death in the 1920s. Resulting in the public ban of hazardous refrigerants, General Motors' research laboratory founded R21, which is the first invention of the CFCs. R21 followed by R11 and R12 and commercial production was started in 1931. CFCs were non-toxic, non-flammable and with good thermodynamic properties and oil miscibility characteristics. The CFCs R11, R12, R114 and R502 together with the hydrochlorofluorocarbon (HCFC) R22 became the definitive refrigerants [3, 4, 6, 7]. HCFCs are molecules composed of methane or ethane in combination with a halogen. Since then, many refrigerants used in the refrigeration systems and the timeline for refrigerants is given in Figure 1.3.

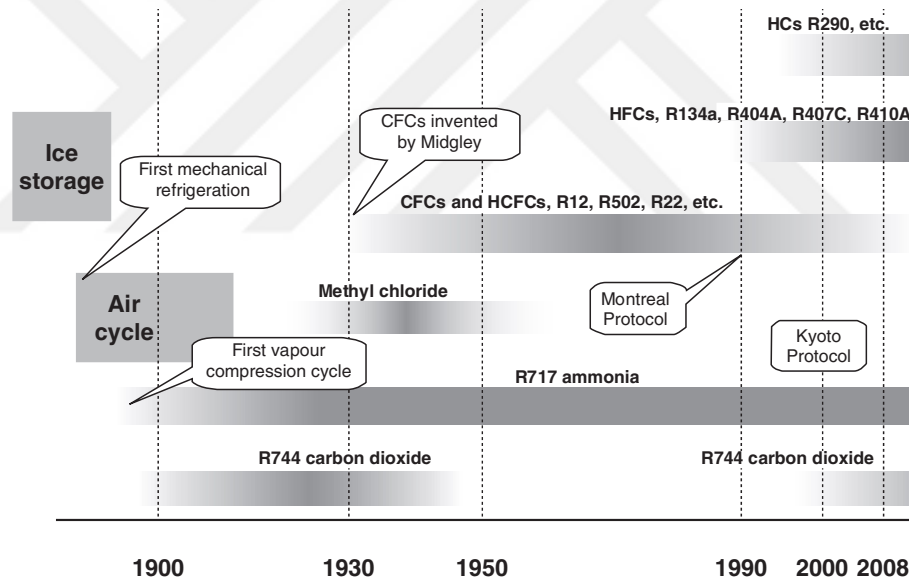


Figure 1.3 : Time line for refrigerants [7].

It is found out that CFCs allow more ultraviolet radiation into the earth's atmosphere in the 1970s. The ozone layer destruction is hazardous to public health by increasing the rate of skin cancer and burns induced by continued exposure to solar radiation. Such refrigerants include chlorofluorocarbons (CFCs), hydrochlorofluorocarbons (HCFCs), halons, and other ozone-depleting substances (ODSs), which are recognized as the main cause of the observed depletion of the ozone layer. The 1985 Vienna Convention for the protection of the Ozone Layer and the 1987 Montreal Protocol on substances that deplete the ozone layer formally recognized the significant threat that ozone-depleting substances posed to the ozone layer and human health, as well as other

potential effects, such as changes in climate. The Montreal Protocol has successfully protected the stratospheric ozone layer. The protocol has been an effective instrument for protecting the Earth’s stratospheric ozone layer by providing an international framework for phasing out ODSs, including CFCs and HCFCs. The phase-out of ODSs has been accomplished by curtailing their production and consumption. HCFCs have Ozone Depletion Potentials (ODPs) that are 10-50 times smaller than CFCs and were classified under the protocol as ‘transitional substitutes’ to be used during the time it took to commercialize new ozone-safe alternatives and replacements are presented in Figure 1.4. It is stated that the ozone layer will return to its 1980 levels towards the 2050s and that the ozone hole will disappear late in the 21st century [8].

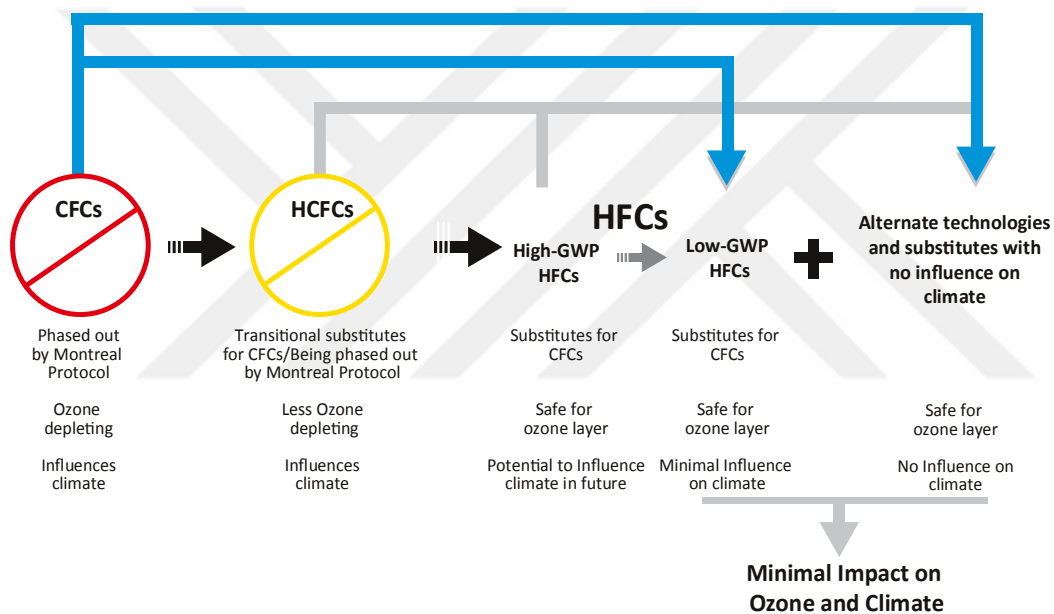


Figure 1.4 : Flow diagram of ODSs phase-out process [8].

The phase-out of ODSs requires either substitute chemicals or other approaches, and hydrofluorocarbons (HFCs) have become the major replacements in many ODS applications. HFCs, which have no known natural sources, are used because they do not deplete the stratospheric ozone layer and can be used with relative ease (technically) in place of CFCs and HCFCs. The phasing in of HFCs as replacements for CFCs is evident from the decrease in CFC usage concomitant with the increasing usage of HFCs. The use of HCFCs also increased with the decreasing use of CFCs. HCFCs are being replaced in part by HFCs as the 2007 Adjustment to the Montreal Protocol on HCFCs continues to be implemented. Thus, HFCs are increasing primarily because they are replacing CFCs and HCFCs as shown in Figure 1.5.

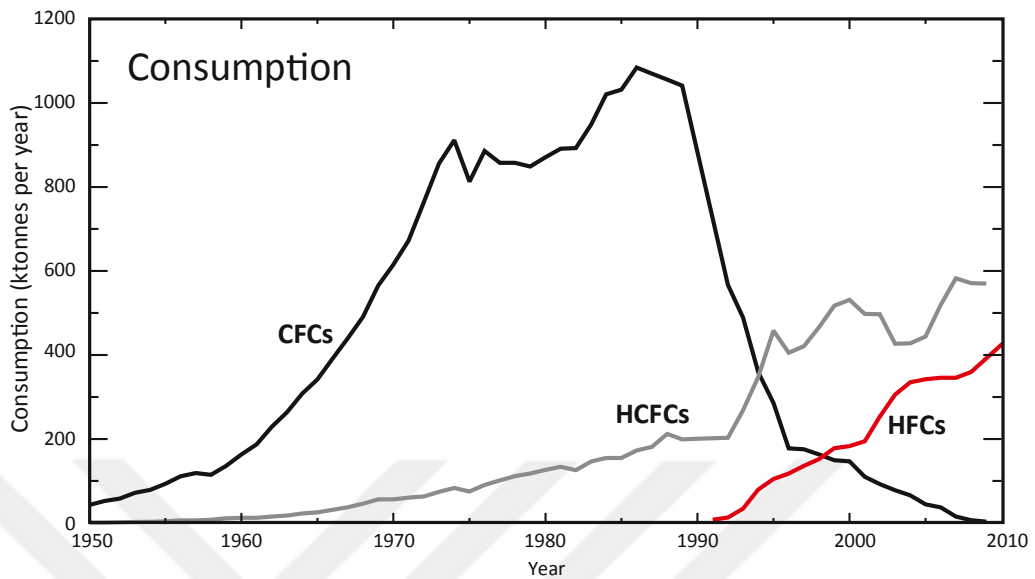


Figure 1.5 : The transition in global consumption from CFCs to HCFCs and to HFCs [8].

HFCs have found widespread use in various applications. They are used in refrigeration and air-conditioning equipment in homes, other buildings and industrial operations ($\sim 55\%$ of total HFC use in 2010, expressed in CO_2) and for air-conditioning in vehicles ($\sim 24\%$). Smaller amounts are used for foam products ($\sim 11\%$), aerosols ($\sim 5\%$), fire protection systems ($\sim 4\%$) and solvents ($\sim 1\%$). The use of HFCs is increasing rapidly as a result of global economic development and population growth.

Many HFCs are potent greenhouse gases. Although their current contribution to climate forcing is less than 1% of all other greenhouse gases combined, HFCs have the potential to influence climate in the future substantially. As a consequence, the abundances of HFCs in the atmosphere are also rapidly increasing. For example, R134a, the most abundant HFC, has increased by about 10% per year from 2006 to 2010. If HFC emissions continue to increase, they are likely to have a noticeable influence on the climate system. By 2050, the buildup of HFCs is projected to increase radiative forcing by up to $0.4 \text{ W}/\text{m}^2$ relative to the year 2000. However, the future radiative forcing by HFCs in 2050 would be relatively small, at the same level as it is today ($<1\%$ of CO_2), if the current mix of HFCs were replaced with low-GWP substances with lifetimes of a few months or fewer [8,9].

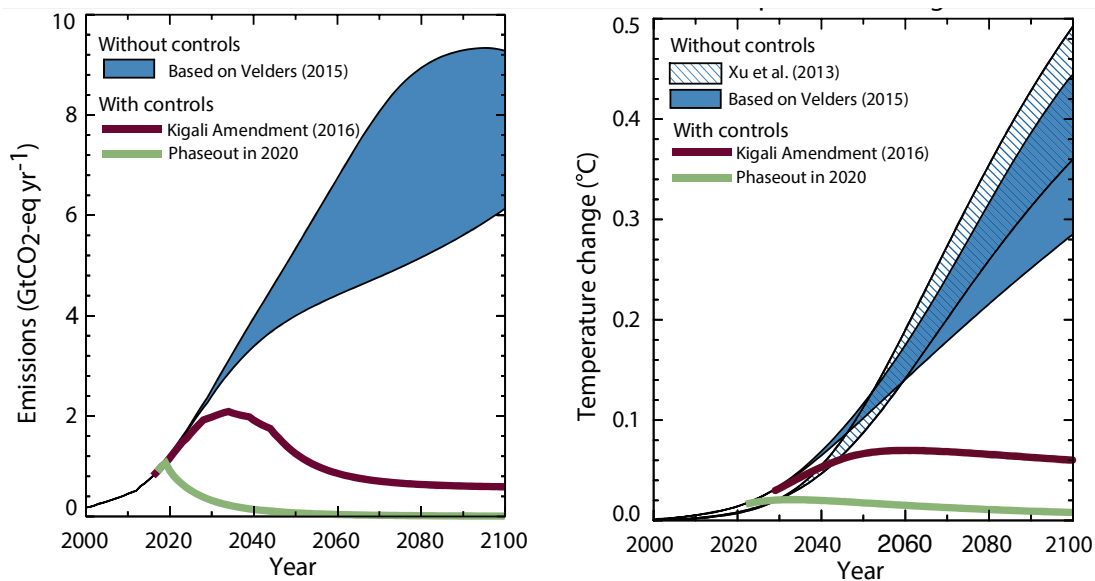


Figure 1.6 : Scenarios of HFC emissions and global average surface-temperature response [10, 11].

The EU Regulation No 517/2014 is going to phase out most of the refrigerants used in refrigerators and air conditioning systems such as R134a, R404a and R410A because of their extended use and their high GWP (Global Warming Potential) values. It was aimed at the EU's F-gas emissions will be cut by two-thirds by 2030 compared with 2014 levels. Moreover, The Kigali Amendment is applied to reduce future global average warming in 2100 due to HFCs from baseline of 0.3°C - 0.5°C to less than 0.1°C.

It is stated that improvements in energy efficiency in refrigeration and air-conditioner equipment during the transition to low GWP alternative refrigerants can potentially double the climate change benefits of the HFC phase-down [10].

As mentioned before, refrigeration, air-conditioning and other sectors are constantly evolving in response to a wide range of commercial, environmental, and other pressures. Technological change is a continuing process in the industry, with new developments occurring every year. Climate change issues, as well as developments in refrigerant options, will continue to stimulate equipment innovations in refrigeration and air-conditioning. Companies are in the process of developing new substances and blends and associated lubricants and equipment components.

1.3 Lubricants

Lubricants are mainly used to lubricate moving parts in the compressor. The life of the wearing parts can be extended several years with careful selection of the lubricants. On the other hand, ineffective lubrication leads to the life of the compressor may be only minutes. The main tasks of lubricants are given below [12].

- Reduce the friction between moving parts.
- Carry heat away from bearing surfaces.
- Prevent corrosion both during operation and when the compressor is at rest.
- Reduce gas leakage between seal faces and close clearances.

Lubricant oil is expected to perform its lubricating function continuously and effectively without undergoing any chemical change for long periods. Especially in the hermetic compressors, changing the oil is not practical and the same oil frequently remains in the compressor through the life of the refrigerator, which is approximately ten years or more.

Another important rule for selecting lubricants is the viscosity, which is essential to prevent wear of the bearings. While using low viscosity oils results wearings of the bearings, high viscosity results in high fluid friction, increasing the power consumption of the compressor. Moreover, high viscosity oil may thick enough not to penetrate between various bearing clearance, particularly where tolerances are close resulting in inadequate lubrication of the compressor parts [13].

Some lubricants penetrate to the compression line in the compressor, i.e. the gap between the cylinder and rod in the reciprocating compressor, resulting in oil travels through in refrigerant cycle which ranges up to 5% and even more in some special cases. Type of the compressor, design of the refrigeration system, operating parameters, the refrigeration oil selection, etc. are responsible for varying amounts of the oil circulation rate in the system. In this context, the refrigerant miscibility of the lubricating oil in the refrigerant circuit is of decisive importance to oil circulation and the overall efficiency of the refrigerator. Phase separation between the refrigerant and the oil leads to malfunction of the condenser, evaporators and oil collectors. Moreover,

collecting oil in the refrigerant cycle could lead to inadequate lubrication resulting in compressor breakdowns [14].

1.4 Compressors

In a refrigeration cycle, the compressor provides a pressure difference across the expansion valve, thereby causing a steady and positive flow of the refrigerant. Refrigerant compressors, which are outlined as the heart of the vapor-compression refrigeration systems, may be divided into two main categories named as positive displacement and dynamic compressors. Compression of the vapor being accomplished mechanically using a compression chamber in the positive displacement compressors whereas, in dynamic compressors, compression provided essentially by the action of the centrifugal force which is developed as the vapor is rotated by a high-speed impeller.

The most commonly used types in the refrigeration and air conditioning industry are reciprocating, rotary, scroll, screw and centrifugal compressors. The approximate range of refrigeration capacities of the compressors is given in Figure 1.7. The majority of domestic, commercial and industrial HVAC systems use reciprocating compressors [7, 13].

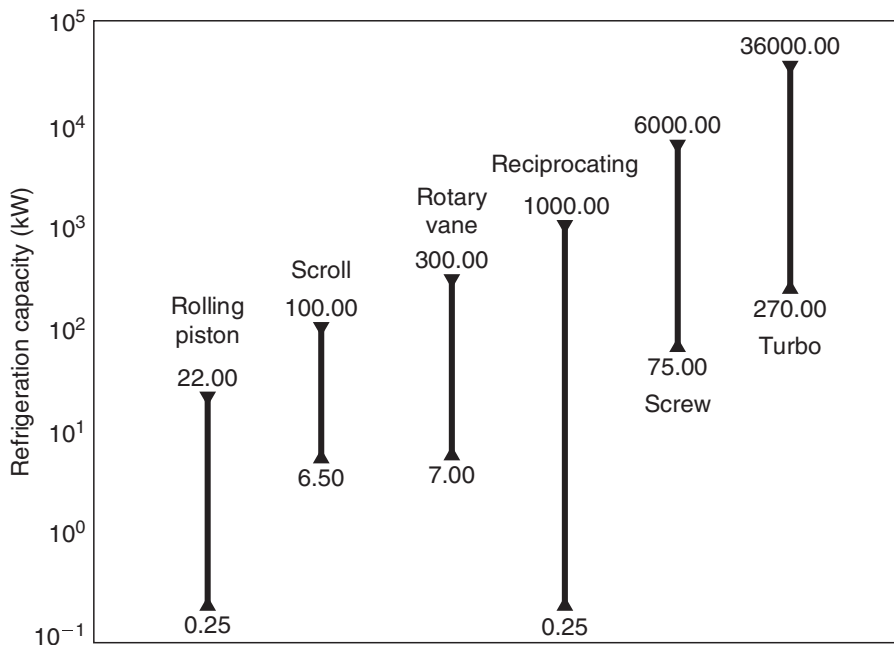


Figure 1.7 : Approximate range of capacity covered by various compressor types [7].

Depending on the position of the electrical motor, the compressors are classified as hermetic, semi-hermetic and open type. The open compressors having external

drive require a gland or seal, where the shaft passes out of the crankcase, are termed open compressors. The semi-hermetic compressor has the rotor of its drive motor integral with an extended crankshaft, and the stator is fitted within the extension of the crankcase. Semi-hermetic compressors are built in a very wide range of sizes for commercial and industrial markets. Hermetic compressors contain the motor and all working parts sealed within a steel shell called the crankcase. Therefore, it is not accessible for repair or maintenance.

The domestic refrigerators and freezers contain hermetic type reciprocating compressor in sizes of up to tens of kW. They are generally lighter and compact than a semi-hermetic compressor. The traditional AC synchronous motor, together with its protection system, is developed in different versions for the various voltages and frequencies existing in different countries. This complexity is solved by introducing a DC motor while it is universal and additionally provides variable speed capacity. DC motors require a converter to convert the supply from the AC source. Inverters, which are designed to control the electronic motor power and speed by generating electrical waveforms of controllable frequency, are used in the compressors. There is a trade-off between the energy consumption and the lubrication system of the compressor. Due to the lubrication requirements, there is likely to be a minimum speed limit in the compressor where limits also the energy consumption [7].

1.5 Literature Survey

In this section, the literature review of the refrigerant/refrigerant mixtures used in the vapor compression refrigeration cycles is presented. The review mainly focused on environment-friendly refrigerants and refrigerant mixtures to replace HFCs and CFCs. Besides the selection of the refrigerant, a lubricant is also crucial since household refrigerators are installed with lubricated compressors. Thereafter, a comprehensive review of the lubricants and lubrication system of the hermetic compressor is provided in this section.

Mulroy *et al.* [15] investigated glide matching with binary and ternary zeotropic refrigerant mixtures. It is concluded in the study that matching temperature profiles of the refrigerant mixture and the heat transfer fluid increases the COP of the refrigeration cycle.

Domanski *et al.* [16] used a semi-theoretical model for evaluating the performance of different working fluids, including refrigerant mixtures in the vapor compression cycle. It is showed that the addition of a low boiling point component to a binary zeotrope to increase the volumetric capacity and zeotropic temperature glide might be useful.

Hansen *et al.* [17] investigated thermodynamical performance, chemical stability, compatibility, wear and a lifetime of a small hermetic compressor using pure R600a as a refrigerant. They stated with disregarding the inflammability hydrocarbons, e.g. R290, R600, R600a could be a candidate to replace HFC R134a. They stated that standard refrigerator design needs modifications to use a zeotropic blend of R600a/R290, which has the same pressure characteristics as CFC R12. Therefore blends are not seen as universal alternatives to use in household refrigeration systems. They concluded that it is possible to use R600a in small hermetic compressors with the necessary redesign of the system.

Camporese *et al.* [18] tested several domestic hermetic refrigeration compressors with different displacements in a secondary refrigerant calorimeter. Tests were performed with R12, R134a, R290/R600a (50%/50%) and R600a. They concluded that both the mixture and R600a has advantage and disadvantages and long term tests are required to define the risks of use hydrocarbons in refrigeration.

Uchida *et al.* [19] experimentally studied the heat transfer performance of a zeotropic refrigerant mixture in horizontal tubes. They concluded that the cross-grooved surface provides the highest heat transfer coefficients for evaporation and condensation among the flat and corrugated surfaces of heat exchangers.

Yilmaz [20] examined the performance of pure and zeotropic refrigerant mixtures used in air to water heat pump system and reported that the mixture ratio of blends affects the COP and second law efficiency. It is concluded that zeotropic refrigerant mixtures with smaller ODP and GWP can also yield a high COP and second law efficiency and they can be a good option to replace CFC and HCFC refrigerants.

Navarro *et al.* [21] tested five hermetic compressors covering different capacities, stroke-to-bore ratios, and several cylinders with propane as a refrigerant and the results are compared to performance with R-407C. They measured volumetric efficiency and

isentropic efficiency, as well as other parameters. They reported that the COP value increased by 9% with R290 instead of R410.

Park & Yung [22] analyzed the thermodynamic performance of two pure HCs and seven mixtures containing R1270, R290, R152a and RE170 in residential air conditioners. The comparison of test results is given in Figure 1.8. 45%R1270/40%R290/15%DME mixture showed the best thermodynamic performance results in increase COP by 5.7% than base fluid R22. They resulted that tested fluids produce good thermodynamic performance with reasonable energy savings without any environmental problem hence can be used as long term alternatives for air conditioning and heat pump applications.

Reference	Refrigerants	COP	Diff. COP (%)	Q_c (W)	Diff. Q_c (%)	T_{dis} (°C)	Diff. T_{dis} (°C)	Charge (g)
[1]	R22	3.78		3600		80.2		1170
[2]	R290(propane)	3.85	1.9	3187	-11.5	63.0	17.3	520
[3]	R1270(propylene)	3.75	-0.7	3808	5.8	69.1	11.7	540
[4]	20%R1270/80%R290	3.90	3.4	3362	-6.6	63.8	16.5	525
[5]	50%R1270/50%R290	3.91	3.5	3589	-0.3	65.5	14.7	550
[6]	80%R1270/20%R290	3.92	3.8	3729	3.6	67.4	12.9	530
[7]	60%R290/40%R152a	3.84	1.8	3572	-0.8	64.9	15.3	630
[8]	71%R290/29%R152a	3.91	3.6	3533	-1.9	64.4	15.9	600
[9]	75%R290/25%R152a	3.91	3.6	3527	-2.0	64.6	15.6	600
[10]	45%R1270/40%R290/15%DME	3.99	5.7	3551	-1.4	67.5	12.7	540

Figure 1.8 : Test results for various refrigerants [22].

Greco [23] carried out an experimental study of the heat transfer performance of pure refrigerants, azeotropic, quasi-azeotropic and zeotropic refrigerant mixtures. It is noted that the heat transfer coefficients of the zeotropic mixtures R407 and R417a are always lower due to the mass transfer resistance in nucleate boiling.

Mani & Selladurai [24] conducted an experimental study on refrigeration system with R290/R600a (68%/32% by weight) refrigerant mixture as a drop-in replacement with R12 and R134a. They noted that the mixture could be a good candidate for the replacement of conventional refrigerants.

Lee *et al.* [25] performed experimental study on the performance characteristics of a small-capacity directly cooled refrigerator using the mixture R290 and R600a with mass fraction of 55:45 as an alternative to R134a. They modified the compressor displacement volume to match the refrigeration capacity of the original system with R134a. They noted that the refrigerant charge and capillary length are optimized for the mixture. They resulted that the power consumption is reduced %12.3 with using the R290/R600a refrigerant mixture. Moreover, they stated that the cooling speed of

the optimized mixture system at the in-case setting temperature of -15°C is improved by %28.8 over that of the optimized R134a system.

Calm [26] provided a comprehensive review of the next generation of refrigerants. Figure 1.9 displays the history of refrigerants divided into four refrigerant generations based on defining selection criteria. The paper investigates the possibility for current options in the contexts of existing global agreements, including the Montreal and Kyoto Protocols to prevent stratospheric ozone depletion and global climate change, respectively. It is concluded in the study that besides all environmental restrictions, new generation refrigerants must offer high efficiency.

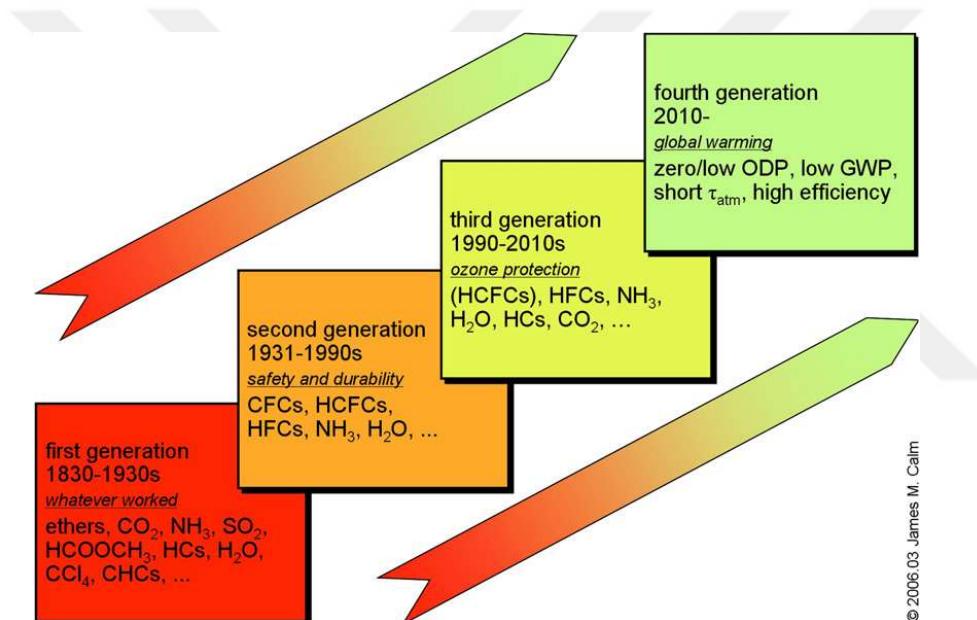


Figure 1.9 : Refrigerant progression [26].

Leighton [27] investigated experimentally and numerically of the household refrigerator with alternative low GWP refrigerants to replace R134a. It is stated that R1234yf would be a good substitute for R134a as a direct drop-in replacement in the household refrigerator. Additionally, the blends of R1234yf and R134a has performance characteristics similar to the pure fluids but has lower GWP than R134a and lower flammability than R1234yf.

Jin & Zhang [28] proposed a new evaluation method for zeotropic refrigerant mixtures. The temperature profiles of pure refrigerant and zeotropic refrigerant mixtures with the heat transfer fluid in the condenser and evaporator are shown in Figure 1.10. They noted that enthalpy varies linearly with temperature in the two-phase region

and the temperature difference between HTF and refrigerant may be close to 0°C , theoretically. By using temperature glide of the zeotropic refrigerant mixtures, they aimed to improve the COP of the refrigeration cycle. They pointed out that the temperature difference between the inlet and outlet of heat transfer fluid should be close to an optimal temperature difference of zeotropic refrigerant mixture to approaching the Lorenz cycle and decreasing the exergy loss.

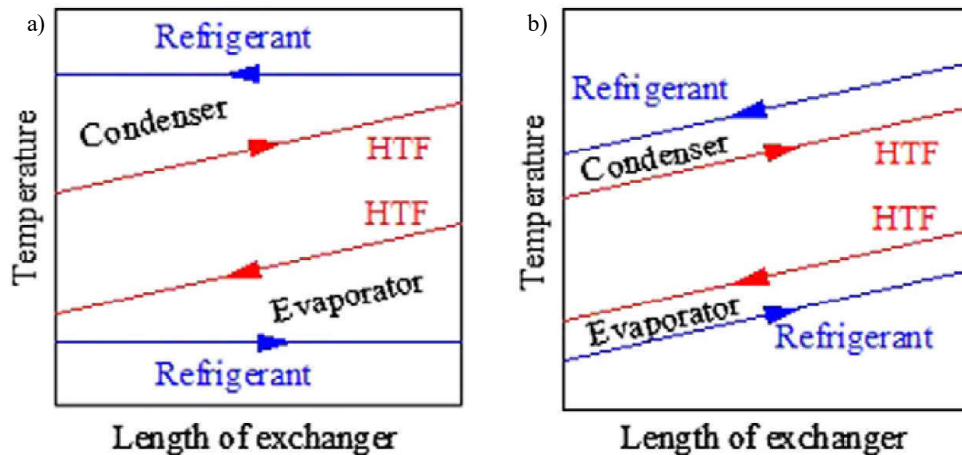


Figure 1.10 : Temperature profiles of refrigerant and HTF in condenser and evaporator: a) pure refrigerant b) zeotropic refrigerant mixture [28]

Navarro-Esbri *et al.* [29] presented experimental analysis of a vapor compression refrigeration system using R1234yf to substitute for R134a. They reported that the cooling capacity and COP decrease 9% and 19% respectively when using R1234yf in the system. They suggested that using an internal heat exchanger reduces the differences in the thermodynamic performance.

Lee *et al.* [30] investigated the drop-in performance of pure R134a, R1234yf mixtures of these refrigerants in a heat pump test bench under summer and winter conditions. They indicated that COP, cooling capacity and discharge temperature of R1234yf and the mixture are similar to those of R134a. They showed that flammability of the mixture reduces with increasing the R134a and compositions after 10% of R134a the mixture becomes non-flammable. They concluded that the mixture of R134a/R1234yf is an environmentally friendly solution for mobile air conditioners with minor modifications.

Mota-Babiloni *et al.* [31] theoretically investigated the energy performance of six refrigerants with four different vapor compression refrigeration cycle taking R404a as a baseline. They stated that with their low flammability and GWP values, long term

alternative refrigerants are L40 and DR-7, which are special refrigerants developed by Honeywell and Dupont respectively.

McLinden *et al.* [32] explored thermodynamic space to find low GWP refrigerants. They examined refrigerants by applying screening criteria to estimates for GWP, flammability, stability, toxicity and critical temperature. They stated that the remaining refrigerant candidates reduced to 62 after the selection criteria. They resulted that no fluid is ideal in all regards due to one or more negative attributes.

Mota-Babiloni *et al.* [33] performed experimental analysis of a non-flammable R1234ze(E)/R134a mixture (R450A) to replace R134a. They reported that the drop-in cooling capacity of R450a compared with R134a is 6% lower as average. The COP of the system with the mixture is even higher than that resulting in R134a. The discharge temperature of R450A is found to be lower than that of R134a, 2K as average. They indicated that R450A could be considered as a good alternative mixture to replace R134a.

In further research conducted by Mota-Babiloni *et al.* [34], different mixtures which are proposed by AHRI as alternative refrigerants used in refrigeration and HVAC systems are investigated theoretically. They concluded that most of the new HFO/HFC mixtures result in decrements in thermodynamic performance compared to those HFC and do not match the GWP limitations approved by the European normative and some of the mixtures proposed would have problems due to their flammability.

In their experimental study, Bohdal *et al.* [35] investigated heat transfer coefficients and pressure drop of condensation in mini-channels using pure R134a and zeotropic mixtures (R404A, R407C, R410A) as a refrigerant. They compared experimental results with correlations available in the literature. They reported that there is a difference between the results of tests and calculations, particularly in zeotropic mixtures. Finally, they proposed correlations for annular and annular-stratified two-phase flow structures.

Deng *et al.* [36] implemented four different condensation models of binary mixtures. They investigated heat and mass transfer resistances on the condensation process and required pipe lengths. They noted the mass transfer resistance in the vapor phase has

a major effect on condensation length. They compared predicted and experimental condensation lengths and concluded non-equilibrium models give better predictions.

Tian *et al.* [37] carried out a theoretical and experimental investigation on refrigeration system performance by using R32/R290 (68%/32% by weight) as a refrigerant to substitute R410A used in household air conditioners. They stated the required refrigerant amount of the mixture is much lower and it provides higher cooling and heating capacities and similar COP compared to R410A. They concluded that the proposed refrigerant is a good candidate to drop-in replacement for R410A in household air conditioners.

Yan *et al.* [38] performed energy and exergy analysis of zeotropic mixture R290/R600a vapor-compression refrigeration cycle with separation condensation. They introduced a phase separator into the system to enhance the overall system performance. A theoretical energy and exergy analysis on the performance of the modified vapor compression cycle (MVRC) is carried out by using the developed mathematical model and then compared with that of the traditional vapor compression cycle using the refrigerant R600a and the mixture R290/R600a. It is shown that MVRC yields the most excellent performances in the COP, the volumetric refrigeration capacity, the total exergy destruction and the exergetic efficiency under the same given operating conditions.

d'Angelo *et al.* [39] presented a performance evaluation of a vapor injection refrigeration system using a mixture R290/R600a. Steady-state simulations are used to accomplish a parametric analysis considering the influence of the refrigerant composition over COP, compressor power, refrigerant mass flow rate, refrigerant temperature glide, mass flow ratio between the vapor and feed streams in the flash tank, liquid and vapor composition of flash tank outlet streams and compression ratio. They resulted that a maximum COP was obtained for a mixture 40% of R290 by weight. Moreover, they showed that COP of vapor injection refrigeration cycle is 16-32% greater than the one of a vapor compression cycle.

Antunes & Filho [40] presented an experimental study on the refrigeration system by using alternative refrigerants. They reported that HCs (R290 and R1270) present the best thermodynamic performance among tested HFC. They reported the advantages of

HCs including reduction of the refrigerant charge, lower purchase price and low GWP values.

Chen *et al.* [41] proposed a modified vapor compression refrigeration cycle of the freezer system with R290/R600 to improve the cycle performance. They included an internal subcooler and an additional capillary tube to employ the temperature glide of the zeotropic mixture. They concluded that even if the theoretical use of the modified vapor compression cycle improves the COP and refrigeration capacity, further experimental work is needed to realize the system.

Popovic [42] experimentally investigated lubricant effects on the performance of R134a refrigeration system. It is noted that the COP could be improved as much as 5% by selecting miscible over an immiscible lubricant. Moreover, the effects of various lubricants on the different types of coils are mentioned. It is concluded in the study that lubricant selection not only important for system reliability but also on improving system performance and efficiency with the use of miscible and lower viscosity lubricants.

Lottin *et al.* [43] investigated effects of synthetic oil in a vapor compression refrigeration cycle using R410 as refrigerant. They showed that when the lubricant does not exceed 0.5% of the total refrigeration weight, the effects of oil are negligible on the system performance, above that limit, the performances of the system decrease significantly.

Wei *et al.* [44] experimentally investigated two-phase flow patterns and heat transfer characteristics of refrigerant-oil mixture flow boiling inside small tubes. As shown in Figure 1.11, the test bench consists of three loops, namely, the main refrigerant loop, a refrigerant bypass loop, and a lubricant oil loop. They concluded that the detrimental impact of oil on heat transfer performance becomes more significant with decrements of the tube size. Moreover, they proposed a new correlation of two-phase heat transfer multiplier with local properties of refrigerant-oil mixture flow boiling [45]. They reported that the new correlation shows a good predictive ability. They concluded that more experimental investigation is required for the development of general correlations.

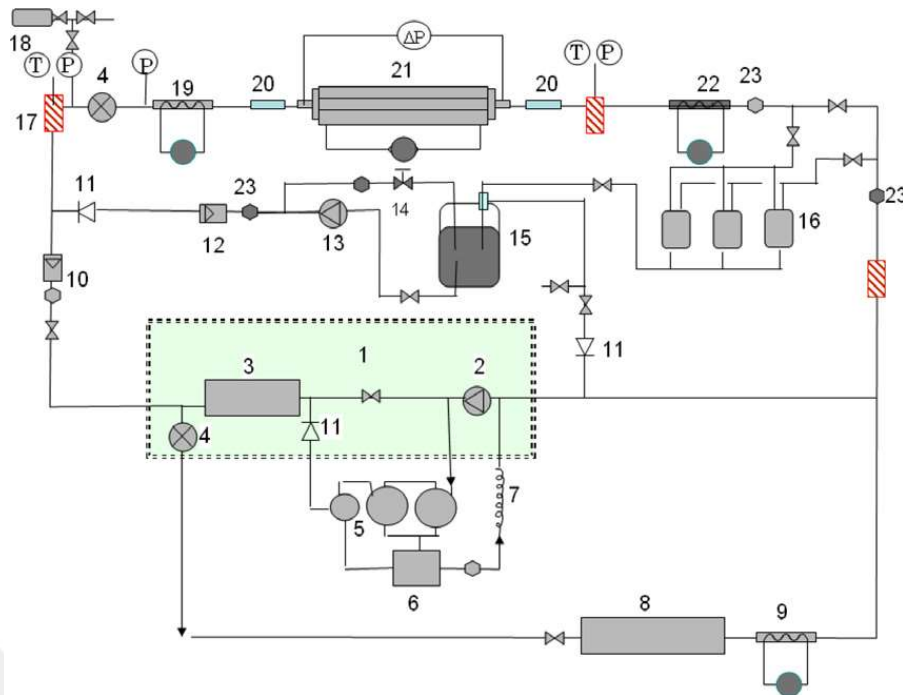


Figure 1.11 : Layout of flow circuits in test facility [44].

Hu *et al.* [46] conducted an experimental study on the heat transfer characteristics of refrigerant-oil mixture flow boiling inside a straight, smooth tube. They resulted that oil presence in the test section improves heat transfer at the range of low and intermediate vapor qualities. They reported that when the local oil concentrations are higher than 8%, the local heat transfer coefficients of the mixture decrease. Additionally, they developed a new correlation to predict the mixture flow boiling inside the straight tube. It is noted that the new correlation agrees with 90% of test data within the deviation of 25%.

Youbi-Idrissi & Bonjour [47] reviewed the effect of oil in refrigeration. They stated that a lubrication agent is required in almost all the refrigeration vapor compression systems, especially for the reliable operation of the compressor besides a certain portion of the oil always circulates with the refrigeration system which results in using a deviation from the theoretical analyses based on pure refrigerant. They stated that more research on the refrigerant/oil mixtures is required to overcome oil circulation problems in the refrigeration.

Prata & Barbosa [48] provided a comprehensive review of the role of thermodynamics, heat transfer, and fluid mechanics of lubricant oil in a hermetic reciprocating compressor. They reported the lubricants main role to lubricate moving parts in the hermetic compressor and effective lubrication system design is key to provide

necessary lubrication. Moreover, they stated that besides its lubrication expectations, refrigerant absorption by lubricant plays a crucial role in the compressor performance; therefore, oil-refrigerant mixture effects compressor design and performance.

Tas *et al.* [49] investigated experimentally the lubrication system of the hermetic compressor. Measurements are conducted to observe the effect of oil temperature, rotational speed and submersion depth on oil mass flow rate. In another study, Tas [50] experimentally investigated the lubrication system of the hermetic compressor. A new experimental setup is designed and same parameters are investigated for two different type hermetic compressor. The experimental results of the two systems are compared for the compressor type in the study.

Kim *et al.* [51] studied the flow characteristics of refrigerant and oil mixture in the compressor suction line. The effects of refrigerant mass flux, oil circulation rate, inner pipe diameter and pipe configuration on the oil retention are discussed in the study. They reported that oil retention increases with decreasing mass flux and increasing the oil circulation ratio. They resulted that oil retention in the vertical pipe is higher than the horizontal pipe.

Gorny *et al.* [52] investigated the lubricity evaluation of oil-refrigerant mixtures with R134a and R290. They proposed a new method of lubricity evaluation of oil-refrigerant mixtures. They noted that additives might improve the lubricity properties of the oils as well as oil-refrigerant mixtures. They concluded that the same viscosity grade oils show significant differences in lubricity properties.

Pizarro-Recabarren & Barbosa [53] investigated the effect of lubrication oil on heat transfer in a hermetic reciprocating compressor. They proposed a numerical model and predicted results are validated with experimental data. The schematic diagram of the oil heat transfer model is shown in Figure 1.12. The lubricating oil is expelled from the top of the crankshaft at point (1). Trajectories of oil in the shell and fall on the internal components are pointed in (2) and (3), respectively. The oil that returns from the compressor components into the oil sump is shown as (4). (5) represents the oil is sucked by the reed pump at the bottom of the crankshaft and finally (6) represents the oil pump. They reported that the highest temperature occurs in the top region of the compressor shell. They concluded that the oil circulation pattern in the crankcase

is important; however, its influence on the cooling capacity and the COP of the system is quite small.

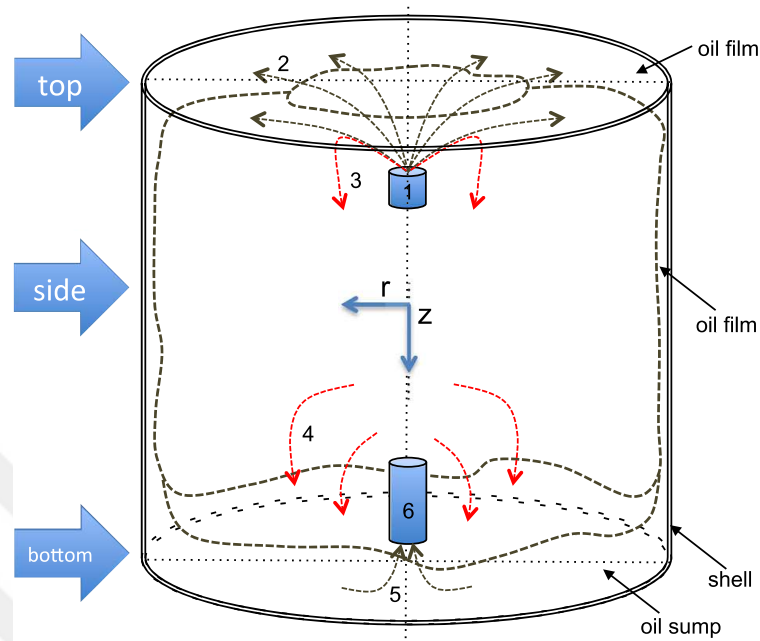


Figure 1.12 : Schematic diagram of the oil heat transfer model geometry [53].

Ido *et al.* [54] worked on tribological properties of sliding elements in compressors lubricated by low GWP refrigerant/oil mixtures. They measured the viscosity of lubricating oil mixed with liquid refrigerant and performed the seizure resistance under severe compressor operating conditions. They concluded that increasing the molar fraction of HFO results in decrements in seizure resistance.

In the CFD simulations, the MRF method is widely preferred to model the lubrication system of the compressor [55–58]. Important outputs of such CFD calculations are the climbing time of oil and the amount of oil spread from the upper part of the crankshaft at various compressor speeds.

Ozsipahi *et al.* [55] numerically investigated how the amount of oil mass flow rate in constant capacity hermetic compressors was affected by some operating conditions such as crankshaft speed, submersion depth of the crankshaft in the oil sump, oil viscosity and also the shape of the helical oil path on the crankshaft. They showed that the oil mass flow rate was directly proportional to the crankshaft speed, submersion depth and inversely proportional to the oil viscosity. Figure 1.13 displays the components of the constant speed hermetic compressor investigated in the study.

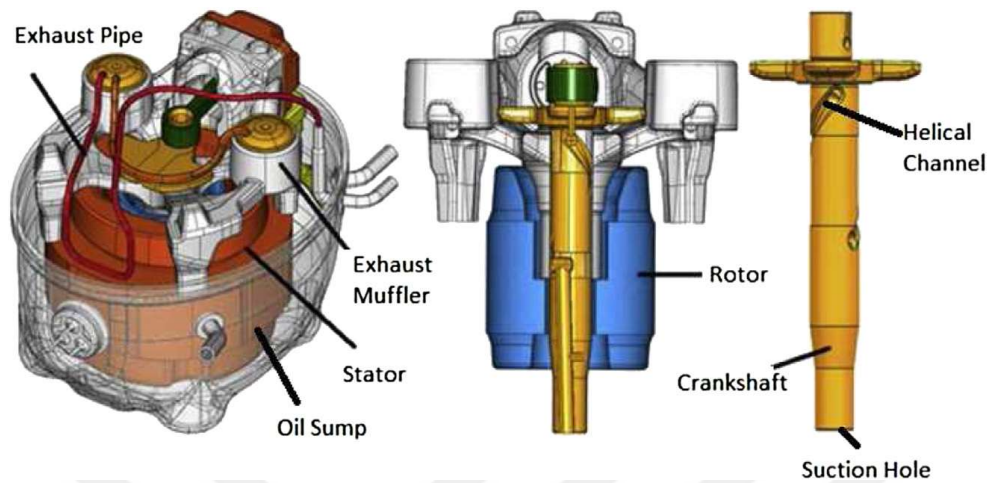


Figure 1.13 : Detailed appearance of the hermetic reciprocating compressor [55].

In another study, Ozsipahi *et al.* [56] suggested an analytical model for the screw pump used in the crankshaft of the hermetic variable capacity compressors to increase the oil mass flow rate at low compressor speeds. They investigated two different fluid flow models in the study, namely rotating crankshaft and stationary screw pump and rotating crankshaft with screw flights and stationary cylindrical apparatus. Schematic views of the fluid flow models are presented in Figure 1.14. The effect of the screw design on maximizing the flow rate was investigated in the analytical model and found to be consistent with the CFD simulations. They resulted that the design with screw flights on the crankshaft wall is more efficient in terms of maximizing the mass flow rate.

Lückmann *et al.* [57] introduced a CFD model of the lubricant flow in the oil pumping system of a reciprocating compressor. They computed the climbing time of the oil and the oil mass flow rate of the system. They concluded that more experimental study is necessary to validate the numerical results.

Tada *et al.* [58] proposed an uncoupled numerical model for the variable capacity compressors which are employed in domestic applications and investigated the effects of the immersion depth of the crankshaft and the compressor speed both numerically and experimentally. They concluded that immersion depth shows an insignificant effect on the experimental oil mass flow rate.

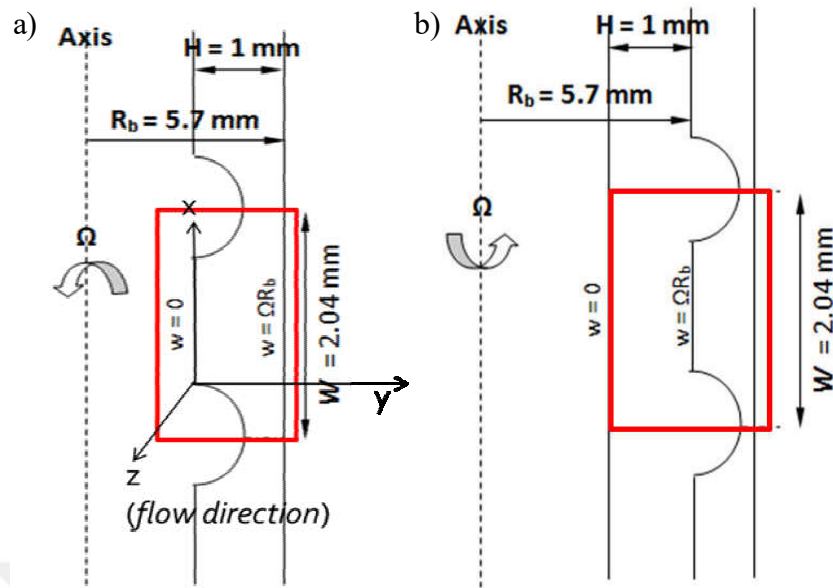


Figure 1.14 : Two different fluid flow models in the crankshaft a) rotating crankshaft and stationary screw pump b) rotating crankshaft with screw flights and stationary cylindrical apparatus [56].

Kerpicci *et al.* [59] performed an experimental and numerical study on the oil flow in a hermetic reciprocating compressor. They performed high-speed camera visualizations to capture oil climbing time. They noted that the Eulerian model predicts an oil mass flow rate better than the VoF model. They mentioned that the flow rate stagnation is observed at high rotational speeds. They concluded that even the small change in the oil viscosity affects the oil mass flow rate remarkably.

Alves *et al.* [60] conducted an analytical analysis of oil flow in the lubrication system for the reciprocating compressors. They proposed a new model to solve laminar, fully developed oil flow inside the system. They performed experimental tests to validate predictions of the mathematical model. They reported that the pumping power of the compressor reduced by %21.9 with respect to the initial design.

Zhu *et al.* [61] studied numerically and experimentally the effect of oil stirrer on the performance of lubrication system for a rolling piston compressor. They reported that good agreement is found between the predicted and experimental results. They resulted that an oil stirrer is efficient to improve the oil mass flow rate of the compressor. They noted that the flow rate stagnation is observed and the oil mass flow rate stays same or decreased even if with the increments of rotational speeds.

In the CFD simulations where the rotating parts are present, there are different techniques to be implemented to approach a more realistic solution. In the literature, dynamic meshes are intensively used in a numerical investigation of the screw and rotary compressors. Kovacevic *et al.* [62] developed the interface program in order to generate numerical grid. It is reported that a good agreement between the predicted and measured performance is a strong indication that CFD is a powerful tool for the design and optimization of the screw compressor.

Liu & Hill [63] suggested frozen rotor model, circumferential average model, and the transient SM method. They noted that depending on the problem definition, such as the existence of non-axisymmetric components or the interaction between the rotating and stationary parts, these models could potentially give different results. They concluded that only the transient SM method is capable of modeling the aerodynamic interaction due to the impeller rotation.

Deng *et al.* [64] simulated a rotary two-stage inverter compressor with SM method and compared the numerical results with experimental tests. They concluded that the offset angle between the upper and lower part of the crankshaft affects slightly the energy consumption of the compressor.

Ozsipahi *et al.* [65] compared the numerical performance of the SM and the Moving Reference Frame methods in modeling the lubrication system of a compact inverter compressor. Oil climbing time with infinite acceleration, instantaneous flow fields of the two-phase flow and the oil mass flow rate predictions obtained by the two methods have been compared in the study.

Ozsipahi *et al.* [66] investigated the lubrication system of a compact inverter compressor both numerically and experimentally. The CFD calculations have been performed for the immiscible two-phase flow under laminar flow conditions using various crankshaft speeds between 1200 and 4500 rpm for oils with kinematic viscosities of 3, 5, 10 and 15 cSt. Two numerical methods, namely MRF and SM were proposed in the prediction of the averaged mass oil flow rates from the outlet of the crankshaft. The formation of oil droplets and their development during the operation of the compressor were observed with a high-speed camera and the oil mass flow rate measurements were carried out on an in-house built setup to confirm the CFD results.

Cavallini *et al.* [67] studied numerically steady-state thermal analysis of a hermetic reciprocating compressor. The numerical results are validated with experimental data obtained for both R600a and R134a. They noted that numerical model able to capture temperatures of different parts, power input and heat transfer rates of the parts. It is stated that a numerical model can be a useful tool for the design and development of the hermetic reciprocating compressors.

Raja *et al.* [68] introduced a numerical model for thermal mapping of a hermetic reciprocating compressor. They obtained temperature distribution of different parts in the compressor and compared with experimental values. They concluded that the selection and position of overload protection relay affect the thermal distribution of the compressor.

Ooi [69] presented an analytical study on the heat transfer and thermal mapping of a hermetic reciprocating compressor. The lumped thermal conductance method is applied to the components in the study. The computer model is introduced to solve equations obtained from the analytical study. It is reported that good agreement found between measurements and predicted solutions. It is concluded that the numerical model can be used for the thermal design of the compressor.

Rigola *et al.* [70] performed an experimental study to validate a mathematical model developed for the numerical simulation of the thermal and fluid dynamic behavior of hermetic reciprocating compressor. The thermocouple positions of the tested compressor are given in Figure 1.15. They tested different compressor geometries and a wide range of working conditions and refrigerants. They reported that the numerical model slightly underestimates the volumetric efficiency and COP for low compression ratios and overestimates at high compression ratios.

In further research conducted by Rigola *et al.* [71], a numerical model for the thermal and fluid dynamic optimization of a hermetic reciprocating compressor is introduced. They performed different parametric studies based on a numerical model. Volumetric efficiency and COP at different evaporation temperatures and compressor speeds are reported. It is concluded that lower stiffness of the valve helps to improve volumetric efficiency and COP of the system.

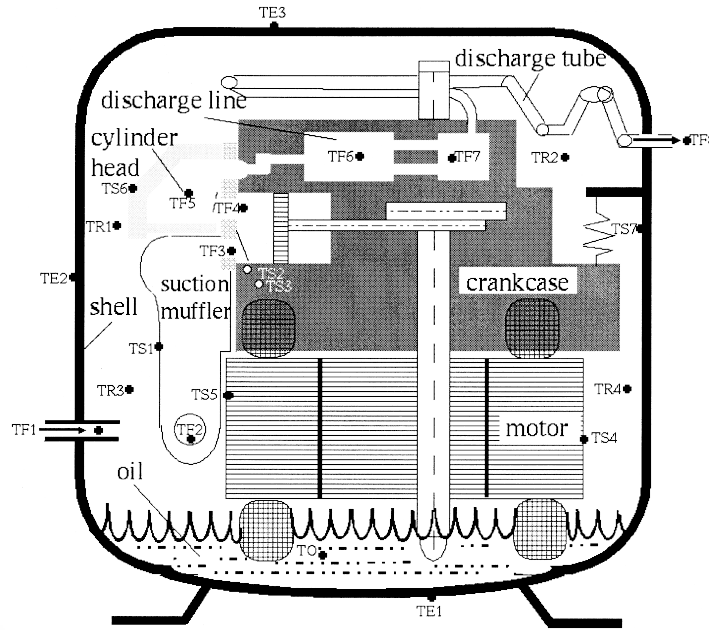


Figure 1.15 : Schematic representation of the hermetic reciprocating compressor with thermocouple positions [70].

Ribas *et al.* [72] reviewed thermal analysis of reciprocating compressors. They reported that major thermodynamic losses are originated in the suction and discharge process due to the pressure losses in the vapor path mostly stem from flow restrictions. In addition to that, superheating accounts for nearly half of the total thermodynamic losses. They reported that various experimental and numerical approaches yield different accuracy and complexity levels. They concluded that the best practice to compressor design is to combine both numerical and experimental methods by allowing more reliable results and a better understanding of the underlying physical phenomena.

Dutra & Deschamps [73] conducted an experimental investigation of the heat transfer distribution of a hermetic reciprocating compressor. They used heat flux sensors and thermocouples to analyze local heat transfer in different positions. They validated the measurements with an energy balance method applied to the compressor. They noted that lubricating oil has a great effect on the heat transfer process at the top region of the compressor shell where oil forms an impinging jet.

Kara & Oguz [74] worked on the thermal analysis of a small reciprocating compressor. They presented a thermal analysis focusing on the role of the crankcase on the heating effect of the refrigerant gas along its flow path. They reported that heat transfers to the crankcase result in superheating of the refrigerant gas. They performed 3D- numerical

simulations to capture the thermal field of the crankcase. They showed that there could be a temperature difference between the solid components directly attached to the crankcase up to 30 K. They noted that the accuracy of the predictions could increase by dividing the gas volume inside the shell due to the temperature difference.

Dincer [75] performed conjugated heat transfer analysis in the hermetic reciprocating compressor. Both experimental and numerical methods are used to determine the heat transfer distribution in the compressor. It is concluded that using aluminum as a material for the crankcase results in increasing thermodynamic efficiency while reducing motor efficiency. It is noted that the valve plate and cylinder head can be made of insulating materials to reduce heat transfer to the refrigerant.

Yesilaydin *et al.* [76] investigated flow losses through the discharge line of the hermetic reciprocating compressor. The effects of geometrical parameters on the discharge line are studied by performing pressure measurements and calorimeter tests. They reported that reducing the number of discharge muffler increases the cooling capacity and COP up to %2. They concluded that the length of the discharge passage significant effects the pressure drop.

Hopfgartner *et al.* [77] studied the thermal behavior of a hermetic reciprocating compressor during transient operation experimentally. They investigated cyclic patterns of the transient behavior of the domestic refrigeration cycle. They used an on/off control compressor equipped with precise measurement instrumentations. They compared steady-state and transient temperature measurements of a compressor operating with 50 Hz. They concluded that both steady and transient measurements show environment temperature influences the temperature levels on the compressor.

Posch *et al.* [78] conducted a numerical study on thermal analysis of a hermetic reciprocating compressor. The simulation model divided into three parts, namely, the gas flow of the compressor, heat conduction in solid parts and energy balance between oil and refrigerant. It is concluded that predictions of the numerical model are in good agreement with experimental measurements. It is noted that unavoidable uncertainties in the determination of the heat transfer coefficients have to be considered in the evaluation of the results.

1.6 Aim of this thesis

The world has faced many problems related to global concerns. As mentioned before, there are several protocols have already applied in both developing and developed countries to reduce global warming and ozone depletion potential. These protocols force producers and suppliers to work with less harmful refrigerants in the refrigeration and air conditioning sector. Besides using environment-friendly refrigerants, it is also demanded to increase the energy efficiency of such devices to compete with the rivals of the market globally.

In this context, environment-friendly HC mixtures R600a/R290 (30%/70% by weight), R600a/R290 (40%/60% by weight) and R600a/R290 (60%/40% by weight) are tested using in house test bench. In addition to the refrigerant mixtures, the optimum lubricant is investigated for the reciprocating compressor both numerically and experimentally. Two different CFD method is employed in the numerical calculations and the oil mass flow rate prediction performance of the methods are validated using experimental data. Moreover, flow visualizations are applied to obtain the oil climbing time and reveal flow patterns inside the compressor.

The main goals of the thesis are given below,

- To increase the energy efficiency of the household refrigeration system by using environment-friendly refrigerant mixtures.
- To improve the knowledge of the lubrication system of the hermetic compressor.
- To compare the performance of the prediction of oil mass flow rate of the numerical methods.
- To reveal oil paths in the compressor using oil flow visualizations.

This dissertation thesis is divided into four chapters. The first chapter introduces the vapor compression refrigeration cycle. The brief introduction of refrigerants, lubricants and compressor used in the vapor compression cycle are given and a comprehensive literature survey is presented. Chapter 2 and Chapter 3 contains the experimental and numerical studies performed in the thesis. Finally, in Chapter 4, the current study is summarized and main conclusions obtained are reported.

1.7 Framework

This dissertation thesis has been carried out within the framework of the 2+2 joint project "REFMIX" with partners Istanbul Technical University, Arcelik A.S., TU Dresden Bitzer-Chair of Refrigeration, Cryogenics and Compressor Technology and Fuchs Schmierstoffe GmbH.

The ultimate goal of the REFMIX is to increase the energy efficiency of the refrigeration and heat pump systems and to decrease Global Warming Potential Rate by developing new refrigerant blends with appropriate lubricants and additives which are less harmless and more environment-friendly compared to conventional refrigerants.





2. EXPERIMENTAL STUDIES

In this chapter, experimental studies carried out in this dissertation are presented. Studies are divided into two sections. In the first part, an experimental set up is constructed to test various refrigerant mixtures on the household refrigeration system. In this context, environment-friendly refrigerants with temperature glide are tested. Examined refrigerants are R600a/R290 (30%/70% by weight), R600a/R290 (40%/60% by weight) and R600a/R290 (60%/40% by weight). The performance outcomes of the tested mixtures are compared with R600a. The effect of compressor speed, evaporation and condensation temperature on the COP of the compressor are investigated in detail. Moreover, calorimeter test results carried out in Arcelik A.S. are compared with in house Refrigerant Mixture Test Bench (REFMIX). In the calorimeter tests, the cooling performance of the R600a/R290 (40%/60% by weight) refrigerant mixture is investigated and the COP of the compressor is reported. Finally, the R600a results of the small refrigeration compressor test stand which is designed for DIN standards are presented.

As mentioned in Chapter 1, the energy is consumed mainly in the compressor of the household refrigeration system. The energy consumption of the compressor limited by the compressor minimum speed. Moreover, the lubrication requirements should be met to avoid any mechanical damage at the minimum compressor speed. In this context, the lubrication system of the hermetic reciprocating compressor is investigated in detail in the second part. In house lubrication test bench is built using various instruments. Experiments are conducted to investigate the effect of viscosity and compressor speed on the oil mass flow rate of the Compact Inverter Compressor (CIC). Then, the results are used to validate the Computational Fluid Dynamics (CFD) predictions in the following chapter.

The structure of this chapter is given as follows. The effect of refrigerant mixtures on the household refrigeration system is summarized in 2.1. Details of the experimental

investigation of the lubrication system of the CIC are given in 2.2. Main conclusions are summarized in 2.3.

2.1 The Effect of Refrigerant Mixtures on the Household Refrigeration System

Nowadays refrigerants are used in the refrigerators, which have a constant temperature during the phase change (in the evaporator and condenser), while the air on the other side of the heat exchanger just increases or decreases its temperature due the dissipation or absorption of heat. Figure 2.1 shows the unfavorable and favorable conditions at the example of an evaporator.

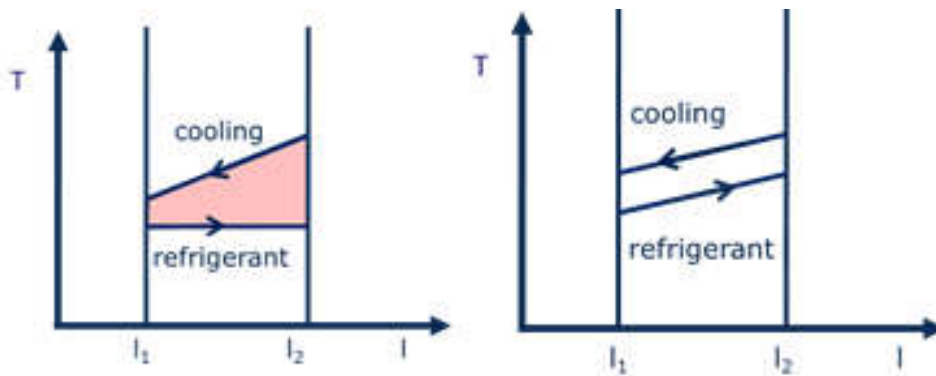


Figure 2.1 : Temperature profiles in evaporator a) different b) constant temperature slope.

Zeotropic refrigerant mixtures change volumetric composition and saturation temperatures as they evaporate or condense at constant pressures. Energy improvement and saving, capacity control, and adaption of hardware components regarding capacity and application limits are some of the advantages of zeotropic mixtures [4]. They have a temperature glide as they evaporate or condense, thus enabling energy efficiency by decreasing irreversibility caused by heat transfer. Glide is defined as the temperature difference between the beginning and phase change of a refrigerant in the evaporator and condenser, as shown in Figure 2.2. In zeotropic mixture, one of the refrigerant molecules moves independently from the other refrigerant molecules. Depending on the pressure of the refrigerants in the mixture, the glides will be different. For different fractions, the temperature changes of the refrigerant and air in the evaporator and condenser will be measured to match temperature glide and to determine its effect on the system.

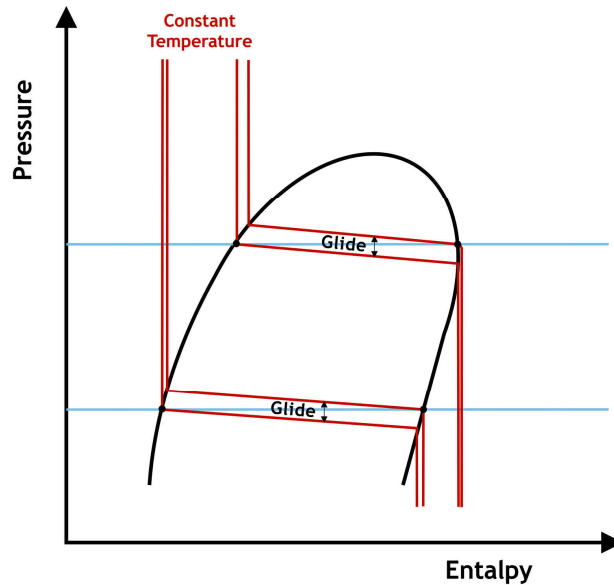


Figure 2.2 : Simplified scheme of glide concept [5].

In this section, environment-friendly refrigerants with temperature glide are tested. Examined refrigerants are R600a/R290 mixtures with three different mass fractions. The performance outcomes of the tested mixtures are compared with R600a. Moreover, calorimeter test results carried out in Arcelik A.S. are compared with in house Refrigerant Mixture Test Bench. The principal aim of these investigations is to enhance the energy efficiency of the refrigeration system.

2.1.1 Refrigerant mixtures test stand (REFMIX)

Experiments related to different zeotropic refrigerant blends with different temperature glides for the refrigeration applications are important to discuss the effects of the new blends associated with efficiency increase. To test the effect of zeotropic blends with different temperature glides on the energy efficiency of the refrigeration system, an experimental set up is built and the schematic view of the test bench is given in Figure 2.3. The red and blue lines represent the high and low pressure sides, respectively. The main components of the experimental system are given in Table 2.1. In addition to the test stand, the insulated room is built to prevent additional heat transfer from/to the system. The air conditioner and heater are used to condition the ambient temperature during the experiments.

Table 2.1 : List of instruments.

Data Acquisition	Keysight 34970A
Data Acquisition	Rheonik Mass Flow Transmitter-RHE16
Calibration Bath	Labo C400-H13
Calibration Bath	Labo C300-H13
Power Supply	Yıldırım CY 306 DC
Power Supply	Yıldırım CYS152 DC
PID controller	Autonics TX4S
Power Controller	Autonics SPC1-35
Needle Valve	Hamlet H300U
Refrigerant Charger	Smart Charge 600
Superheater	Cable type resistance (750 W)

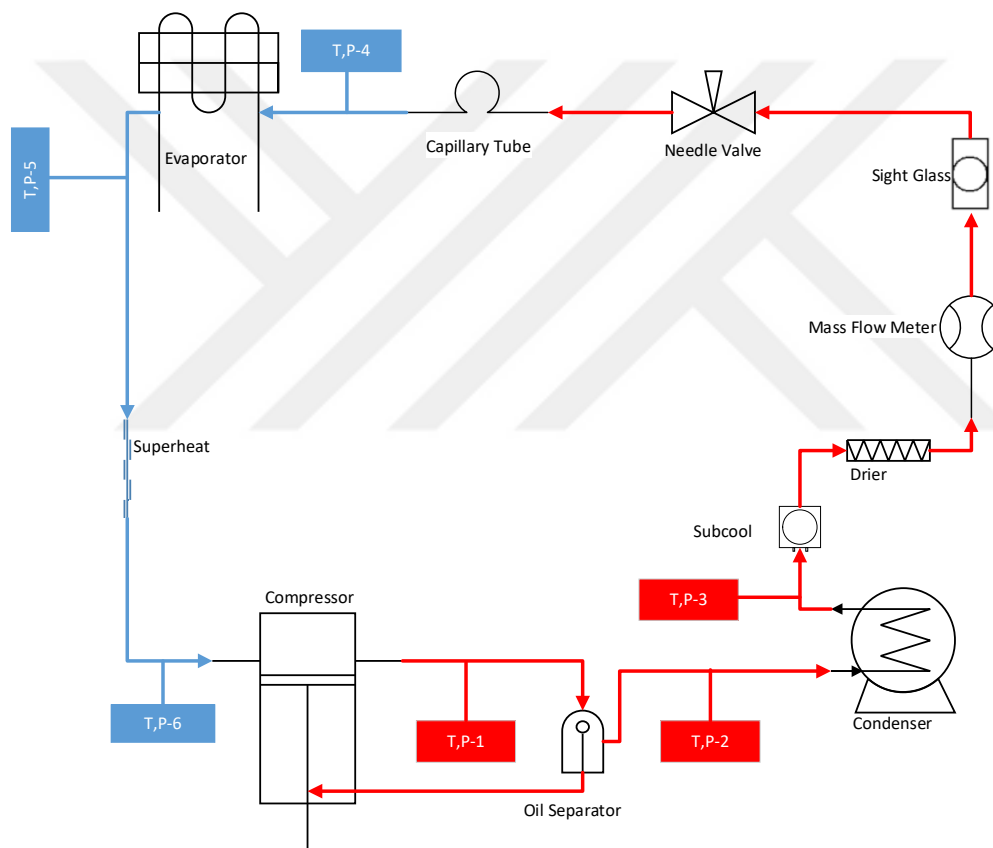


Figure 2.3 : Schematic view of the test stand.

The details of measuring devices included in the test apparatus are temperature sensors (RTD, T type thermocouples), pressure sensors and Coriolis type mass flow meter integrated into the system. Measurement range and accuracy of the sensors are shown in Table 2.2.

The refrigerant is charged into the system with Smart Charge 600. Smart Charge 600 is a fully automated vacuum and charging machine for accurately repairing domestic and commercial refrigeration units that run on R600a. A gas sensor, which detects the

Table 2.2 : List of the sensors.

Sensor Type	Model	Measurement Range	Accuracy
Mass flow meter	Rheonik-RHE16	0.15-600 g/min	0.21%
Pressure Transducer	Keller PA-25HTC	0-20 bar	0.50%
Pressure Transducer	Keller PA-21Y	0-10 bar	0.25%
Thermocouples	RTD	-50 to 260 °C	0.20%
Thermocouples	T Type	-270 to 370 °C	0.40%

presence or concentration of gases in the atmosphere, is able to detect 200—1000ppm LPG, iso-butane, propane, LNG. Device has a precision balance which allows gas filling automatically with +/- 1 g accuracy. The refrigerant charged into the system is gradually increased starting from 60 grams and the amount of charge required is determined as 175 grams.

The working principle of the test apparatus is as follows. A compressor of the manufacturer Arcelik of the type "VNTZ 165 M" is mounted on the test stand. This is a frequency-controlled reciprocating compressor for the refrigerant R600a. In order to control the compressor speed additional frequency controller is used to adjust the rotational speed. A power meter is used to monitor power consumption of the compressor. When the compressor operates (as detailed in the previous work packages), the oil circulates in the refrigerant cycle. Therefore, the oil separator is used to separate the oil from the refrigerant. The separated oil is returned to the compressors' service line. The refrigerant passing through the oil separator comes to a condenser placed in a calibration bath. The refrigerant is left from the condenser as a saturated liquid. An additional calibration bath is provided for subcooling the refrigerant. Liquid refrigerant passes through a filter drier, which is used to hold the contaminants, and Coriolis type mass flow meter, respectively. The refrigerant expands in the needle valve and capillary tube in the cycle. The refrigerant enters as wet steam to an evaporator and left as a vapor. Additional 12 thermocouples are placed on the evaporator to monitor the temperatures. PID controlled superheater is applied to the refrigerant to ensure that it returns compressor in a vapor state. The main components of the REFMIX is shown in Figure 2.4. The numbers denoting the components are given as follows. (1) Compressor, (2) oil separator, (3,4) calibration bath for the heat exchanger, (5,6) calibration bath for the subcooling, (7) Coriolis mass flow meter, (8) sight glass, (9) Needle valve and capillary tube, (10,11) cabin and

evaporator, (12) superheater isolated with rock wool, (13) data acquisition system, (14) PC for recording, (15) air conditioner, (16) frequency controller with electrical card and (17) refrigerant charger and vacuum pump.

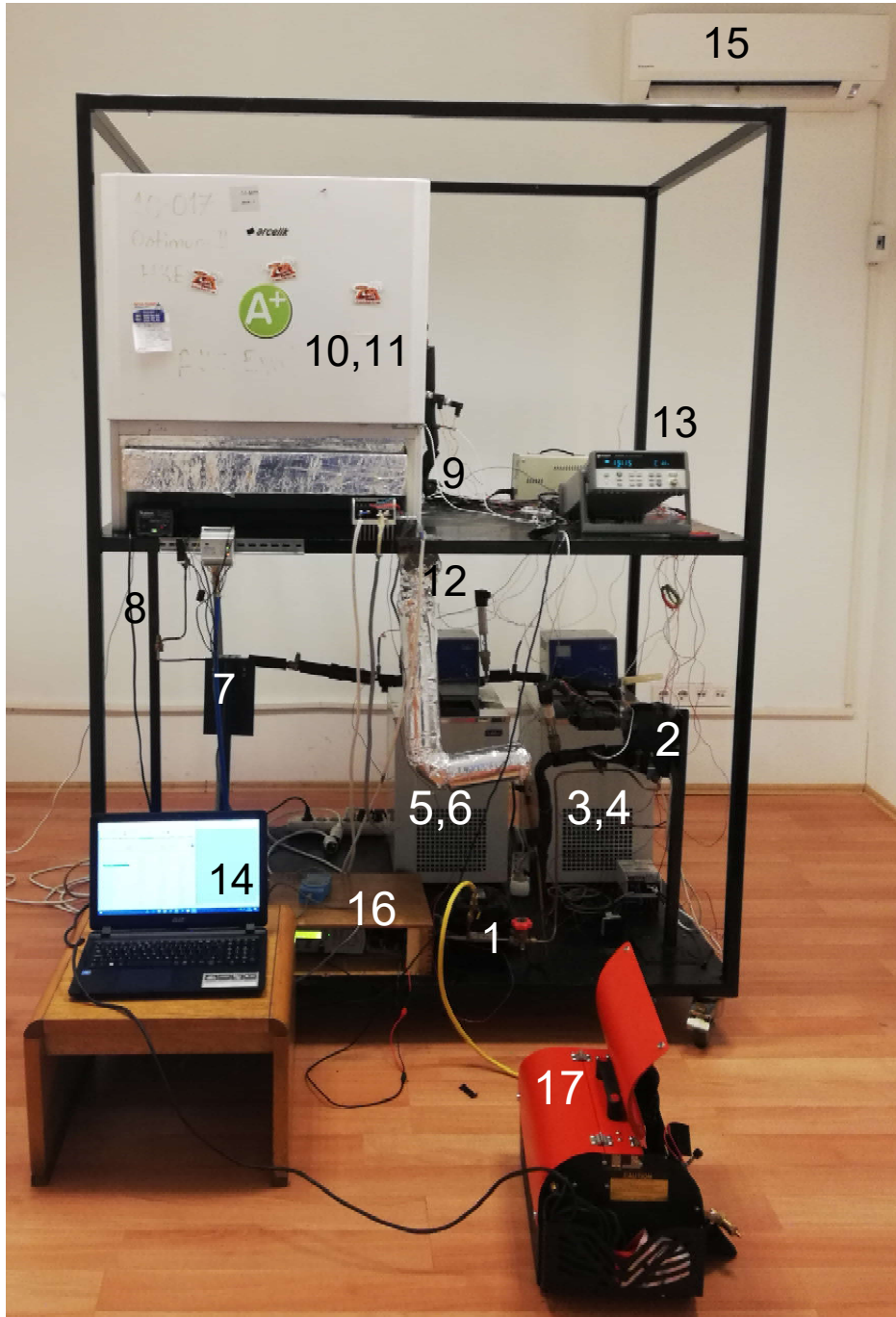


Figure 2.4 : Detailed view of REF MIX.

Test routine is described as follows. The compressor operates for a couple of hours to reach steady state conditions. The temperatures and pressures of the discharge and suction line are monitoring during these period. After reaching the steady state conditions, the tests are started. Each test run minimum of 15 minutes. Temperatures and pressures are sampled each 5 seconds and refrigerant mass flow

rate is sampled each 0.5 seconds. Averaged pressures and temperatures are used to calculate refrigeration capacity. AHRI standard is followed for the special points for the calculation [79]. CoolPack and REFPROP are used to calculate thermophysical properties of R600a and R600a/R290 mixtures. The COP of the compressor is calculated using refrigerating capacity and power consumption of the compressor. It should be noted that, the refrigerant mixtures test bench are able to follow several test standards due to the adjustable superheat and subcool temperature of the refrigeration cycle.

$$\dot{Q} = \dot{m} \times (h_{g1} - h_{f2}) \quad (2.1)$$

$$COP_R = \frac{\dot{Q}}{\dot{W}} \quad (2.2)$$

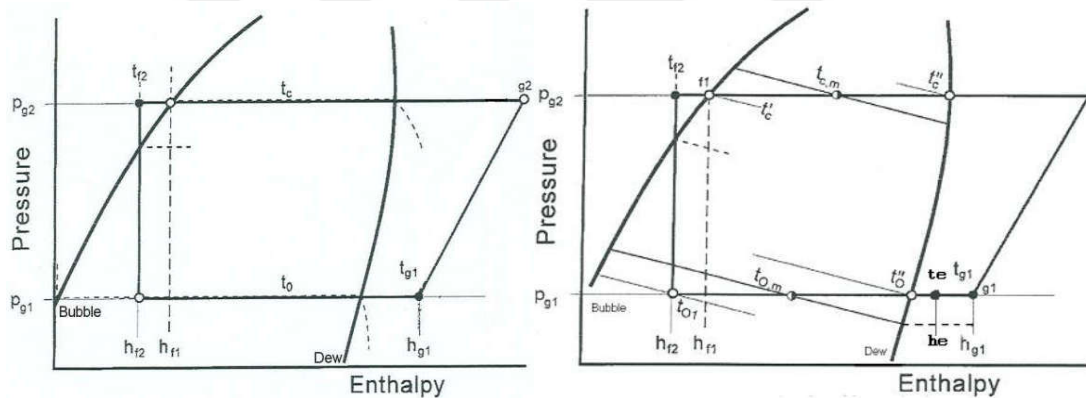


Figure 2.5 : Cycle process for single component refrigerants and zeotropic refrigerant mixtures [79].

2.1.1.1 Leakage tests

Figure 2.6 and Figure 2.7 shows high and low-pressure leakage tests, respectively. Nitrogen is used in high pressure tests. Both tests are performed for a minimum of 20 hours. Since the temperature values affect the pressure, the temperature and pressure are plotted together. To achieve a leak tight system, many tiny faults are found and lock-tight seals are used to prevent losses. As a result of these studies, system tightness is tested and possible refrigerant losses are prevented.

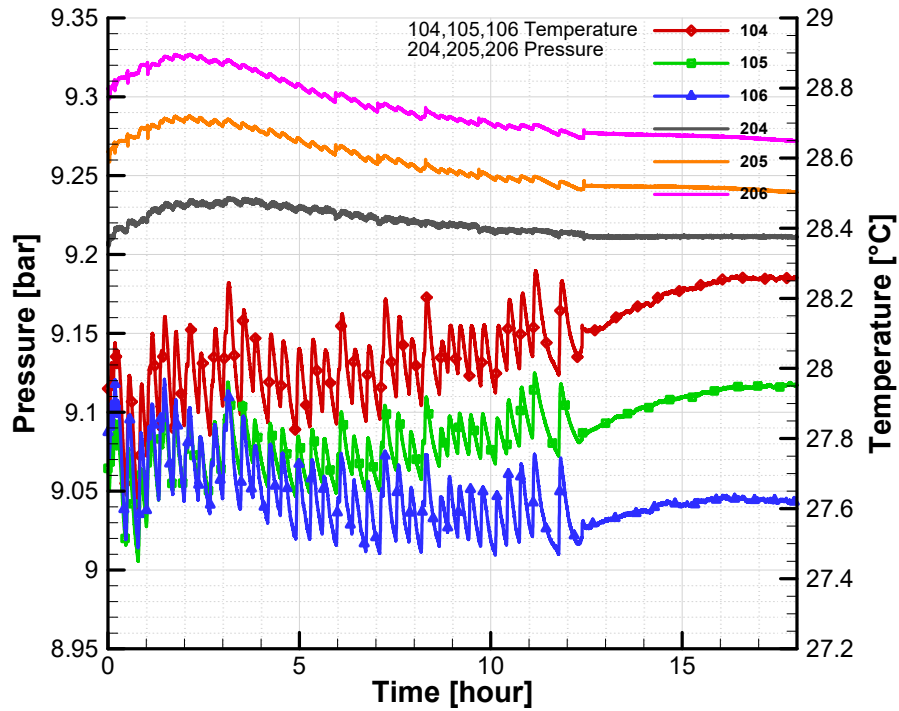


Figure 2.6 : High pressure leakage test.

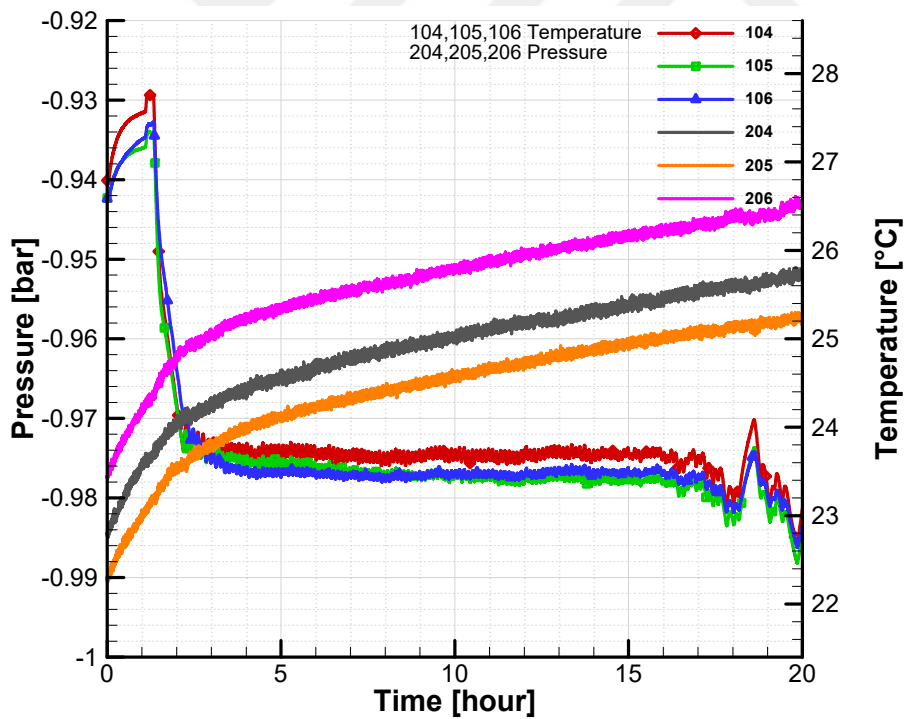


Figure 2.7 : Low pressure leakage test (Negative values indicate the vacuum medium).

2.1.1.2 Start-up behavior of the system

Figure 2.8 shows temperature history the time zone between the compressor start-up and steady state conditions for R600a/R290 mixture at 3000 rpm. It should be noted

that increasing refrigerant mass flow meter decreases the required time notably for reaching steady state conditions.

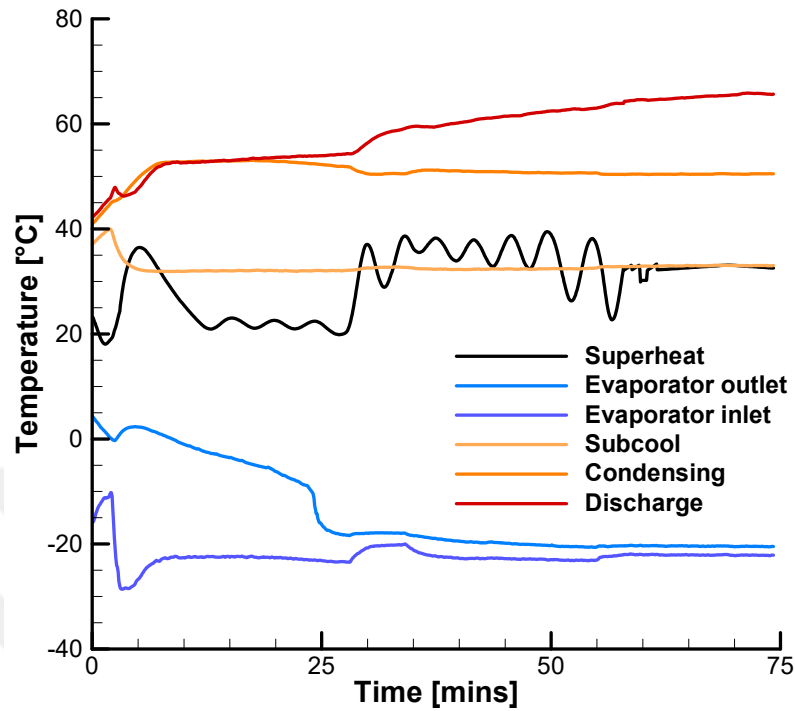


Figure 2.8 : Temperature variations after the compressor start-up.

Figure 2.9 shows pressure history of the same interval with the temperature. It should be noted that several tunings are performed to meet ASHRAE requirements. Since the compressor runs with constant rotational speed, pressure fluctuations are mainly disturbed by the needle valve positions.

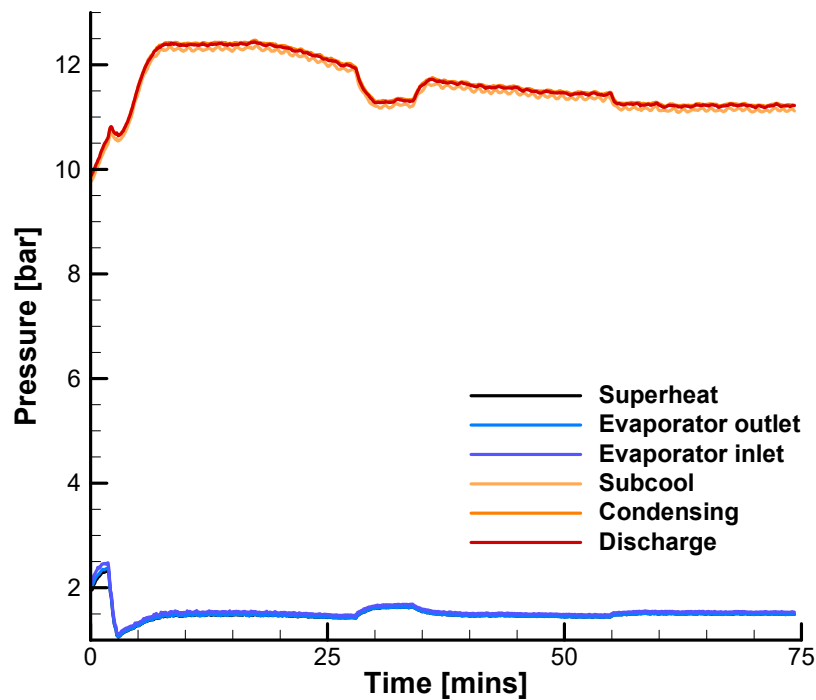


Figure 2.9 : Pressure variations after the compressor start-up.

2.1.1.3 Sensor fluctuations during the experiments

A steady-state test described as the controlled test parameters are regulated to remain constant within the specified tolerances while the unit operates continuously in the same mode. Time dependent change of the pressure, temperature and mass flow rate during the test are important to show that results are gathered in steady-state conditions. Suction and discharge pressure fluctuations during the experiments are shown in Figure 2.10 and Figure 2.11, respectively. It should be noted that negligible fluctuations are observed during the tests.

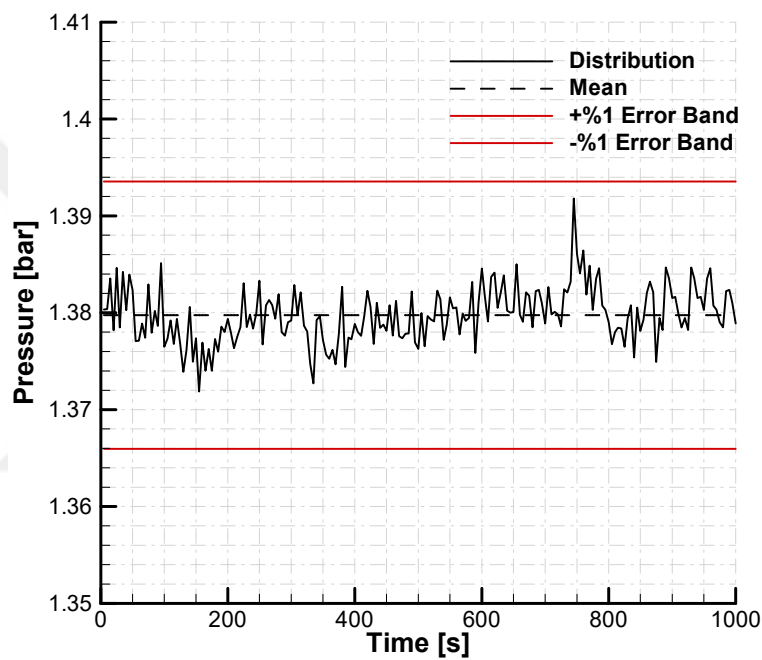


Figure 2.10 : Time-dependent change of suction pressure during the experiment.

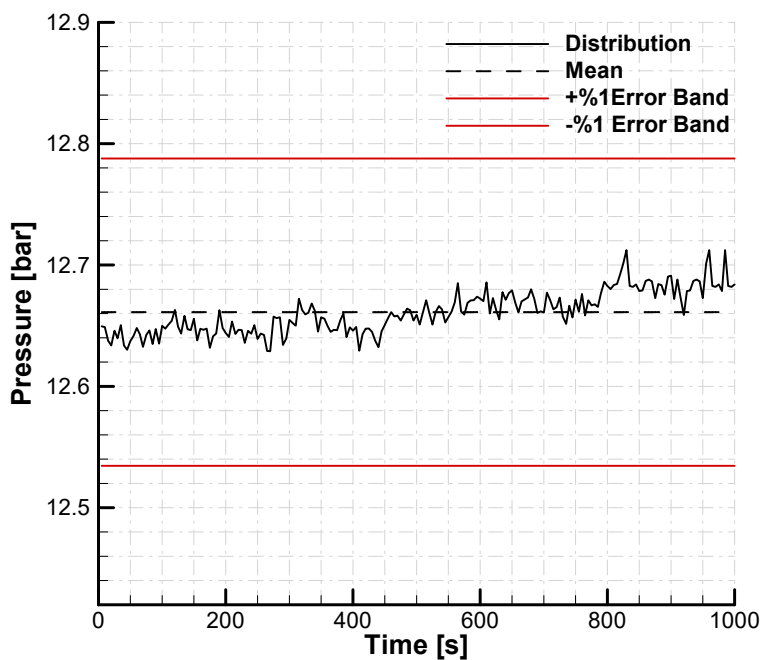


Figure 2.11 : Time-dependent change of discharge pressure during the experiment.

In addition to that, time-dependent change of suction temperature and refrigerant mass flow rate are plotted in Figure 2.12 and Figure 2.13, respectively. The error band of the suction pressure is narrow, even in this case distribution of the suction pressure are in the range of the error. Other readings are also within the range of $\pm 1\%$ error band. It is shown that the measurement results meet the tolerance ranges for the readings in the standards.

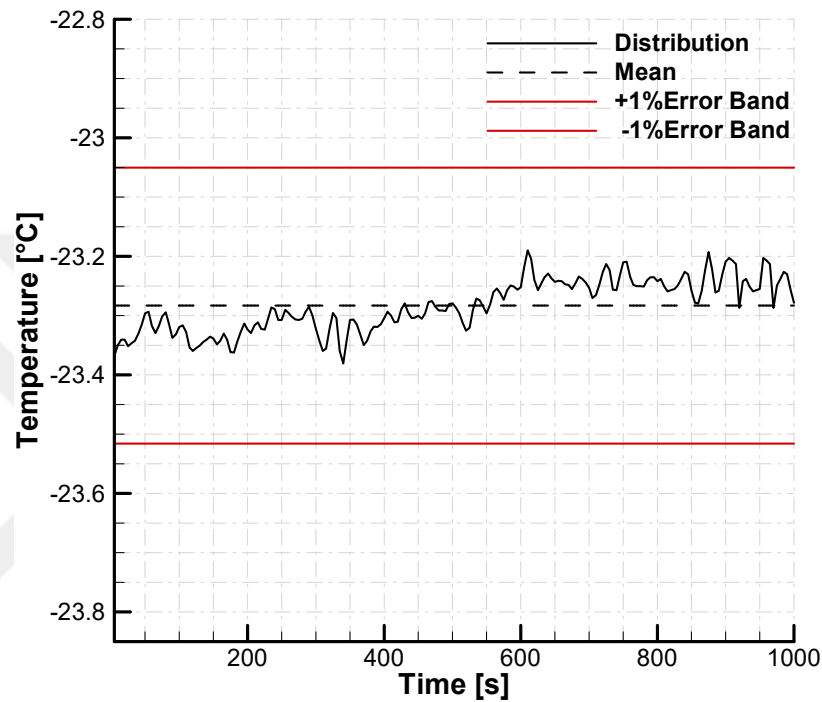


Figure 2.12 : Time-dependent change of suction temperature during the experiment.

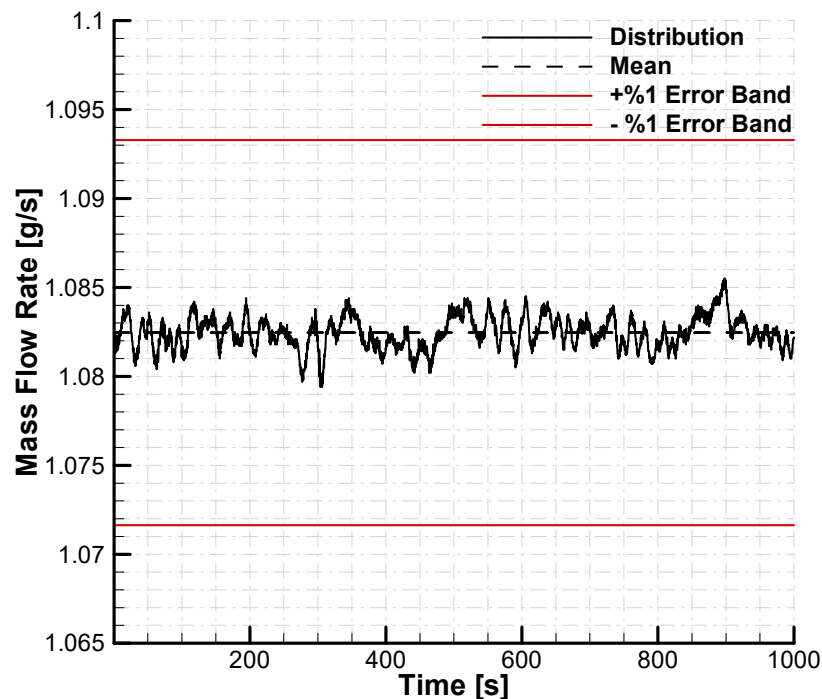


Figure 2.13 : Time-dependent change of refrigerant mass flow rate during the experiment.

2.1.1.4 Results

In the refrigerant mixtures test bench, the COP depends on various parameters such as the rotational speed of the compressor, the position of the needle valve and the calibration bath temperatures. These are the main parameters that affect condensation and evaporation pressure in the system. In addition to these parameters, the evaporation fan speed is taken constant in each of the experiments to eliminate this parameter.

ASHRAE conditions are followed in general to compare the results with calorimeter tests. To meet the requirements, subcool and superheat temperature are set to 32.2°C and condensing temperature set to 54.4°C . As shown in Table 2.3, ASHRAE standards sets evaporating pressure to 0.65 bar which correspond evaporating temperature to -23.3°C .

Pressure-enthalpy diagram at ASHRAE standards are given in Figure 2.14. It is shown that subcool temperature is critical for vapor quality of the refrigerant. Decreasing subcool temperature is decreasing the vapor quality and therefore increases the refrigerant effect.

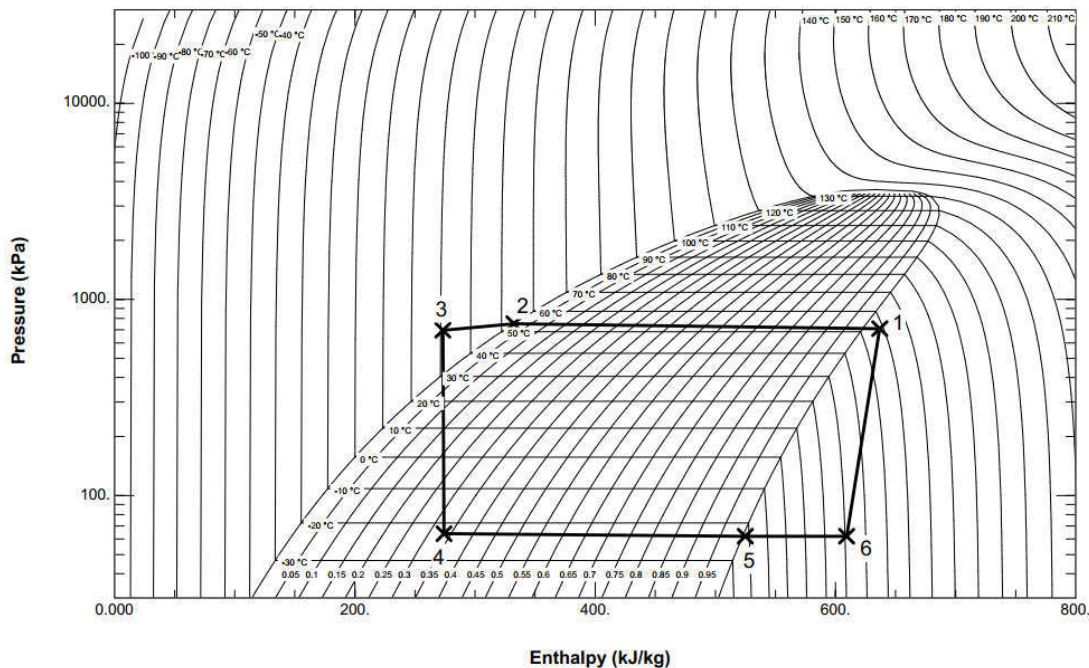


Figure 2.14 : Pressure-enthalpy diagram of R600a plotted at ASHRAE standards.

In addition to ASHRAE standards, the effect of evaporating pressure on the compressor performance is investigated. In these tests, superheating, subcooling and condensing

Table 2.3 : Summary of investigated cases for R600a.

Case ID	Compressor Speed	Evaporating Pressure	Abbreviation
1	1500	0.62	1500.062
2	2100	0.62	2100.062
3	3000	0.62	3000.062
4	4500	0.62	4500.062
5	2000	0.56	2000.055
6	2000	0.69	2000.069
7	3000	0.54	3000.054
8	3000	0.72	3000.072
9	4500	0.54	4500.054
10	4500	0.71	4500.071

temperature set same as ASHRAE standards. To investigate effect of condensing pressure, condensation temperature are adjusted to different values, which are given explicitly in that section.

Table 2.3 shows the investigated cases and corresponding abbreviations that made for simplify the identify investigated the cases. Abbreviation indicates that the rotational speed and evaporating pressure of the corresponding test.

To compare in-house test stand REFMIX with calorimeter tests several experiments are conducted. Table 2.4 presents detailed results for refrigerant R600a conducted at ASHRAE standards. ASHRAE standard requires a 32.2°C ambient temperature however it is fixed around 25°C in the REFMIX. Table 2.4 shows that with increasing compressor speed, the mass flow rate of the refrigerant is also increasing. Thus, the cooling capacity is increasing with increments of the compressor speed. Moreover, the discharge temperature is notably increasing towards to higher compressor speed.

COP and input power of the compressor is presented at ASHRAE standard for various rotational speed in Figure 2.15. It is shown that the COP is maximizing between the compressor speed 2000-2200 rpm. As the compressor speed increases, both the refrigerant mass flow rate and the power consumption is increased. However, since the rate of increase in power consumption is higher than the refrigerant mass flow rate, COP is decreasing towards to high compressor speeds. It is shown that power consumption of the compressor is increasing almost linearly in the tests.

Table 2.4 : Detailed results for R600a tested at ASHRAE standards.

Case ID	1500.062	2100.062	3000.062	4500.062
Cooling c. (W)	94.09	131.77	172	211.49
Input power (W)	52.90	72.75	101.3	144.4
COP_R	1.78	1.81	1.70	1.46
Mass flow rate (g/s)	0.28	0.39	0.52	0.64
Superheat (°C)	33.59	32.10	30.15	29.45
Evap. outlet (°C)	-21.05	-22.79	-23.82	-24.43
Evap. inlet (°C)	-22.71	-22.92	-22.46	-22.13
Subcool (°C)	30.62	31.81	32.43	33.20
Condensation (°C)	54.5	54.23	54.32	54.78
Discharge (°C)	56.42	57.96	70.71	79.95
Ambient (°C)	24.08	24.17	24.99	25.56
Cabin (°C)	-21.08	-21.08	-21.19	-21.44
Superheat (bar)	0.6	0.58	0.56	0.52
Evap. outlet (bar)	0.6	0.59	0.58	0.57
Evap. inlet (bar)	0.62	0.63	0.62	0.62
Subcool (bar)	6.79	6.72	6.69	6.79
Condensation (bar)	6.89	6.82	6.78	6.87
Discharge (bar)	6.90	6.83	6.80	6.90

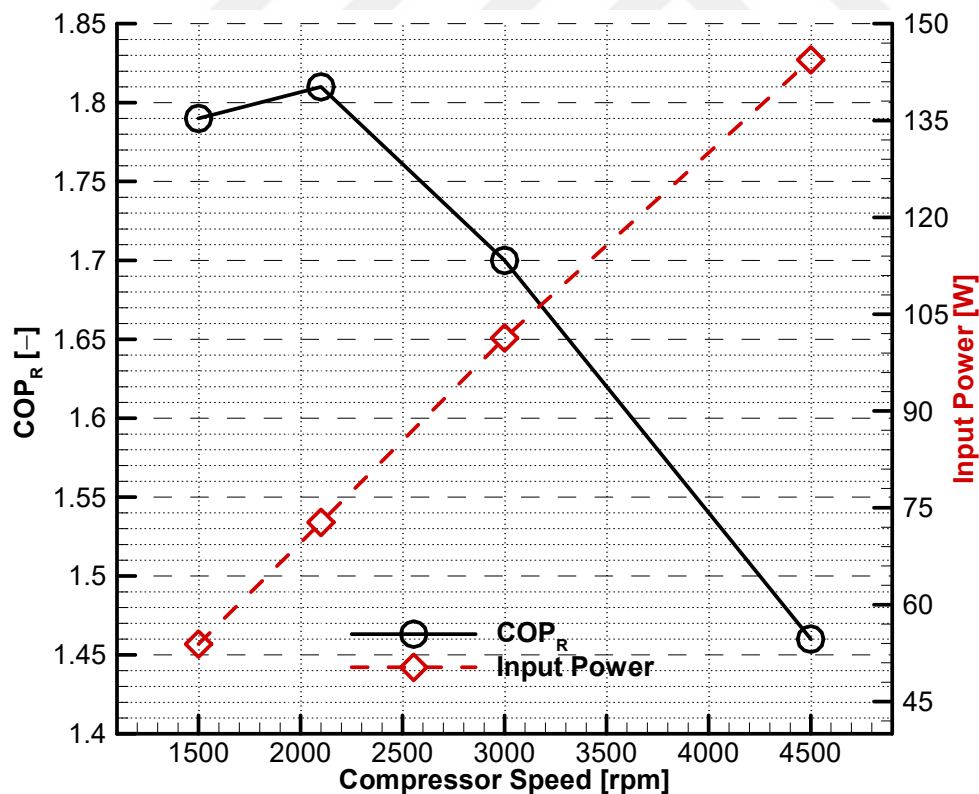


Figure 2.15 : Effect of compressor speed on the COP and input power, tested with refrigerant R600a.

Figure 2.16 shows the effect of three different evaporator temperatures on the compressor COP. The results are obtained by changing the needle valve position by

keeping the compressor speed constant, which selected as 2000, 3000 and 4500 rpm. It is seen that with increasing evaporator pressure, the COP of the compressor is increasing.

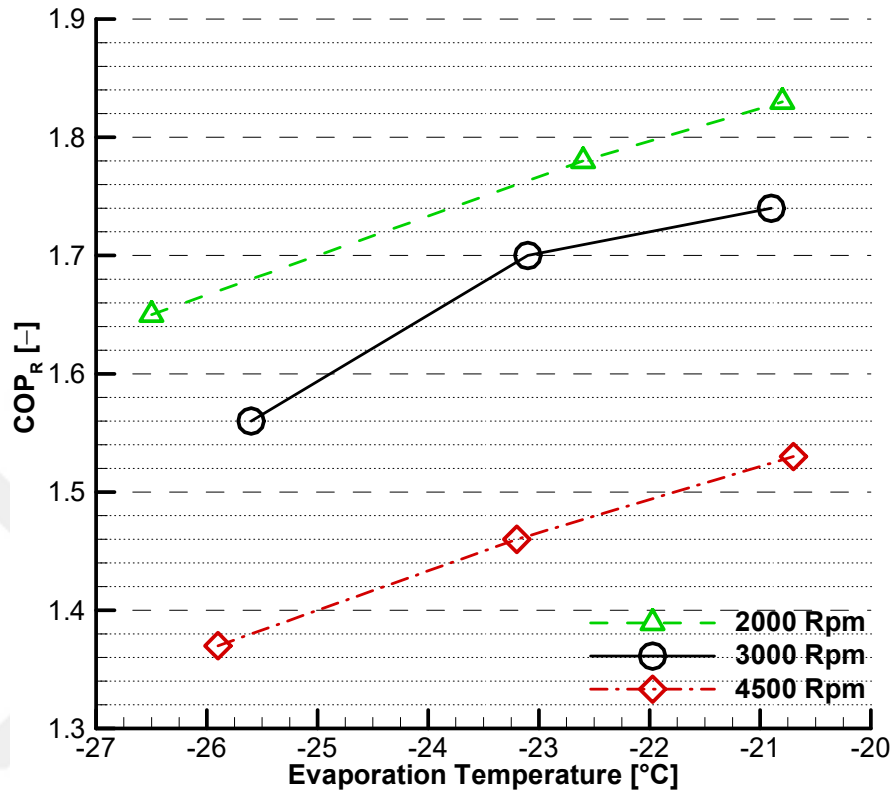


Figure 2.16 : Effect of evaporator temperature at different compressor speeds on the COP, tested with refrigerant R600a.

The R600a/R290 (40%/60% by weight) refrigerant mixture is charged to the test system and the experiments are repeated. Fuchs GmbH provided Reniso WF 10 A-59 mineral oil which is compatible with selected refrigerant mixture. Table 2.5 presents detailed results for R600a/R290 refrigerant mixture tested at ASHRAE standards.

Refrigerant mass flow rate, input power and discharge and suction pressures are increased notably compared to R600a. Due to the high discharge pressures, discharge temperature is increased around 15°C. The optimum compressor speed is found in the vicinity of 2100 rpm whereas the COP values are fairly close between 1500-3000 rpm. As with the same results of the R600a, the COP drops significantly at 4500 rpm.

Figure 2.17 presents the effect of compressor speed on the COP and input power. It is seen that with increasing compressor speed, input power increasing almost linearly up to the 3000 rpm, and then the slope is decreasing between 3000 to 4500 rpm.

Table 2.5 : Detailed results for R600a/R290 (40%/60% by weight) refrigerant mixture tested at ASHRAE standards.

Case ID	1500.153	2100.151	3000.154	4500.151
Cooling c. (W)	225.07	314.15	424.28	464.17
Input power (W)	116.02	154.00	214.00	258.00
COP_R	1.94	2.03	1.98	1.80
MassFlowRate (g/s)	0.62	0.81	1.08	1.21
Superheat (°C)	30.92	30.86	30.63	29.51
Evap. outlet (°C)	-21.72	-23.47	-23.34	-23.89
Evap. inlet (°C)	-22.91	-23.74	-23.18	-23.06
Subcool (°C)	32.14	33.30	33.54	33.80
Condensation (°C)	50.37	52.04	52.82	53.27
Discharge (°C)	72.47	77.69	88.35	93.61
Ambient (°C)	25.20	24.20	24.62	25.04
Cabin (°C)	-20.83	-21.94	-21.79	-21.71
Superheat (bar)	1.49	1.42	1.38	1.31
Evap. outlet (bar)	1.48	1.44	1.44	1.42
Evap. inlet (bar)	1.53	1.51	1.55	1.55
Subcool (bar)	11.40	12.13	12.57	12.88
Condensation (bar)	11.49	12.22	12.66	12.98
Discharge (bar)	11.49	12.22	12.69	13.01

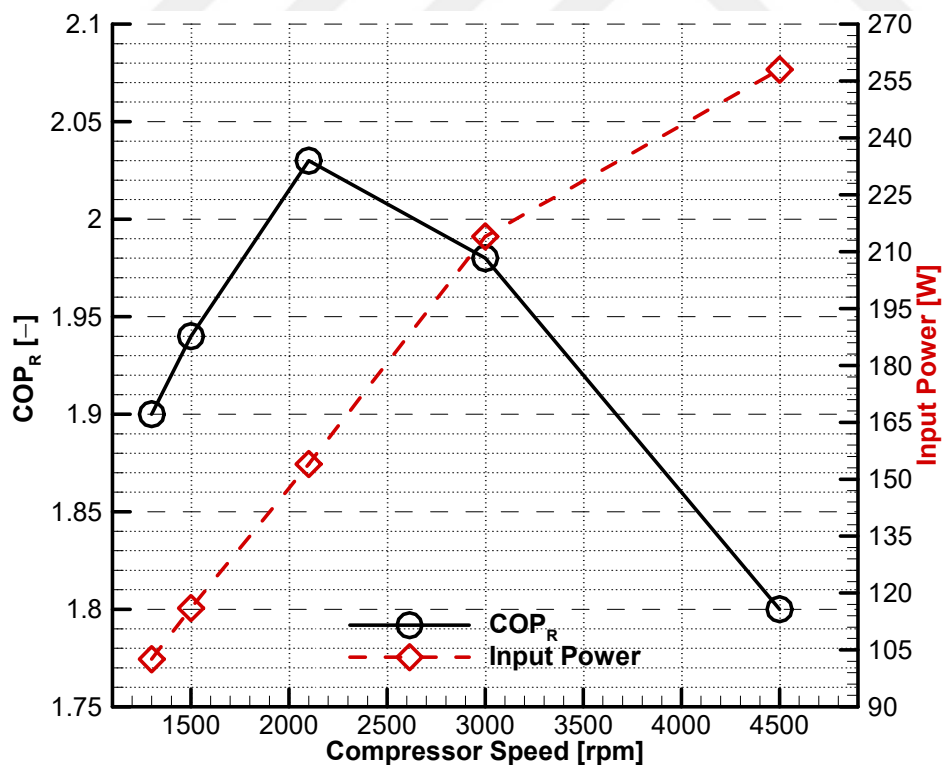


Figure 2.17 : Effect of compressor speed on the COP and input power, tested with R600a/R290 (40%/60% by weight).

Figure 2.18 presents the effect of evaporator pressure on the COP for various compressor speed. Experiments are carried out for three different evaporation pressure,

at the 1.35, 1.52 and 1.72 bar, and corresponding evaporation temperatures are around -20°C , -23°C and -26°C , respectively. 1500 rpm is also included in the Figure 2.18, due to the fact that refrigerant mass flow rate is significantly higher than those of R600a.

It is seen that the COP values are fairly close to each other until 1.55 bar except for 4500 rpm. The COP is increasing with increments of the evaporation pressure as expected. Maximum COP is found 2.26 at 3000.171, which indicates that the optimum working speed range is increasing at the higher evaporation pressure.

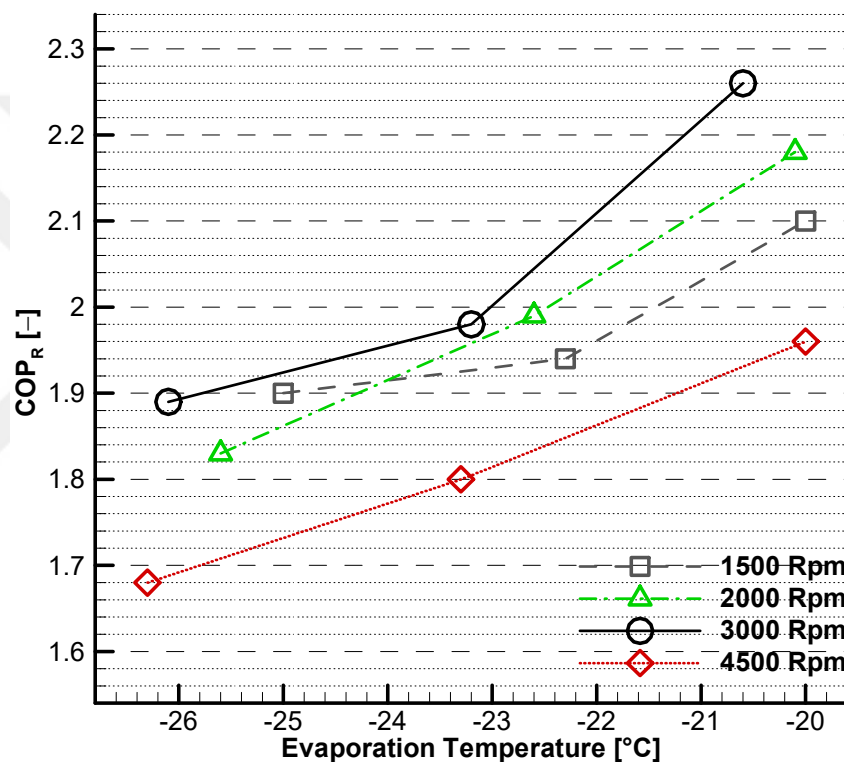


Figure 2.18 : Effect of evaporator temperature on the COP, tested with R600a/R290 (40%/60% by weight).

Table 2.6 presents the effect of condensation temperature on the compressor performance. It is shown that with decreasing condensation temperature, the discharge and condensation pressure is also decreasing as expected. The slight increase in refrigerant mass flow rate and decreasing power consumption yields 9.27% increase in COP with reducing condensation temperature 2.29°C .

In addition to the R600a/R290 (40%/60% by weight), R600a/R290 (60%/40% by weight) refrigerant mixture is charged into the system and the results are given in Table 2.7.

Table 2.6 : Effect of condensation temperature on the COP, tested with R600a/R290 (40%/60% by weight).

Case ID	1500.153	1500.171	1500.153	1500.181
Condensation (°C)	50.37	52.58	48.08	48.06
Condensation (bar)	11.49	11.86	11.01	10.97
Discharge (°C)	72.47	72.24	72.80	74.82
Discharge (bar)	11.49	11.87	11.01	10.97
Cooling c. (W)	225.07	260.95	237.86	290.69
Input power (W)	116.02	124.10	112.40	124.20
COP_R	1.94	2.10	2.12	2.34
MassFlowRate (g/s)	0.62	0.69	0.61	0.75
Superheat (°C)	30.92	31.85	32.23	32.20
Evap. outlet (°C)	-21.72	-19.56	-22.35	-18.58
Evap. inlet (°C)	-22.91	-20.40	-23.39	-19.13
Subcool (°C)	32.14	32.20	32.23	33.54
Ambient (°C)	25.20	24.35	23.64	23.48

Refrigerant mass flow rate, input power and discharge and suction pressures are increased notably compared to R600a. The optimum compressor speed is found in the vicinity of 3000 rpm.

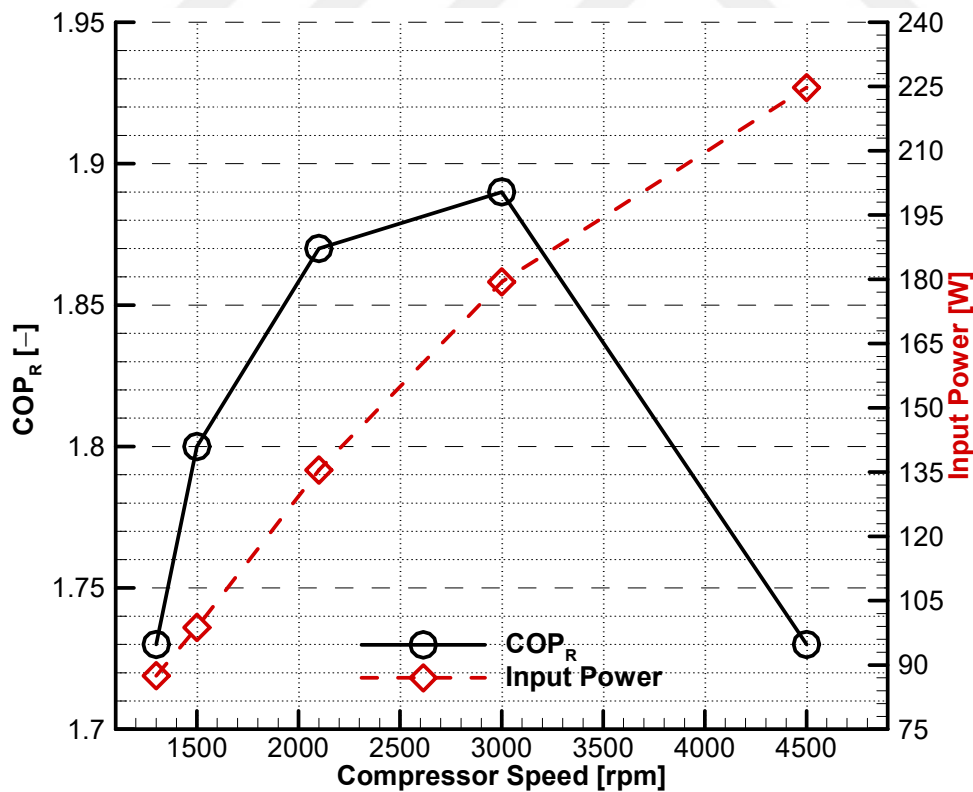


Figure 2.19 : Effect of compressor speed on the COP and power consumption, tested with R600a/R290 (60%/40% by weight).

The effect of compressor speed and evaporation pressure are given in Figure 2.19 and Figure 2.20, respectively. It is seen from Figure 2.19 that, decreasing R290 fraction in

Table 2.7 : Detailed results for R600a/R290 (60%/40% by weight) refrigerant mixture tested at ASHRAE standards.

Case ID	1500.153	2100.151	3000.154	4500.151
Cooling c. (W)	177.8	253.57	339.04	388.94
Input power (W)	98.75	135.5	179.4	224.75
COP_R	1.80	1.87	1.89	1.73
MassFlowRate (g/s)	0.48	0.67	0.88	1.02
Superheat (°C)	30.0	29.6	28.52	28.33
Evap. outlet (°C)	-20.15	-21.52	-22.55	-23.08
Evap. inlet (°C)	-23.00	-23.43	-23.48	-23.29
Subcool (°C)	32.26	31.94	32.39	32.53
Condensation (°C)	55.49	55.51	54.88	55.25
Discharge (°C)	70.05	76.71	85.27	92.49
Ambient (°C)	28.24	24.24	26.44	25.34
Cabin (°C)	-19.55	-20.75	-21.30	-21.40
Superheat (bar)	1.19	1.17	1.10	1.06
Evap. outlet (bar)	1.19	1.18	1.14	1.12
Evap. inlet (bar)	1.22	1.21	1.22	1.22
Subcool (bar)	11.96	12.17	11.75	11.96
Condensation (bar)	12.08	12.27	11.84	12.04
Discharge (bar)	12.10	12.30	11.87	12.08

the mixture results in decreasing in COP. Thus R600a/R290 (30%/70% by weight) are charged into the system.

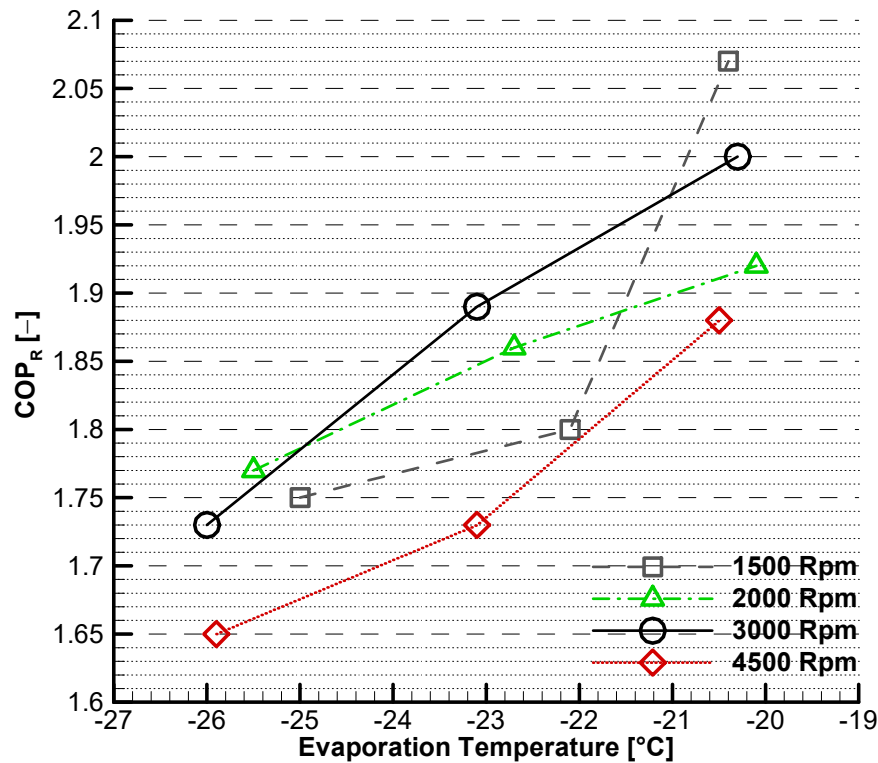


Figure 2.20 : Effect of evaporator temperature on the COP, tested with R600a/R290 (60%/40% by weight).

The effect of R600a/R290 refrigerant mixture on the household refrigeration system is investigated at three different mass fractions. Figure 2.21 presents the COP values for R600a, R600a/R290 (30%/70% by weight), R600a/R290 (40%/60% by weight) and R600a/R290 (60%/40% by weight) measured with REFMIX. The experiments are conducted at similar conditions to ASHRAE standards.

It is seen from Figure 2.21 that R600a/R290 refrigerant mixtures provide higher COP value than R600a. The COP difference between refrigerant mixtures and R600a appears to increase with increasing compressor speed. R600a/R290 (40%/60% by weight) refrigerant mixture provides the highest COP values. Although R600a/R290 (40%/60% by weight) provides higher values than R600a/R290 (30%/70% by weight) up to 1500 rpm, COP values after 1500 rpm are almost the same.

There is a clear COP superiority of these two refrigerant mixtures compared to the R600a/R290 (60%/40% by weight) refrigerant mixture.

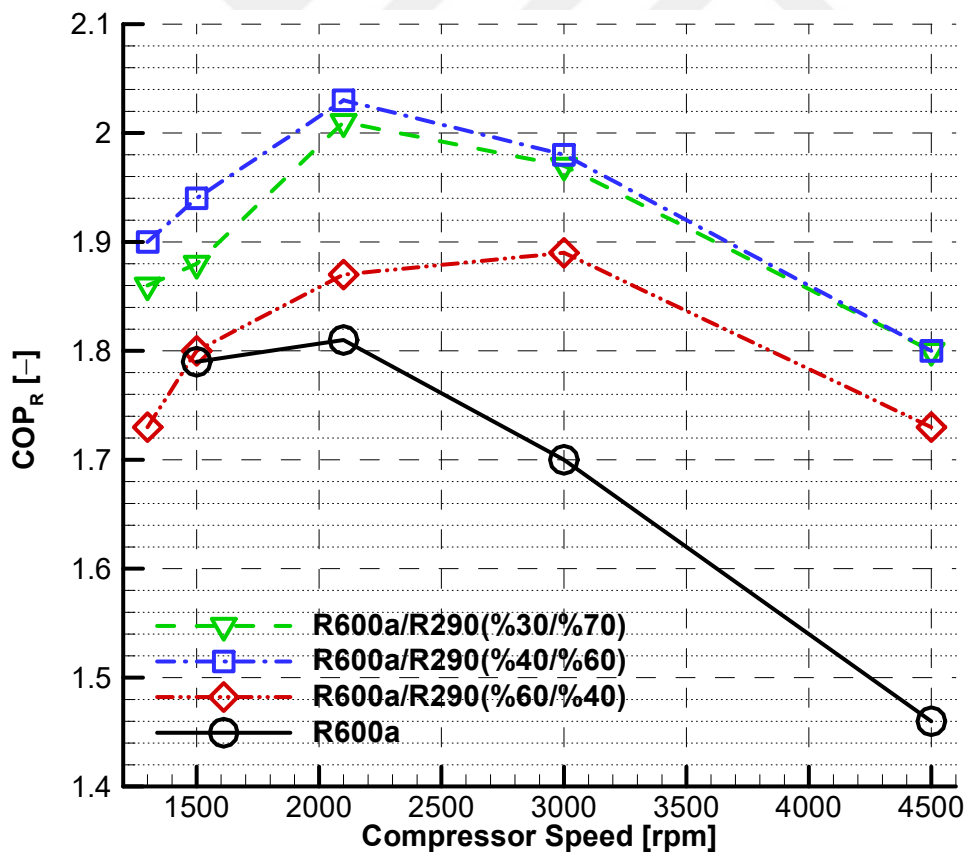


Figure 2.21 : COP values obtained from REFMIX at ASHRAE standards for various refrigerant mixtures.

2.1.2 Calorimeter test stand

The calorimeter tests to measure the performance of the hermetic compressor are conducted at Arcelik A.S. using the Re/genT brand calorimeters. Figure 2.22 shows the temperature-controlled vessel room for two compressor positions. The calorimeters have specially produced for engineering goals, enabling the use of several refrigerants, including flammables. In addition, refrigerant mixtures such as hydrocarbon mixtures can be used in the calorimeter [80].

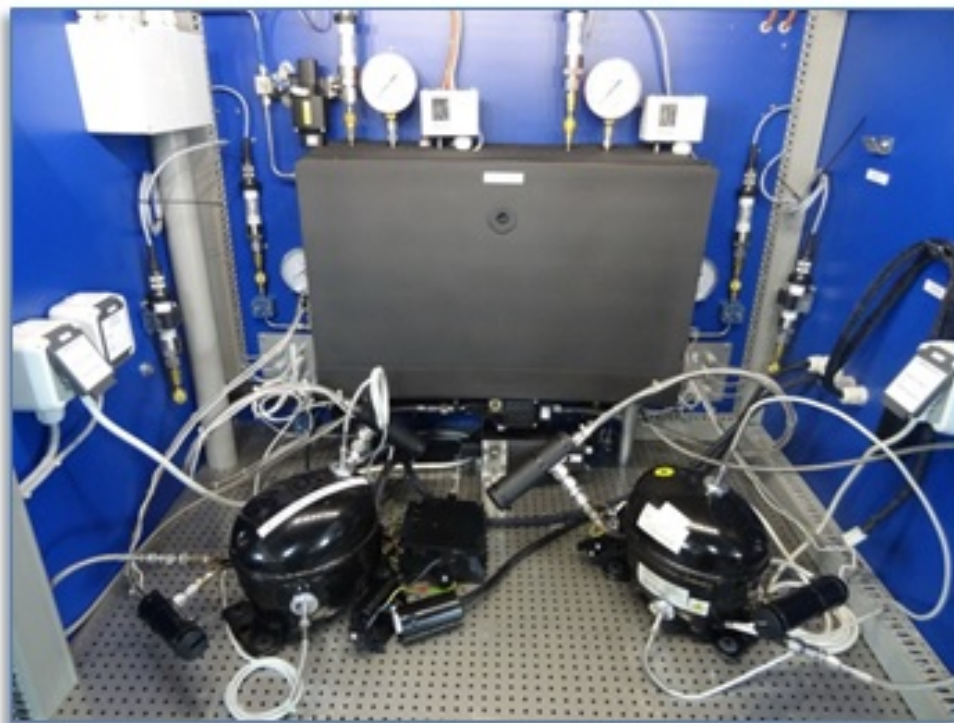


Figure 2.22 : Temperature-controlled vessel room [80].

The scheme of the test set-up is given in Figure 2.23. Main components of the test system are reciprocating compressor, water cooled condenser, mass flow meter, capillary tube and calorimeter. ASHRAE test standards are followed in the experiments. Since no oil separator is used in the system, oil circulates with refrigerant in the circuits. Thus mass flow meter measures the refrigerant oil mixture before the capillary tube. The COP is calculated using refrigeration capacity and power consumption of the compressor.

Table 2.8 : Results of calorimeter tests for R600a/R290 (40%/60% by weight) refrigerant mixture at ASHRAE standards.

Refrigerant	R600a				R600a/R290			
Comp. speed (rpm)	1300	2100	3000	4500	1300	2100	3000	4500
Condensation (°C)	54.4	54.4	54.4	54.4	54.4	54.4	54.4	54.4
Evaporation (°C)	-23.3	-23.3	-23.3	-23.3	-23.3	-23.3	-23.3	-23.3
Discharge (°C)	61.5	66.9	79.5	92.4	73.3	92.1	103.9	113.1
Superheat (°C)	32.2	32.2	32.2	32.2	32.2	32.2	32.2	32.2
Subcool (°C)	32.2	32.2	32.2	32.2	32.2	32.2	32.2	32.2
Ambient (°C)	32.2	32.2	32.2	32.2	32.2	32.2	32.2	32.2
Mass flow rate (g/s)	0.28	0.40	0.59	0.77	0.48	0.86	1.22	1.45
Input power (W)	53.5	77.9	115.1	163.4	90.5	142.4	199.2	250.1
Cooling c. (W)	93.9	135	197.5	257.5	170.2	306.2	432.9	513.9
COP (W/W)	1.75	1.73	1.72	1.58	1.88	2.15	2.17	2.05

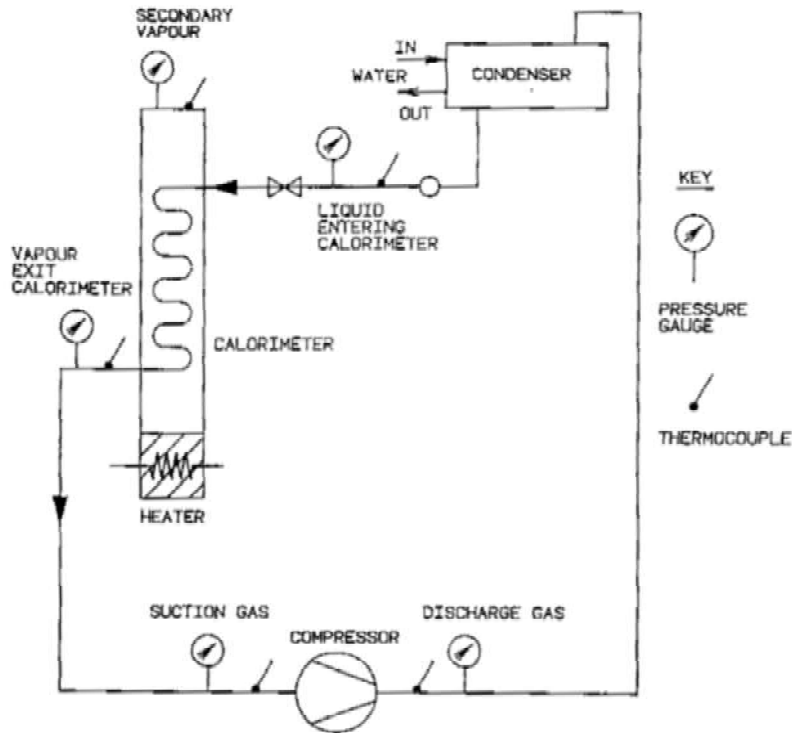


Figure 2.23 : Calorimeter test set up.

The results for R600a and R600a/R290 (40%/60% by weight) mixture are presented in Table 2.8. It is shown that COP value increases drastically for 2100, 3000 and 4500 rpm. An increase in COP is observed between 7.4% and 29.7%, with an increase towards higher speeds. Main reason for such a drastic increase may be that the calorimeter test system is designed for high back pressure compressors.

Figure 2.24 shows the test results for R600a and R600a/R290 refrigerant mixture conducted at ASHRAE conditions. Red line indicates the results of the refrigerant

mixtures test stand while the dashed black line stands for calorimeter tests. Circle and square symbols in the lines represent the refrigerant R600a and R600a/R290 mixture, respectively. It is seen that the COP values are fairly close between 1300 to 3000 rpm for R600a. Although the values of the COP of R600a/R290 mixture and R600a are relatively close at 1300 rpm, the differences in COP are increased significantly as the compressor speed increases. It should be noted that the trends of the square symbols are similar to each other. The optimum compressor speed of R600a/R290 mixture is obtained close to the 3000 rpm at calorimeter test stand while refrigerant mixtures test stand found close by 2100 rpm.

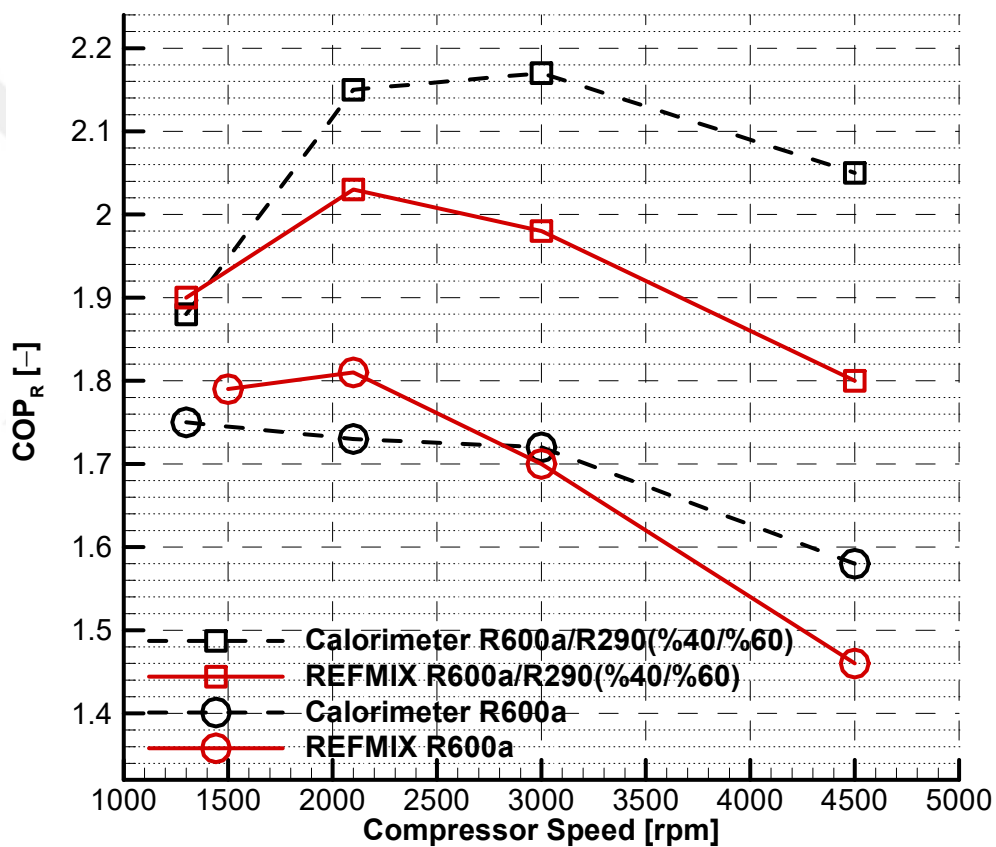


Figure 2.24 : Comparison of results for R600a and R600a/R290 (40%/60% by weight) refrigerant mixture.

Figure 2.25 demonstrates increase in COP using R600a/R290 mixture relative to R600a results. It is seen that the calorimeter test stand depicts a greater COP increase compared to the refrigerant mixture test stand at all speeds. The minimum increase in COP is calculated as 6.15% at 1500 rpm for the refrigerant mixture test stand. It is seen that the relative increase to R600a results for the REF MIX is 12.15%, 16.47% and 23.29% for 2100, 3000 and 4500 rpm, respectively. It is clear that the use of

R600a/R290(40%/60% by weight) in household refrigeration compressors is more beneficial in terms of energy efficiency.

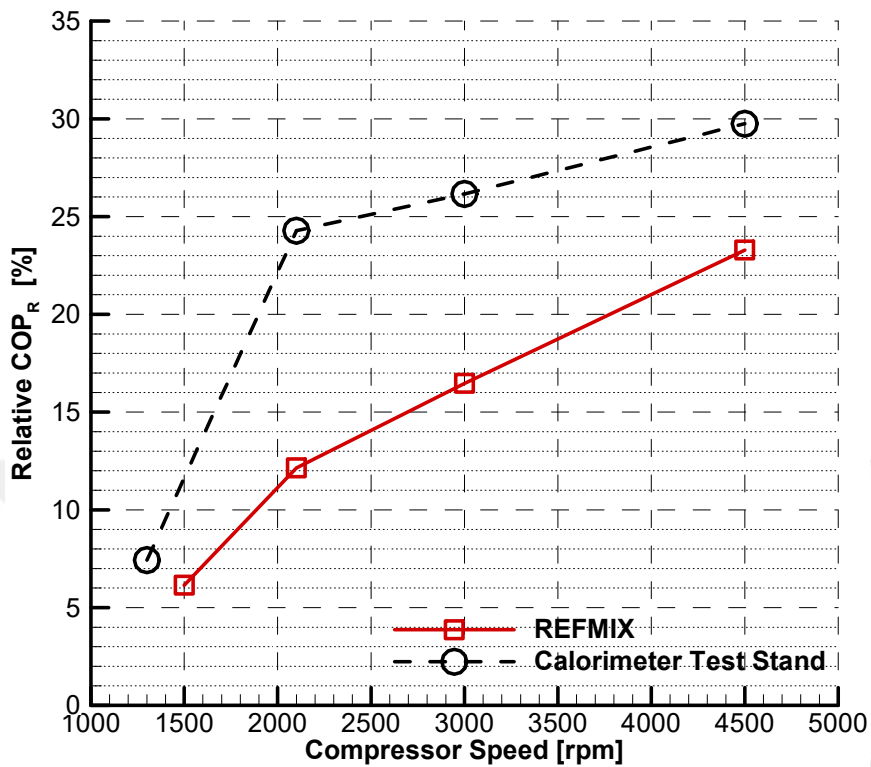


Figure 2.25 : Increase in COP relative to R600a results.

2.1.3 Small refrigeration compressor power test stand

Small refrigeration compressor test stand is used in the experiments. Test stand is built from several student works in TU Dresden [81]. Main purpose of the test system is to measure the efficiency of the hermetic compressor. The measurements are carried out in accordance with DIN EN 13771-1. The layout of the experimental system is given in 2.26.

Blue and red labels indicate pressure and temperature respectively while yellow label indicates the mass flow meter. A Yokogawa type WT333E is used for power measurement of the compressor. The calorimeter serves as evaporator in the design and R134a is used as refrigerant. The electrical heater placed in the calorimeter and can be adjusted by the user continuously. The superheat at the compressor inlet is set to the required 32°C. WT310E used to measure applied heat power. The condensation temperature is controlled via a fan which can be controlled via signal control. WIKA type pressure sensors having a measuring range 0-16 and 0-25 bar are used for high and low pressure side. The Bronkhorst mass flow meter has a working range of

0-1.3 g/s. The temperature sensors are Pt100 resistance thermometers. Mass flow, pressure and temperature measurements are delivered to NI type data acquisition card. The measurement program LabVIEW is used to monitor and transfer the data to the computer.

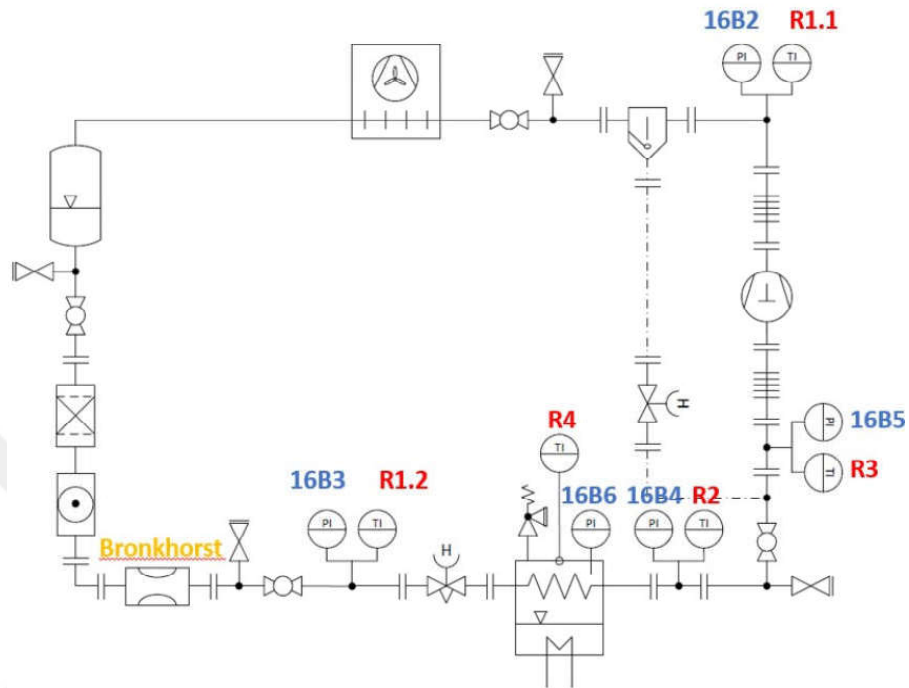


Figure 2.26 : Layout of the compressor power test stand

R600a is used in the system to measure the performance of the compressor. R134a is used as a refrigerant in the calorimeter. Measurements carried out for hermetic type compressor manufactured by Embraco model number "VEM XTC". Cooling capacity and COP are calculated by using following equations according to the DIN EN 13771-1 standard.

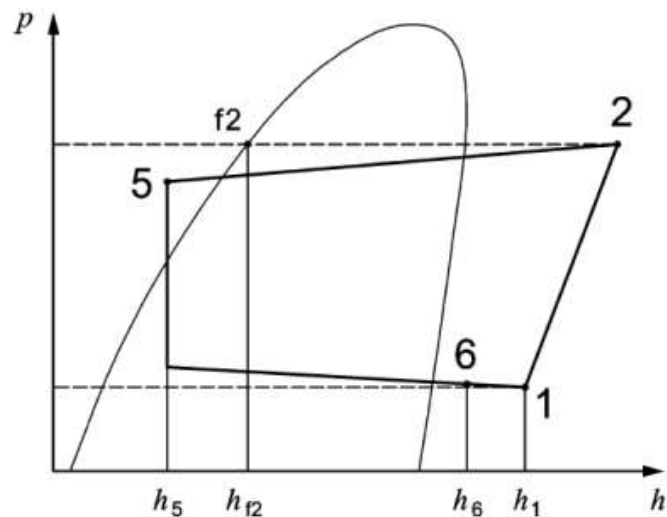


Figure 2.27 : Pressure enthalpy diagram.

Table 2.9 : Temperature readings of experiments at 3000 rpm.

Temperature (°C)	Standard	Test 1	Test 2	Test 3
Evaporation	-25	-25.9	-25	-25.1
Condensation	55	59.8	60.2	60.3
Superheat	32	31.4	30.8	30.5
Ambient	32	31.4	30.8	30.5

$$\dot{Q} = \dot{m} \times (h_1 - h_{f2}) \quad (2.3)$$

$$COP_R = \frac{\dot{Q}}{\dot{W}} \quad (2.4)$$

The cycle temperatures are given in the 2.9. The compressor speed is set to 3000 rpm in the measurements. The experiments are carried out for 15 minutes and the pressure, temperature and mass flow rate data are sampled each 5 seconds. The average mass flow rate of the refrigerant/oil mixture is around 0.31 g/s.

Cooling capacity and COP of the compressor are given in Figure 2.28. As Figure 2.28 states, the COP and cooling capacity of the system is determined between 1.56 to 1.6 and 80 to 82 W, respectively.

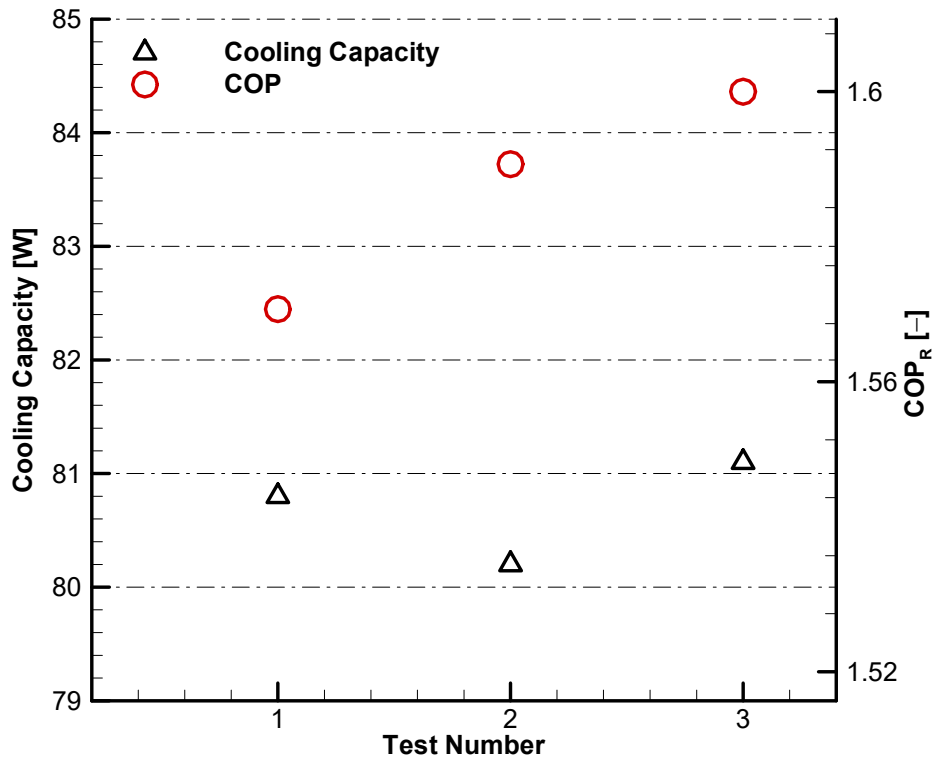


Figure 2.28 : Experimental results of the compressor power test stand tested at DIN EN 13771-1.

2.1.4 The compatibility of the refrigerant with oil

The importance of refrigeration oil is mentioned in Chapter 1.3. The influence of the refrigerant dissolved in the oil on viscosity is demonstrated by the PVT diagram known as Daniel Plots. In these, saturation vapor pressure and mixture viscosity at defined concentrations are shown against temperature. The resulting mixture viscosity can be found from the given temperature and the corresponding percentage of oil dissolved in the refrigerant. Figure 2.29 and Figure 2.30 presents the Daniel Plots for the 5 and 10 cSt Reniso brand mineral oils, respectively [14]. In this context, the corresponding mixture viscosity drastically changes for the 95%, 90% and 85% refrigerant-oil mixtures. In this regard, the lubrication performance of the various viscosities is studied in the next chapter. Moreover, the effect of refrigerant dissolving in the oil is studied numerically in Chapter 3.

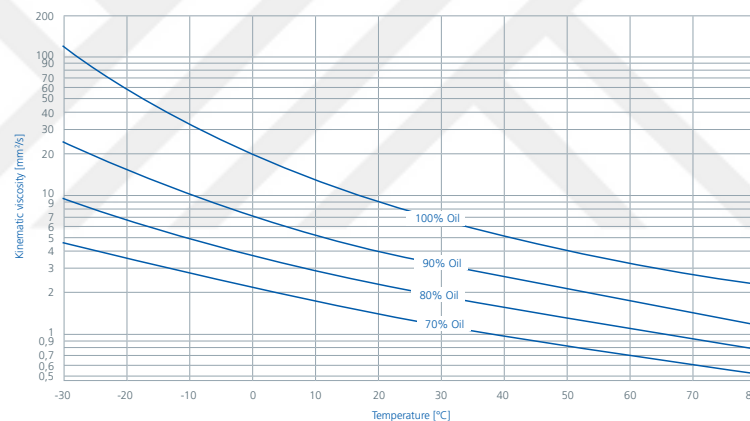


Figure 2.29 : Kinematic viscosity of RENISO WF5 A-R600a mixture.

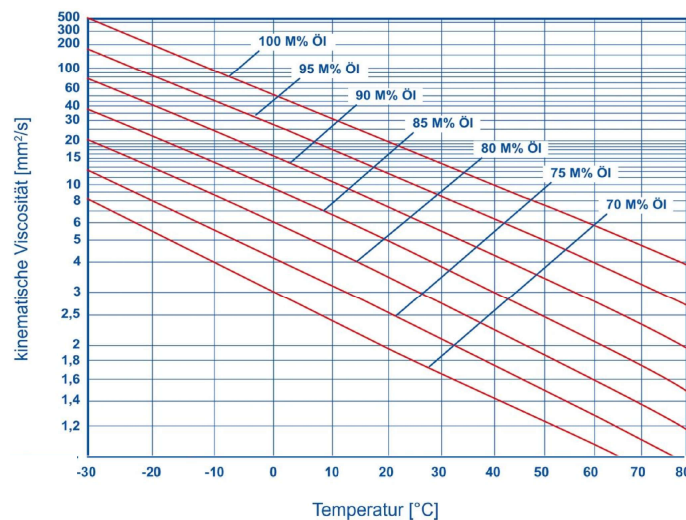


Figure 2.30 : Kinematic viscosity of RENISO WF10 A-R600a mixture..

2.2 Lubrication System of the Compact Inverter Compressor

Environmental laws, legislation, and regulations are forcing the manufacturer to improve their products. With improved manufacturing techniques and novel compression concepts, the variable capacity hermetic compressors are designed more compact for both reducing the production cost and increasing cooling domain in the refrigerator. Moreover, due to the changing energy regulations, the expectancy of the higher isentropic and volumetric efficiencies are still a challenging issue in the design of compact inverter compressors. Depending on the refrigeration capacity, inverter type compressors operate at various rotational speeds. Oil management and lubrication mechanism in journal bearings may change drastically between compressor maximum and minimum speeds. Nevertheless, sufficient lubrication should be provided to the bearings and all moving parts to avoid any mechanical damage on the compressor.

In this thesis, the compressor of interest is a compact inverter compressor (CIC) for household appliances, which is shown in Figure. 2.31. The technical specifications and dimensions of the compressor used in this study are shown in Table 2.10. In this context, some of the recent studies in the household refrigerator compressors focus on the improvement of the oil management system [55, 65].



Figure 2.31 : Compact Inverter Compressor (CIC).

Table 2.10 : The details of the compressor model.

Model	VNTZ type
Weight	6 kg
Motor Type	Brushless DC
Displacement	11.28 cc
Cooling Capacity	173 kcal at 3000 rpm
COP	1.9 W/W at 3000 rpm (ASHRAE condition)
Working Speeds	1200-4500 rpm
Height of the crankshaft	9.8 cm
Dimensions ($W \times L \times H$)	$14.5 \times 15 \times 13.5$ cm

2.2.1 Problem description

The crankshaft, which acts as an oil pump, delivers oil from the sump to the rotating and moving parts of the compressor. Oil is sucked from the bottom of the crankshaft and transferred with the centrifugal forces caused by the rotation and the viscous effects. Oil climbs through the eccentric hole up to the first journal bearing. It further moves on the double-helical paths which join to each other before the main journal bearing. Finally, oil is spread out from the hole located at the uppermost of the crankshaft. The crankshaft mechanism of the CIC is given in Figure 2.32.

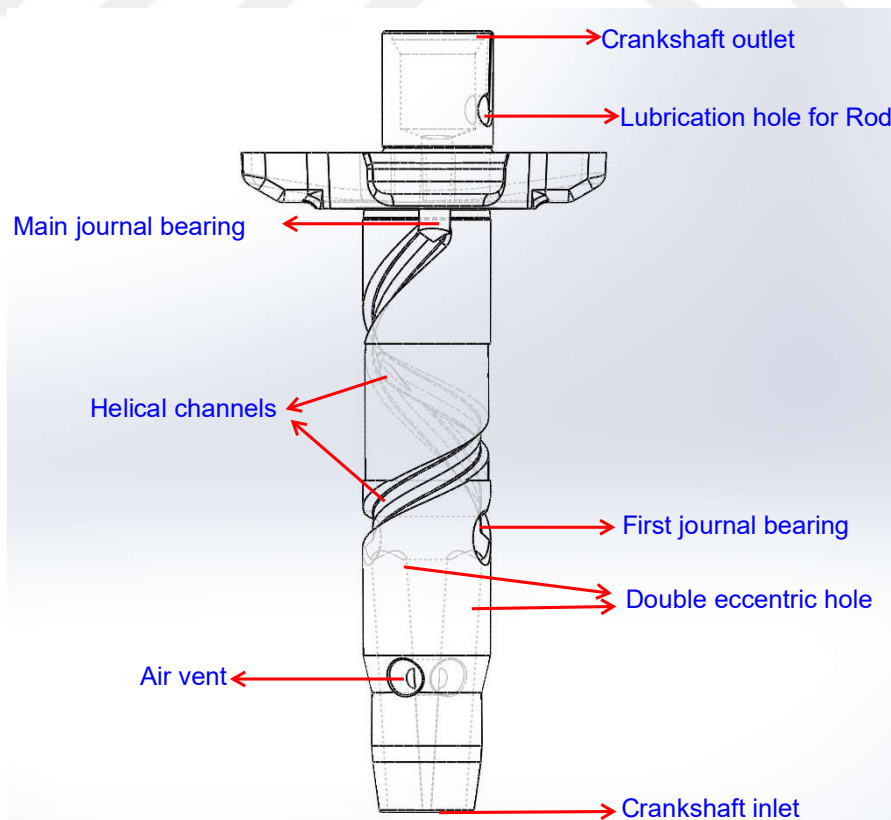


Figure 2.32 : Crankshaft of the CIC.

The lubricants which are widely used in hermetic reciprocating compressors are synthetic and mineral-based oils with various kinematic viscosities depending on the operating conditions [14]. Lubrication oil is filled into the compressor in the assembling process and the compressor is expected to self-lubricate during the operation of the refrigerator.

2.2.2 Oil mass flow rate measurements

The measurement devices of the experimental set up of the oil flow rate are shown in Figure 2.33. CIC is located inside a plexiglass housing to gather the oil which is emanated from the crankshaft. The heating capacity of the heater are controlled via the PID feedback control system to maintain the oil viscosity in the operating range. Temperatures are measured with a data acquisition system via thermocouples located in the oil tank and compressor. To monitor the temperatures carefully, seven T-type thermocouples are used, three of them in the oil tank (T1, T2, T3) the other three in the oil sump (T4c, T5c, T6c) and the last one (T7) in the cylinder head of the compressor. The locations of the thermocouples are given in Figure 2.34.

Measurement is started right after the oil temperatures reached the desired operating conditions. Steel sheets are used to cover the upper part of the compressor to prevent oil leakage to the oil sump. Aluminum tapes are applied both to tighten the sheets and close the small gaps between the CIC and sheets. Crankshaft speed is adjusted by a signal generator. The details of the instrumentations are given in Table 2.11.



Figure 2.33 : Instruments of the experimental set up: 1. CIC 2. Pre-heated oil sump 3. Control panel 4. PID controller 5. Direct current relay 6. Frequency generator 7. Precision balance 8. Beakers

Table 2.11 : The instrumentation list of the test stand.

Data Acquisition	Keysight 34970A
Thermocouples	T type (%0.4 accuracy)
High speed camera	Photron 512 PCI 32K
Spotlights	dedocool COOLH
PID Controller	Autonics TX4S
Power Controller	Autonics SPC1-35
Heater	Sheet type adhesive flexible resistance (1200 W)

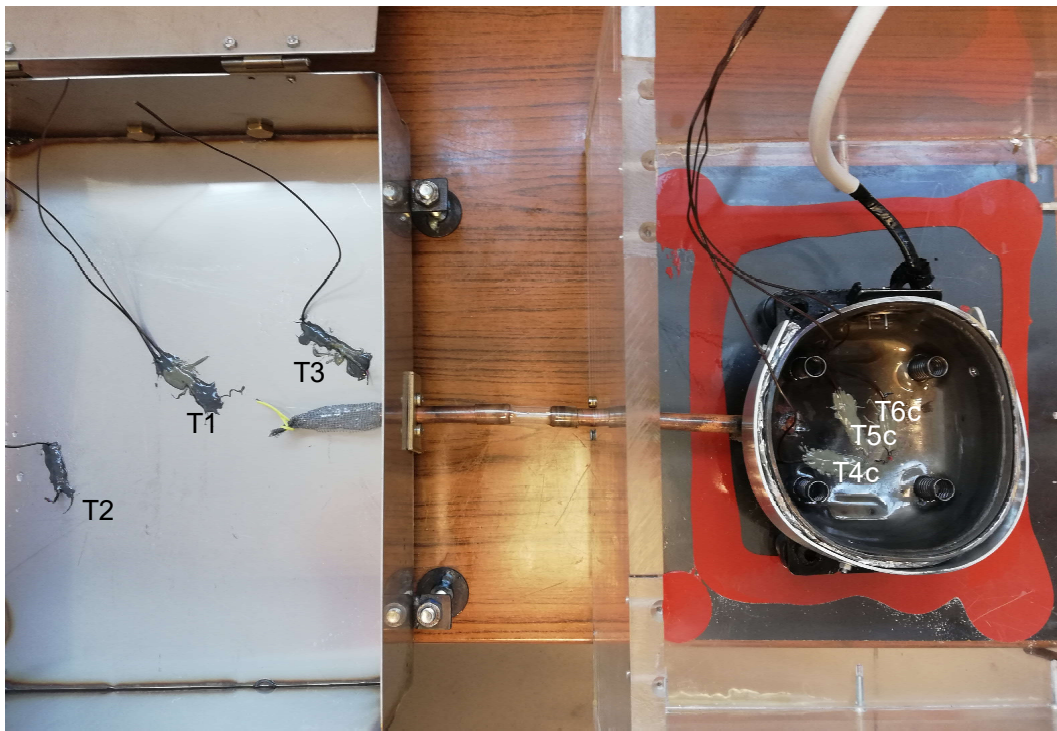


Figure 2.34 : Thermocouple positions in the pre-heated oil sump and compressor case.

The test routine is described as follows. At steady-state conditions, the compressor operates for a minimum of ten minutes and oil is collected in a beaker. The run time for oil collection is about two minutes and the measurements are repeated at least fifteen times. If the working speed of the compressor is higher than 2400 rpm, the run time of the test is one minute and measurements are repeated thirty times. Kinematic viscosities of the oil at 40°C and 65°C are 3 and 5 cSt, respectively [14].

2.2.3 Results

Figure 2.35 shows the temperature fluctuations during the tests. It is seen that there are only negligible deviations in the temperatures' changes. The only considerable fluctuation is observed for the thermocouple T2 which is located on the left side of

the oil tank since the collected oil in the beaker is returned into the left side of the oil tank for a new measurement. The oil temperature is decreased due to heat loss from the oil to the environment, therefore, the temperature of the oil sump kept over 40°C. The thermocouples T4 and T5 measure the oil temperature in the compressor and T6 measure the skin temperature of the case and they are important to track the viscosity of the oil. It is shown in Figure 2.35 that the time zone between 1000 to 2000 seconds is ideal to carry out oil flow rate measurements for the oil viscosity of 5 cSt.

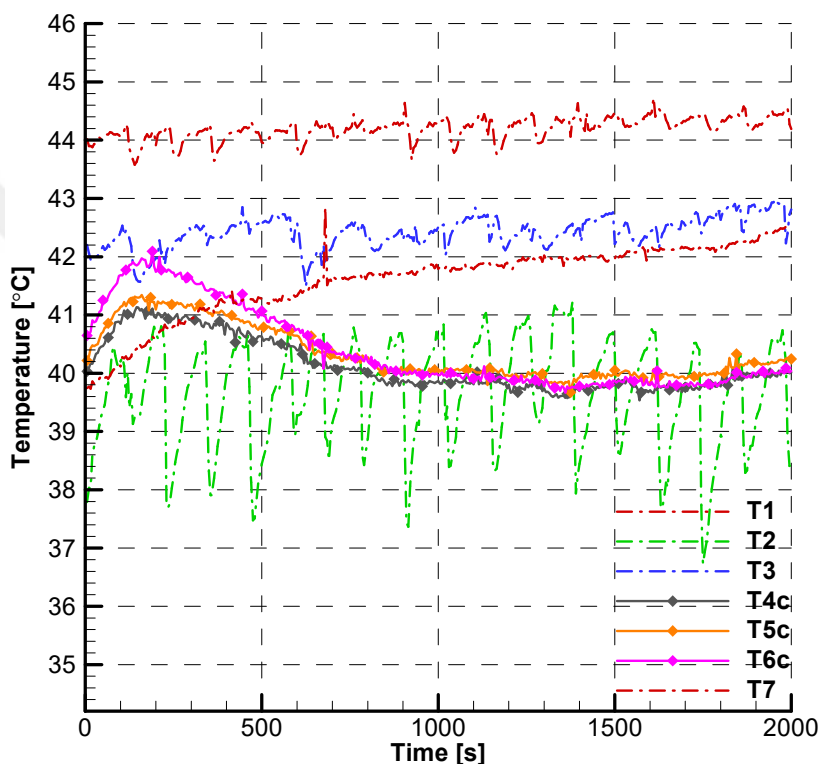


Figure 2.35 : Temperature fluctuations during measurement.

Figure 2.36 shows the repeatability of the measurements reflected in the standard deviation with 2σ using thirty measurements. The repeatability analysis indicated that the standard deviation in the oil mass flow rates is calculated $\sigma = 0.034$ g/s from the mean value of 1.69 g/s. The analysis showed that half of the total measurements are in the bandwidth of 1.67-1.69 g/s, thus the measurements are reliable at the standard operating conditions of the CIC. The Equation 2.5 is used to calculate sample standard deviation. The standard deviations of oil mass flow rate measurements in the operating range of the CIC for 3 and 5 cSt oil viscosity are given in Table 2.12. It is shown that maximum standard deviation is 0.13 g/s and it corresponds the 5.5% of the measurement.

Table 2.12 : Standard deviation values of the experiments.

Rotational Speed	3 cSt	5 cSt
1200	0.004	0.037
1400	0.007	0.064
1600	0.006	0.072
1800	0.008	0.113
2000	0.006	0.071
2200	0.006	0.069
2400	0.011	0.061
2600	0.009	0.019
2800	0.02	0.026
3000	0.014	0.034
3300	0.009	0.045
3600	0.02	0.077
4000	0.022	0.085
4500	0.016	0.13

$$SD = \sqrt{\frac{\sum_{i=1}^n (x_i - \bar{x})^2}{n - 1}} \quad (2.5)$$

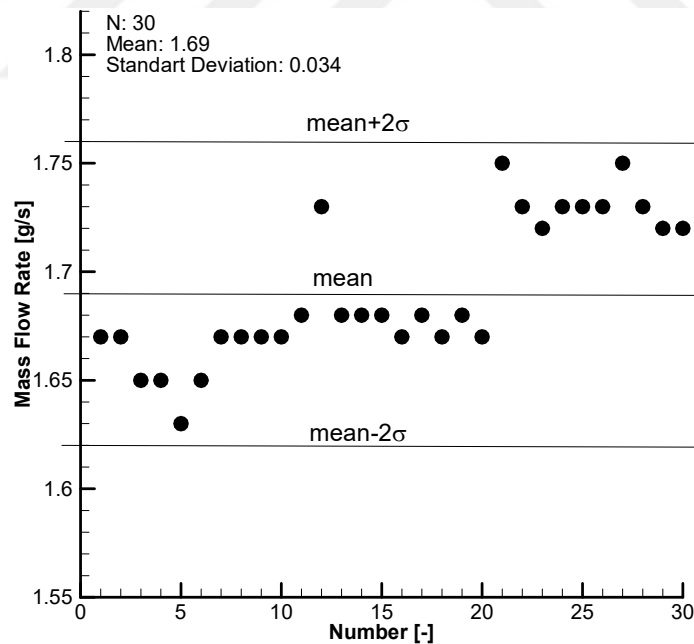


Figure 2.36 : Standard deviation of the oil mass flow rates at 3000 rpm, 5 cSt.

The working speed of the compressor and the viscosity of the oil are two main parameters affecting the oil mass flow rate. To investigate these effects, three different oil viscosities are tested in a wide range of working speed of the compressor. Figure 2.37 shows the experimental oil mass flow rate results for 3, 5 and 10 cSt. The operating range of the compressor is examined in fourteen different speeds. It is

observed that 5 cSt yields higher oil flow rate than 3 cSt below 1800 rpm. There is no considerable change between the 3 and 5 cSt results are observed after this working speed. Moreover, 10 cSt has been found to provide higher oil flow results below 2200 rpm, except for 1200 rpm. It is observed that after this interval, 3 and 5 cSt viscosity provide a higher oil mass flow rate than 10 cSt. There are two different flow zone in the crankshaft mechanism. The first one is up to a first journal bearing. The flow inside the double inclined hole is mainly dominated by centrifugal forces and viscous forces have a negative effect on the oil mass flow rate in this flow zone. The second flow zone is defined the location between first and main journal bearing. In this zone, double-helical channel carved on the crankshaft acts like an extruder which higher viscosity yields higher oil flow rate due to oil is transferred mainly with viscous forces in that region. The trade-off between these two flow zones reveals that viscous forces are dominant until 2200 rpm in CIC. It is worth the note that the oil mass flow rates are fairly close to each other after 1800 rpm for 3 and 5 cSt.

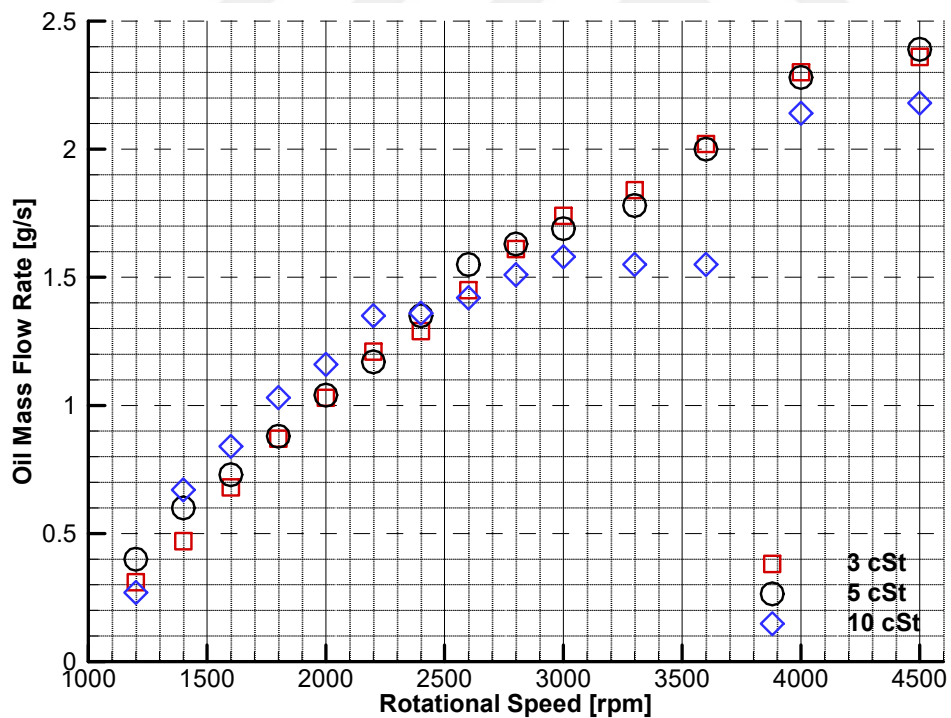


Figure 2.37 : The oil mass flow rate results for 3,5 and 10 cSt.

Figure 2.38 shows the effect of viscosity on the oil mass flow rate at 3000 rpm. It is revealed that with increasing viscosity oil mass flow rate decreases. It should be noted that the relative difference between the 3 and 5 cSt is 6.5% for 3000 rpm. Lubrication tests are confirmed that the lubrication performance of the CIC compressor is higher than previous variable speed compressors.

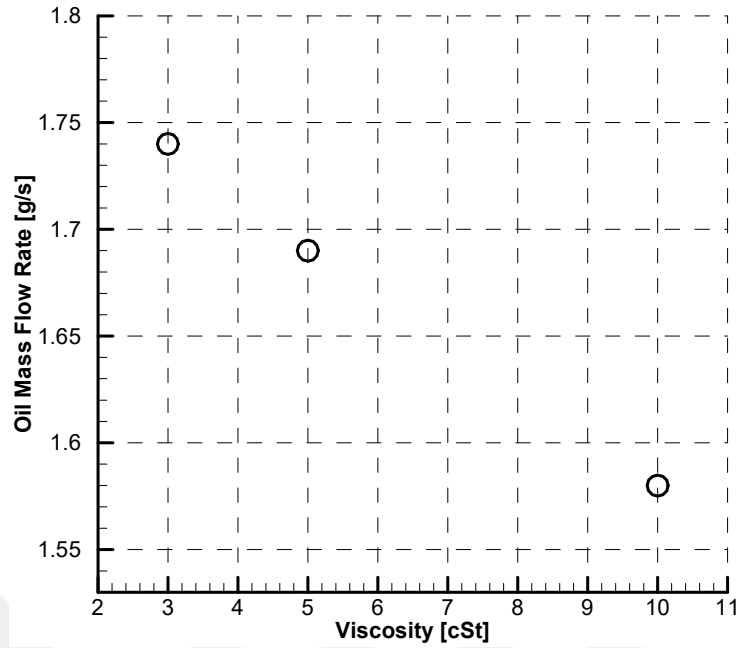


Figure 2.38 : The effect of viscosity on the oil mass flow rate at 3000 rpm.

2.2.4 Flow visualizations

Figure 2.39 shows the experimental setup with flow visualization equipment, which consisted of one Photron 512 PCI 32K model high-speed camera, two spotlights for illumination, PC for recording and storage. The steady-state oil lubrication pattern inside of the compressor is visualized at 2000 fps. These flow patterns will be used to validate CFD model predictions in the following chapter.

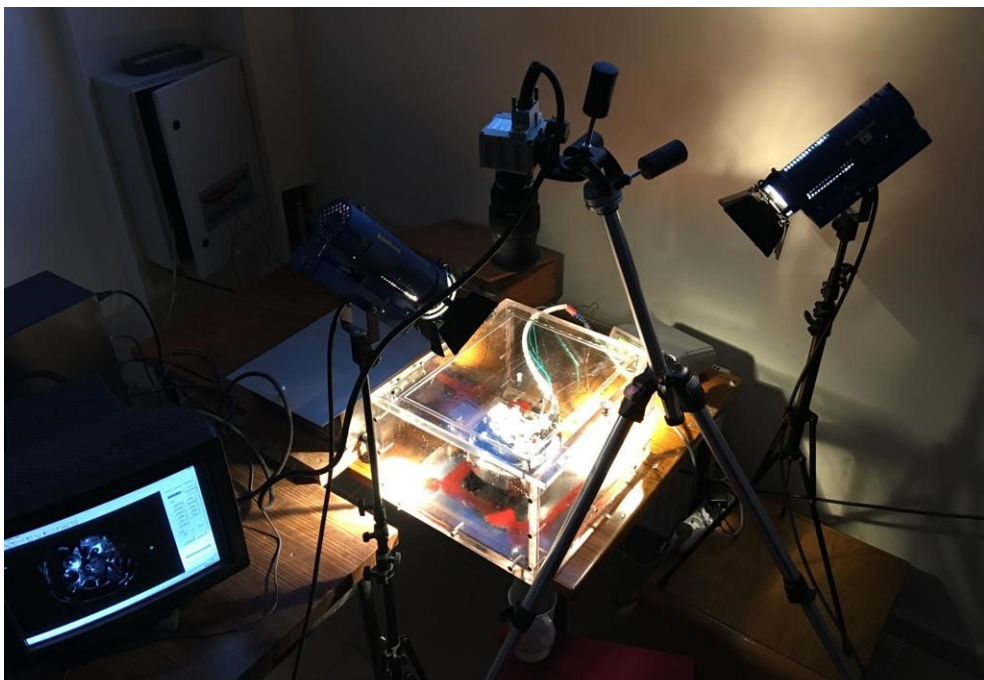


Figure 2.39 : Flow visualization test bench.

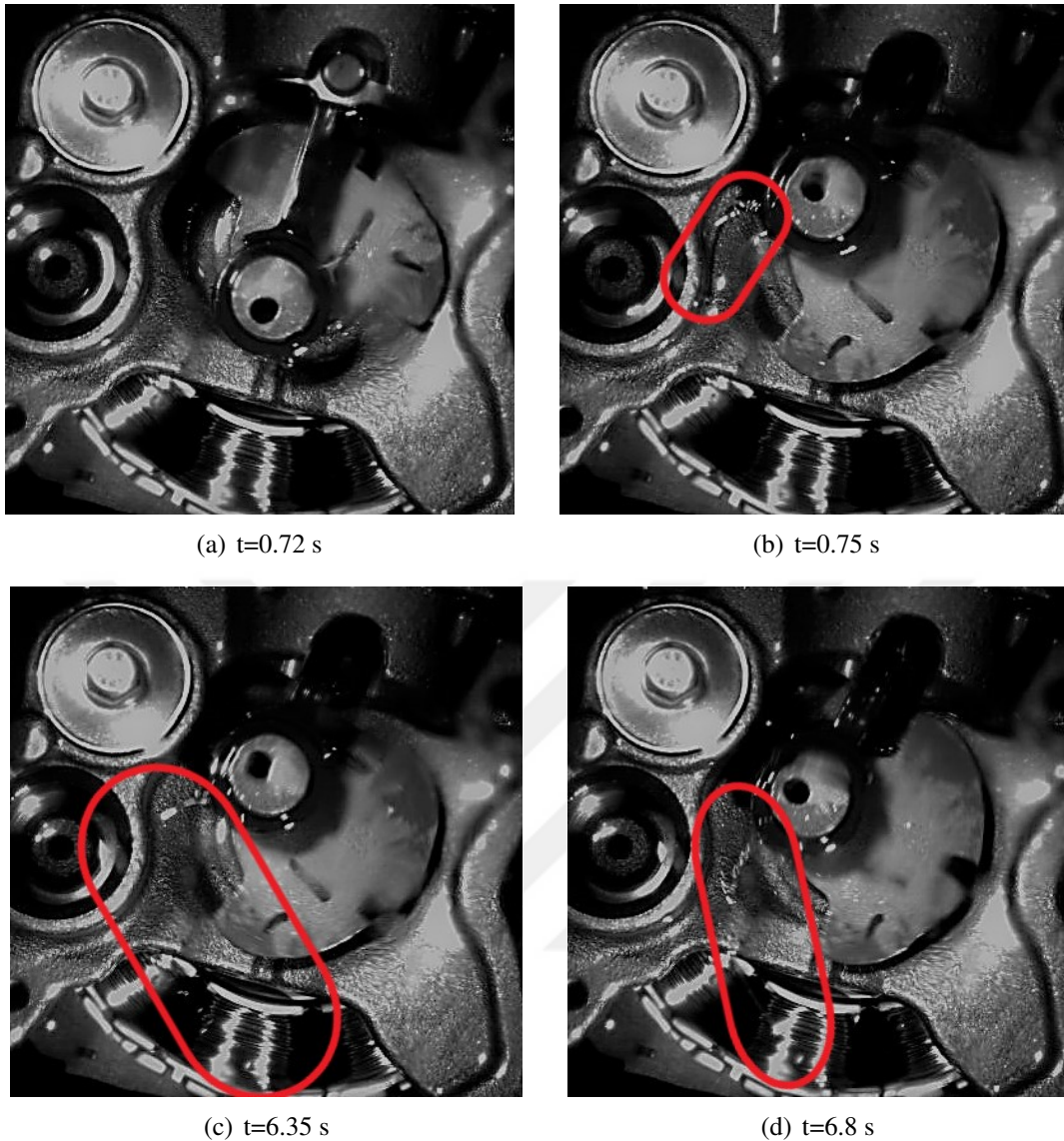


Figure 2.40 : Instantaneous snapshots of the CIC at 3000 rpm, high speed camera at 1000 fps.

The acceleration of the crankshaft between the initial time $t=0$ to 7.8 seconds is monitored at 500 fps (see Figure 2.40). Then using the location of the crankshaft, the rotational speed is found from captured pictures. After the crankshaft speed increases to 750 rpm in 1 second, it reaches 3000 rpm with an increase of 100 rpm per second. Although the oil climbing time is seen at 0.75 seconds, oil droplets appear in snapshots up to 6.35 seconds. The transition from oil droplets to an oil film is captured around 6.8 seconds, which is called, the required time for sufficient lubrication. In that time, corresponding crankshaft speed is around 1200 rpm which is the lowest operating speed of the CIC. Measurements show that below this range it could be unsafe to run the compressor.

2.3 Concluding Remarks

Extensive experimental studies carried out and a brief summary is given in this section.

The main conclusions can be summarized as follows:

- The performance evaluation of refrigerant/refrigerant mixtures on the household refrigeration compressors studied several experimental test stands, namely refrigerant mixtures test stand, calorimeter test stand and small refrigeration compressor power test stand. First two of the stands are designed for the ASHRAE standards and the last one built for the DIN EN 13771-1.
- The effect of the R600a/R290 refrigerant mixtures on the household refrigeration compressor is studied in house refrigerant mixture test stand (REFMIX). Examined refrigerants are R600a/R290 (30%/70% by weight), R600a/R290 (40%/60% by weight) and R600a/R290 (60%/40% by weight). The performance outcomes of the tested mixtures are compared with R600a.
- It is shown that R600a/R290 refrigerant mixtures provide higher COP values than R600a. The COP difference between R600a/R290 and R600a appears to increase with increasing compressor speed.
- It is noted that R600a/R290 (40%/60% by weight) refrigerant mixture provides the highest COP values. The relative increase in COP to R600a is calculated as 6.15%, 12.15%, 16.47% and 23.29% for 1500, 2100, 3000 and 4500 rpm, respectively.
- R600a/R290 (40%/60% by weight) refrigerant mixtures is tested with a calorimeter test bench. A relative increase in COP to R600a is observed between 7.4% and 29.7%, with an increase towards higher speeds. The main reason for such a drastic increase may be that the calorimeter test system is designed for high back pressure compressors.
- It is clear that the use of R600a/R290 refrigerant mixtures in household refrigeration compressors is more beneficial in terms of energy efficiency.
- The main difference in the DIN EN 13771-1 standards is no subcooling applied which affects dramatically to the enthalpy of the refrigerant at the evaporator inlet. The evaporation and condensation temperature are slightly different than ASHRAE

standards. The enthalpy of the refrigerant at the inlet of the evaporator is calculated from pressure and temperature at the discharge line of the compressor.

- The influence of the refrigerant dissolved in the oil on viscosity is demonstrated by the PVT diagram known as Daniel Plots. In these, saturation vapor pressure and mixture viscosity at defined concentrations are shown against temperature. It is shown that the mixture viscosity decreases with increasing the amount of refrigerant dissolving in the oil.
- The lubrication experiments are carried out between 1200 to 4500 rpm and oil mass flow rates are given in Figure 2.37 for 3, 5 and 10 cSt oil viscosity. The results reveal that the oil mass flow rate of the lubrication system is increasing with the rotational speed.
- It is observed that 5 cSt yields higher oil mass flow rate than 3 cSt below 1800 rpm except for 1200 rpm. There is no considerable change between the 3 and 5 cSt results are observed after this working speed.
- 10 cSt has been found to provide higher oil mass flow rate results below 2200 rpm, except for 1200 rpm. It is observed that after this compressor speed, 3 and 5 cSt viscosity provide a higher oil mass flow rate than 10 cSt.
- The effect of viscosity can be explained by the various zones in the crankshaft system. The first one is up to a first journal bearing. The flow inside the double inclined hole is mainly dominated by centrifugal forces and viscous forces have a negative effect on the oil mass flow rate. The second flow zone is the location between the first and second journal bearing. In this zone, a double-helical channel carved on the crankshaft acts like an extruder in which higher viscosity yields higher oil flow rate due to oil is transferred mainly with viscous forces in that region. The trade-off between these two zones reveals that viscous forces are dominant until 2200 rpm in CIC.
- The acceleration of the electrical motor of CIC is derived from flow visualizations. After the crankshaft speed increases to 750 rpm in 1 second, it reaches 3000 rpm with an increase of 100 rpm per second.

- Flow visualizations revealed that oil climbing time is seen at 0.75 s, oil droplets appear in snapshots up to 6.35 second. The transition from oil droplets to an oil film is captured around 6.8 s, which is called, the required time for sufficient lubrication.





3. NUMERICAL STUDIES

Numerical tools are currently receiving great attention. The aim of this chapter is to model the CIC compressor. These studies divided into two parts. In this chapter, the lubrication system of a compact inverter compressor (CIC) is numerically investigated. In the numerical modeling, a finite volume-based algorithm is used to model two-phase (air-oil) flow inside the compressor using the Volume of Fluid Method (VoF) method. Transient behavior of the oil flow under laminar flow conditions is both simulated by imposing Sliding Mesh (SM) and the Moving Reference Frame (MRF) methods at various crankshaft speeds varying between 1200 and 4500 rpm. The measurements are used to compare/validate CFD results obtained from SM and MRF methods. Moreover, the acceleration of the crankshaft is determined via a high-speed camera and employed as a user-defined function to model the start-up period of the compressor. Oil climbing time and the linear increase in oil mass flow rate in the start-up period of the both methods are presented.

This chapter is organized as follows. The numerical modeling of the lubrication system of the CIC is given in Section 3.1. Thereafter, two different modeling approach, SM and MRF methods are given in Section 3.2 and Section 3.3, respectively. Finally, the main findings are summarized in Section 3.4.

3.1 Numerical Investigation of the Lubrication System

Insufficient lubrication of the hermetic compressor causes the compressor to stop working or even become inoperable. Several experimental and numerical studies which are dedicated to overcoming insufficient lubrication problems are given in the section 1.5. Among these studies, numerical investigations are at the forefront especially to provide a chance to investigate the oil management system design of inverter type reciprocating compressors in more detail. As rapid and cost-effective numerical approaches open the way of comparison of the number of various design alternatives with a lesser prototype, peer investigations require higher computation

time for the most realistic approach. CFD is a powerful alternative to experiments in the design phase of a product moreover the results of numerical calculations should be consistent with measurements. Therefore, the selection of a modeling approach is vital to achieving reliable results.

In this section, two different numerical modeling approaches, namely Sliding Mesh (SM) and Moving Reference Frame (MRF) are used to numerically investigate the lubrication system of a Compact Inverter Compressor (CIC). The CAD data of the CIC is given in Figure 3.1.

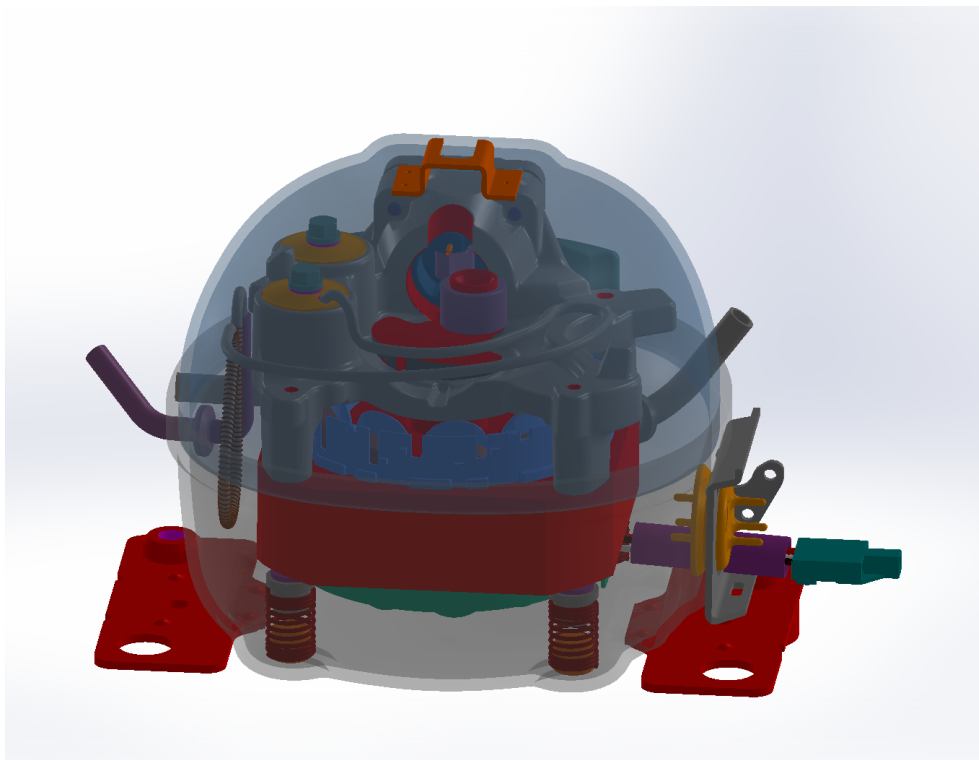


Figure 3.1 : CAD data of the CIC.

3.2 Sliding Mesh Method

The SM method is a special type of dynamic mesh motion in which boundaries and mesh cells move together in a rigid-body motion. As a consequence, the SM method is inherently unsteady due to the motion of the mesh with time. The cells in the zones are not deforming and the governing equations of the fluid motion are different than used in the MRF method. Moreover, SM method ables to model unsteady interactions such as potential, wake and shock caused by the relative motion of moving and stationary

components. SM method is defined as the most accurate method for simulating flows in multiple reference frame, but also the most computationally demanding [82].

3.2.1 Computational model

The CAD data of the CIC is simplified according to the requirements of the SM method. The interface encapsulating the crankshaft is introduced in the numerical model as shown in Figure 3.2. It consists of the crankshaft and the required interface domains. Since the SM method provides the opportunity to track the motion of the crankshaft in the temporal domain, it is possible to obtain instantaneous oil iso-surfaces.

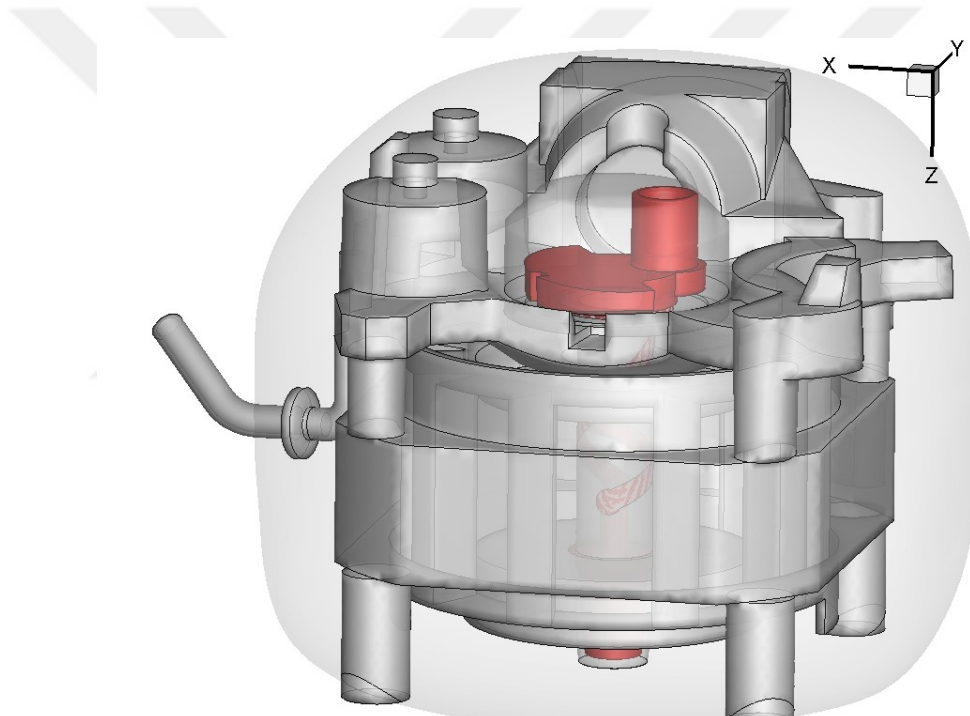


Figure 3.2 : Simplified domain used in SM method: red part: crankshaft, grey part on the top and bottom of the crankshaft: interface.

Due to the complexity of the solid geometry, the unstructured grid is employed in the fluid and solid domains. The tetrahedral and CutCell mesh is used in the numerical calculations. Maximum skewness kept below 0.92 and the average skewness is around 0.23. Figure 3.3 a) and Figure 3.3 b) demonstrate the generated mesh zones for the solid and fluid domain, respectively. As shown in the Figure 3.3, grid refinement is increased close to the solid walls and interfaces between the adjacent domains.

The boundary conditions for the mass and momentum equations are as follows:

The two-phase flow in the oil lubrication system is simulated using the Volume of Fluid Method (VoF) under transient, laminar and incompressible flow conditions by using the finite volume-based ANSYS-Fluent package.

- The mixture is assumed to be immiscible.
- The flow is considered isothermal.
- The refrigerant is replaced with air with a density of 1.23 kg/m^3 and a viscosity of $1.5 \times 10^{-5} \text{ kg/ms}$.
- The lubrication oil with a density of 890 kg/m^3 and the kinematic viscosity of the oil is 5 cSt.
- Rotational speed is taken constant in the analyses and acceleration of the electrical motor is neglected.
- All other remaining walls and interfaces between domains are taken as stationary.

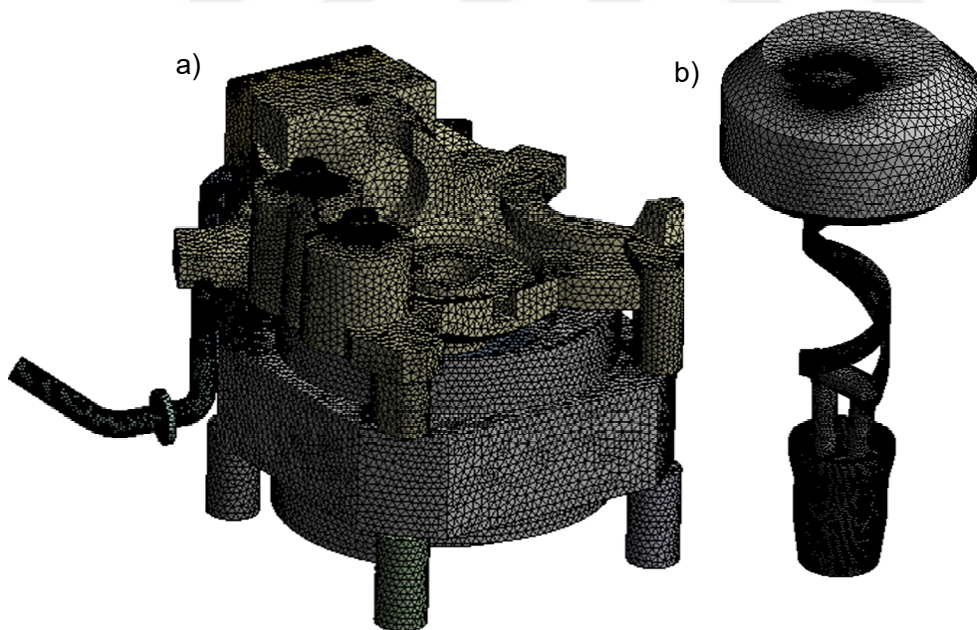


Figure 3.3 : Generated mesh zones a) solid and b) fluid domain.

Parallel computations have been performed on a 28-core processor computer using a second-order upwind scheme with appropriately selected underrelaxation factors for discretizing the continuity and momentum equations. The PISO (Pressure-Implicit with Splitting Operators) algorithm is used for pressure-velocity coupling since it is suitable for small time steps.

3.2.2 Governing equations

The conservation equation in general integral form for any scalar used in the SM method is given in Equation 3.1,

$$\frac{d}{dt} \int_V \rho \phi dV + \int_{\partial V} \rho \phi (\vec{u} - \vec{u}_g) \cdot d\vec{A} = \int_{\partial V} \Gamma \nabla \phi \cdot d\vec{A} + \int_V S_\phi dV \quad (3.1)$$

Since the time rate of change of the cell volume is zero, $V^{n+1} = V^n$ is valid for the SM method. The first order temporal derivative in Equation 3.1, can be rewritten using first-order forward difference formula as given in Equation 3.2,

$$\frac{d}{dt} \int_V \rho \phi dV = \frac{[(\rho \phi)^{n+1} - (\rho \phi)^n] V}{\Delta t} \quad (3.2)$$

In order to satisfy mass conservation, the time derivative of the control volume can be formulated as given in Equation 3.3,

$$\frac{dV}{dt} = \sum_j^{n_f} \vec{u}_{g,j} \cdot \vec{A}_j = 0 \quad (3.3)$$

In the numerical modeling, the VoF model with implicit scheme was used since there is an interface between the free surface of oil and the refrigerant (in the present study air). Air was preferred in CFD calculations because the experiments were carried out at atmospheric conditions without refrigerant. Moreover, R600a and R290 are also performed as refrigerant in the following sections. For the two-phase model, the continuity and momentum equations are given in Equation 3.4 and Equation 3.5, respectively where α represents the volume fraction [82].

$$\frac{\partial}{\partial t} (\alpha_i \rho_i) + \nabla (\alpha_i \rho_i \vec{u}_i) = 0 \quad (3.4)$$

$$\rho \left[\frac{\partial \vec{u}}{\partial t} + \nabla (\vec{u}\vec{u}) \right] = \rho \vec{g} - \nabla p + \nabla [\mu (\nabla \vec{u} + \nabla \vec{u}^T)] \quad (3.5)$$

3.2.3 Convergence tests

To determine the sufficient number of mesh elements to obtain reliable results, a mesh sensitivity study has been performed using tetrahedral and the CutCell mesh and results are shown in Table 3.1. As seen in Table 3.1, the oil mass flow rate released from the

Table 3.1 : Mesh independence tests for SM method.

Case ID	Oil Mass Flow Rate [gs^{-1}]	Relative Error [%]
CutCell, 790 K	3.31	0.6
CutCell, 1.2 M	3.29	-
CutCell, 1.8 M	3.23	-1.8
CutCell, 7.9 M	3.21	-2.4
Tetrahedral, 2.5 M	3.31	0.6
Tetrahedral, 5 M	3.21	-2.4
Tetrahedral, 10 M	3.07	-6.7

crankshaft outlet has approximately the same order for the tetrahedral and the CutCell meshes. Moreover, there is no considerable change in the oil mass flow rate with an increasing number of mesh, therefore the CutCell mesh method with 1.2M cell number is chosen in numerical calculations to reduce the computational cost. The unsteady mesh analysis was performed at a rotational speed of 3000 rpm with oil viscosity of 5 cSt and submersion depth of 15 mm. The relative error in Table 3.1 is calculated taking CutCell 1.2 M case as a selection criteria.

A time independence test is also conducted since the unsteady numerical calculations have been performed in the study. As regarded in any engineering method, the trade-off between the accuracy and computational cost must be considered. Smaller time steps will typically yield more accuracy and stability. On the other hand, that needs a higher number of time steps and therefore results in an increased computational cost. The Courant–Friedrichs–Lewy (CFL) condition indicates that,

$$CFL = \frac{u\Delta t}{\Delta x} \leq 1 \quad (3.6)$$

From this regard in the numerical calculations, time step size is taken as 5×10^{-4} seconds initially and 2.5×10^{-4} , 1×10^{-4} , 5×10^{-5} and 2.5×10^{-5} seconds are performed in the computations. As it is seen in Figure 3.4, the oil mass flow rate of the lubrication system is dramatically decreasing with decrements of the time step size. By reducing the time step size, both the oil climbing time is delayed and the rate of change of the oil mass flow rate is reduced. After 0.3 seconds, time-averaged oil mass flow rates which are released from the outlet of the crankshaft are noted in Figure 3.4. The computational run time is selected 0.5 seconds to reduce computational cost. It is shown that the oil mass flow rate difference between 5×10^{-5} and 2.5×10^{-5} is around 1.5% which is within the acceptable error margin. Therefore, time step

size (dt) is selected 5×10^{-5} seconds to perform the numerical calculations. Parallel computations have been performed on a 28-core processor computer and average simulation can have a wall-clock time approximately 28 and 80 hours for the time step sizes 5×10^{-5} and 2.5×10^{-5} seconds, respectively.

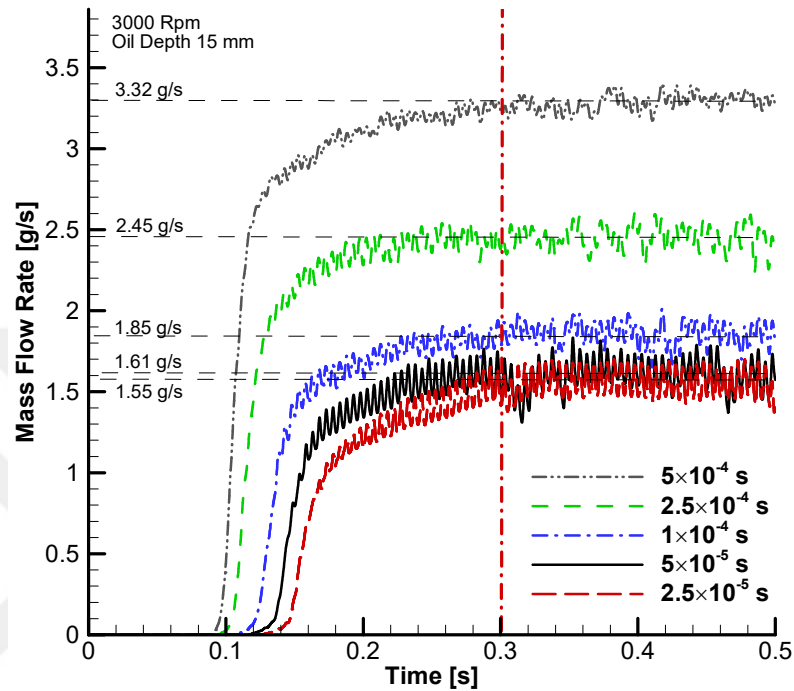


Figure 3.4 : Time step size test carried out with SM method.

3.2.4 Effect of rotational speed

The CFD calculations using SM method at various crankshaft speeds are summarized graphically in Figure 3.5. The effect of rotational speed on the oil mass flow rate investigated for twelve different crankshaft speeds varying between 1200 and 4500 rpm. The transient behavior of the oil mass flow rates and the climbing times with infinite acceleration could be understood well using the SM method. With increasing rotational speed, oil mass flow rates increase as expected. Oil climbing time is increasing with decreasing rotational speed. No oil droplets spread out from the crankshaft outlet at 1200 rpm.

The numerical output of the SM method was fluctuating due to the mathematical nature and mesh topology of the method [82], thus time sampling is used in the quasi-periodic phase after 0.7 seconds. Moreover time-averaged values are used to make a compatible comparison with measurements.

In the time sampling period, the oil mass flow rates are almost identical at 4000 and 4500 rpm. The reason for this is thought to be the constructive constraints in the CIC design. In the analyses, the oil submersion depth and oil viscosity are taken 11.5 mm and 5 cSt, respectively.

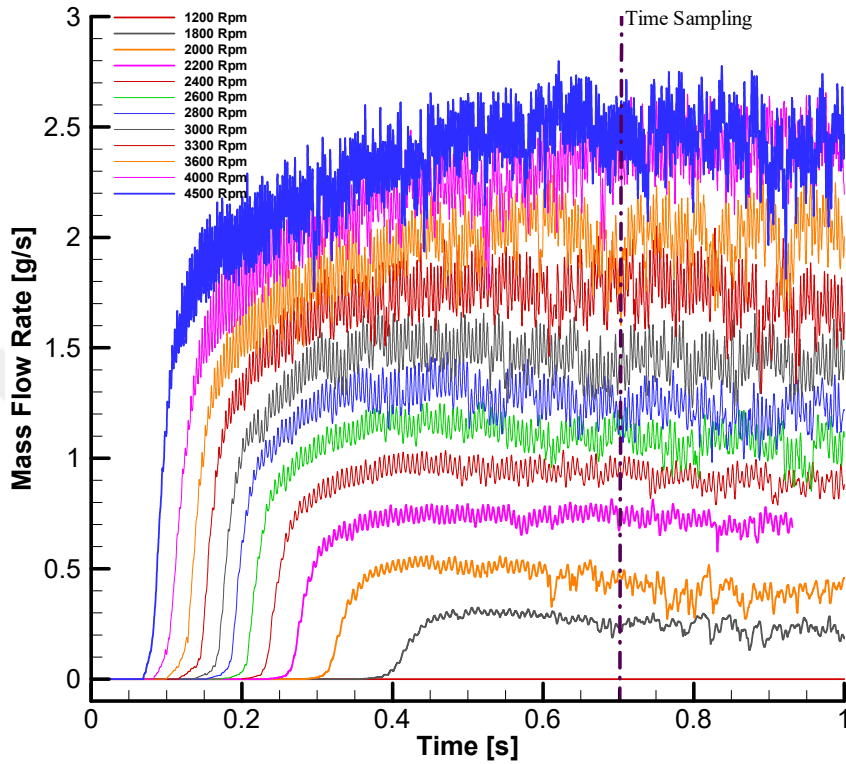
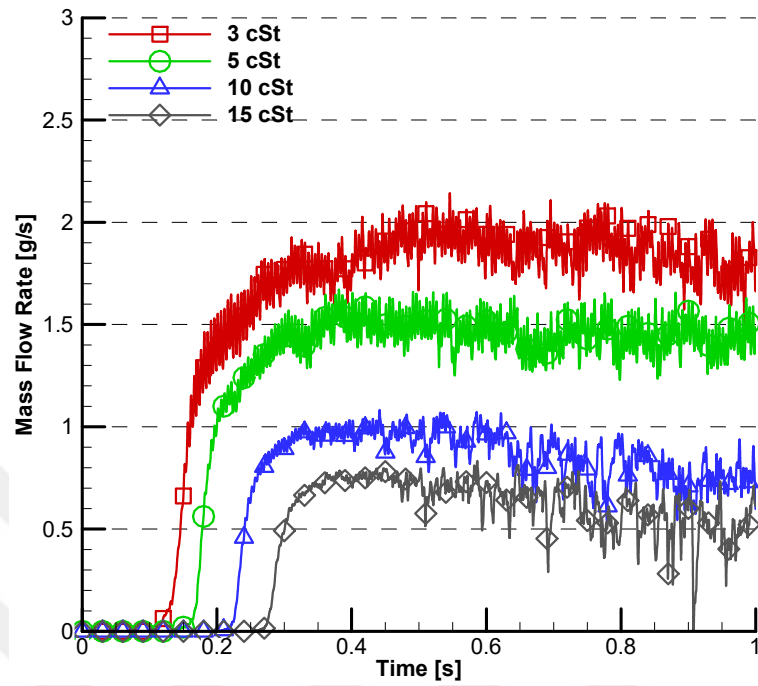


Figure 3.5 : Time dependent change of oil mass flow rate for various rotational speeds.

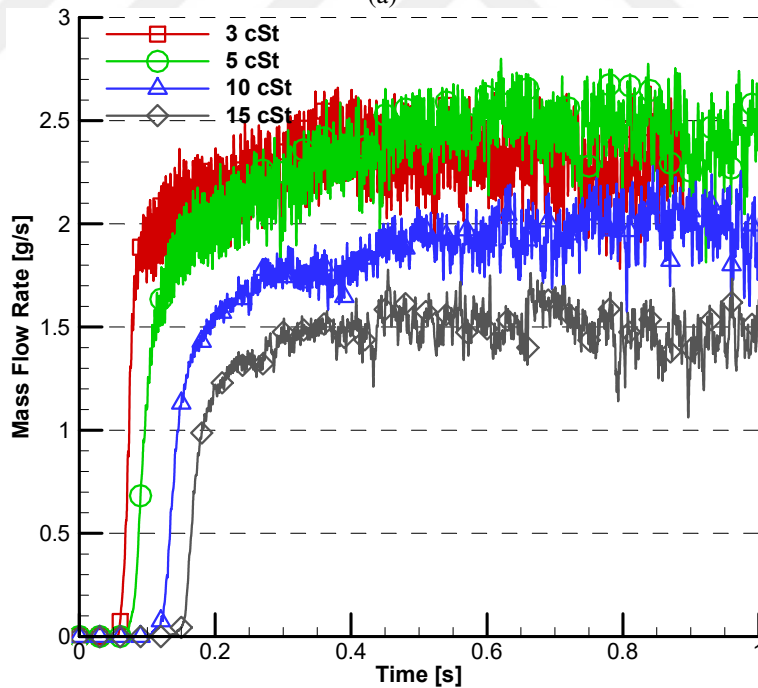
3.2.5 Effect of viscosity

The flow inside the compressor is mainly dominated by centrifugal and viscous forces. The impact of the viscous forces became obvious with increased viscosity. The effect of the oil viscosity on mass flow rates is demonstrated in Figure 3.6 at different crankshaft speeds. Increased viscosity causes more friction forces resulting in decreased oil mass flow rates. This behavior can be explained by the helical channel zone are rotating in the numerical calculations while in reality, the outer surface of the helical channel is sliding in the bearing and not closed. Thus flow confined in the channel and increasing viscosity resulting in decreasing oil mass flow rate in the numerical calculations. Moreover, the oil climbing time is decreasing with decrements of the viscosity. The oil mass flow rates are overlapped for 3 and 5 cSt at 4500 rpm. Sharp fluctuations are observed in the SM results. The difference in oil mass flow rate for 3 and 5 cSt are fairly close in the experiment as seen in Figure 2.37, whereas

SM method under-predicts significantly oil mass flow rate compared to experimental results.



(a)



(b)

Figure 3.6 : Effect of oil viscosity on the oil mass flow rate a) 3000 rpm b) 4500 rpm.

3.2.6 Instantaneous flow fields

In the initial state, the oil level is at rest having a height of 11.5 mm in the crankshaft. The oil is sucked from the oil sump through symmetrically opened two suction holes on

the bottom of the crankshaft and climbs through a helical channel carved on the shaft wall. As time marches, the oil is directed to the outlet of the crankshaft and released into the compressor case. Figure 3.7 shows the instantaneous oil volume fractions at various times. It is seen that oil reaches the outlet of the crankshaft around 0.13 seconds. To observe the oil path in the crankshaft, the position of the crankshaft is fixed in Figure 3.7. The results are obtained at 3000 rpm with 5 cSt oil.

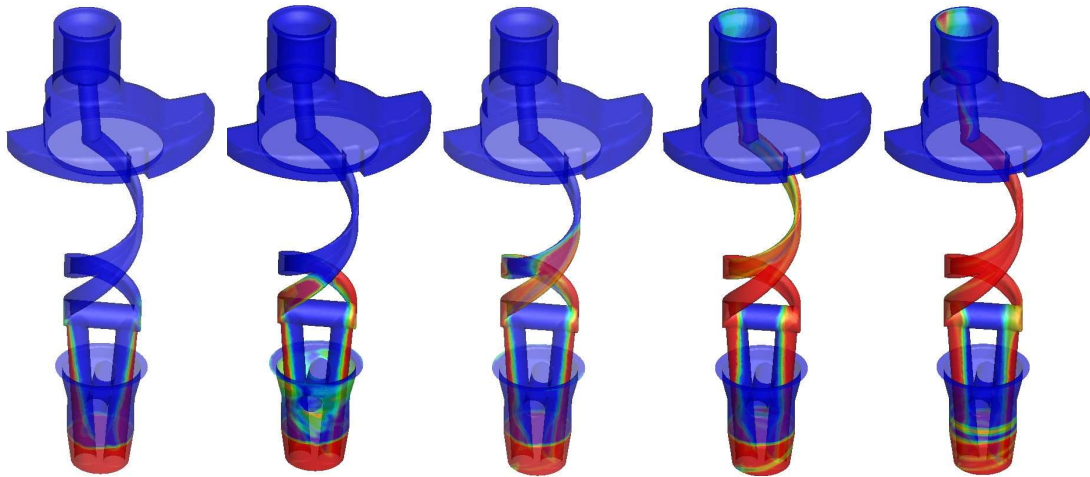


Figure 3.7 : Instantaneous oil phase fields with SM model at $t= 0.02, 0.04, 0.06, 0.14$ and 0.4 s. Oil volume fractions are colored from 0 (blue) to 1 (red).

Figure 3.8 shows the instantaneous isosurfaces of the oil volume fraction which clearly indicated the distribution of the lubricant inside the CIC at various time levels. The instantaneous isosurfaces of the oil volume fraction were obtained from SM method since the sliding mesh enabled to track the crankshaft position. The CutCell mesh had 1.2 million elements and time step was 5×10^{-5} seconds. To show the flow contours of the spreading oil from the uppermost of the crankshaft more clearly, a plane at the top of the crankshaft outlet was created. Oil contours were illustrated as isosurfaces on the plane.

The oil droplets at six different crankshaft positions were visualized from CFD simulations and the steady state conditions for a developed oil film distribution at 3000 rpm with infinite acceleration are given between $t=0.35$ and $t=0.5$ seconds. It is seen from Figure 3.8 that the amount of oil spreading out from the crankshaft is nearly the same in the snapshots. The instantaneous snapshots revealed the oil traveling inside the CIC and revealed how the solid parts of the CIC were lubricated during the operation cycle.

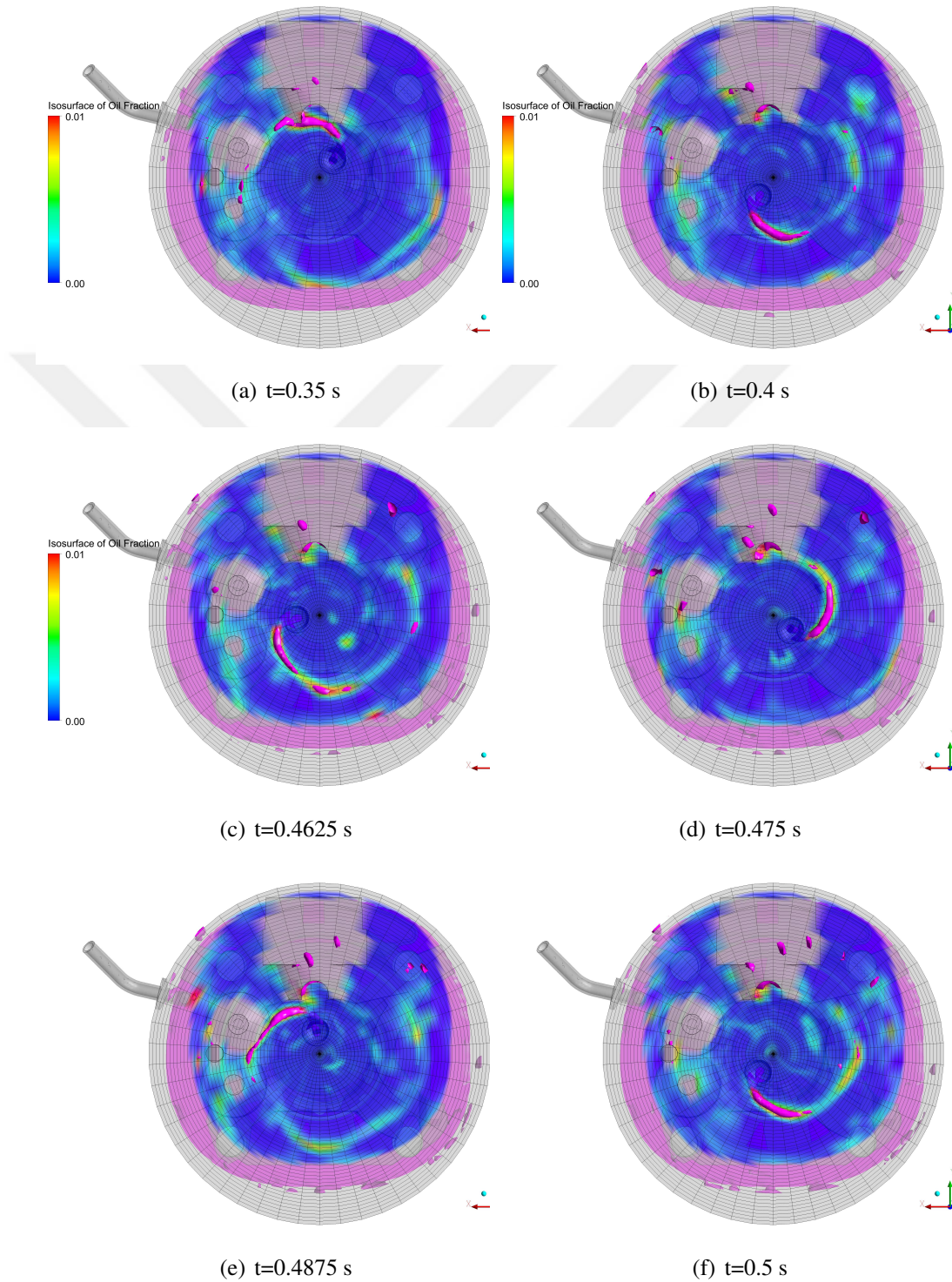


Figure 3.8 : Instantaneous isosurfaces of the oil volume fraction at 3000 rpm from the top-view of the CIC.

3.2.7 Effect of electrical motor acceleration

To test the effect of the crankshaft acceleration on the oil mass flow rates during start-up, linear acceleration data is derived from the flow visualization snapshots and two linear functions are fitted to the visual data as shown in Figure 3.9. These functions are implemented as motor start-up curves in the form of User Defined Function (UDF) into the CFD code which is represented by pink line in the Figure 3.9. This function reaches the 3000 rpm in 25 seconds thus the oil mass flow rates are increasing almost linearly after 8 seconds. Black circles represent the compressor speed obtained from the flow visualizations. The time step size is set equal to 5×10^{-4} seconds to reduce computational time.

As shown in Chapter 2.2.4 time required for sufficient lubrication is found around 6.8 seconds from flow visualizations. The climbing time of the oil is calculated 7.5 seconds with motor acceleration in the SM method. The speed of the electrical motor is around 1300 rpm at 7.5 seconds, which is close to lower operating limit of the compressor. Starting from that time, the oil mass flow rate increasing almost linearly. Figure 3.9 clearly demonstrates the oil climbing time and it also revealed the mass conservation is achieved between the crankshaft's inlet and outlet at 8 seconds.

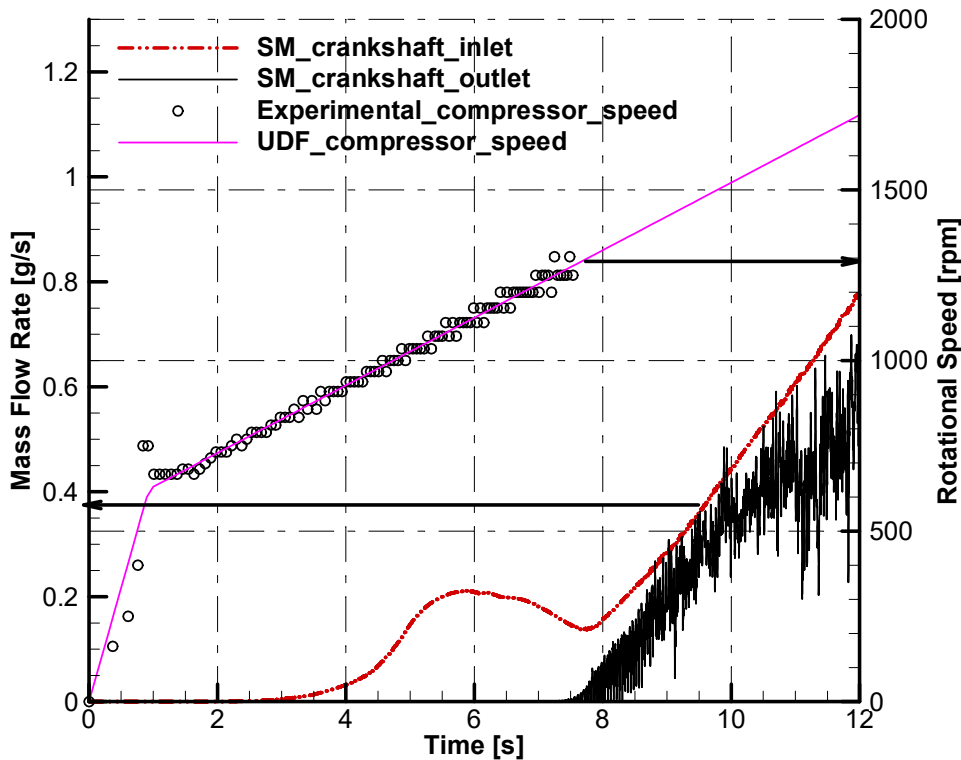


Figure 3.9 : Oil mass flow rate variation during CIC start-up.

Table 3.2 : Properties of investigated refrigerants.

Properties	Refrigerant		
Name	R600a	R290	Air
Density (kg/m^3)	2.46	1.91	1.225
Viscosity (kg/ms)	7×10^{-6}	7.95×10^{-6}	1.79×10^{-6}

3.2.8 Effect of refrigerant

As mentioned before, the air is used as a refrigerant in the analyses to compare numerical results with experiments. In the real operation of CIC, R600a is used as the refrigerant. Additionally, several mixtures of R600a/R290 are studied in the experimental studies. Table 3.2 presents the density and dynamic viscosity of the investigated refrigerants in the numerical calculations.

Figure 3.10 shows the lubrication performance of the CIC using R600a and R290 as the refrigerant. The oil mass flow rate increased relative to air approximately 10.3% and 7.5% for R600a and R290, respectively. It results that the increasing viscosity of the refrigerant has an inverse effect on the oil mass flow rate.

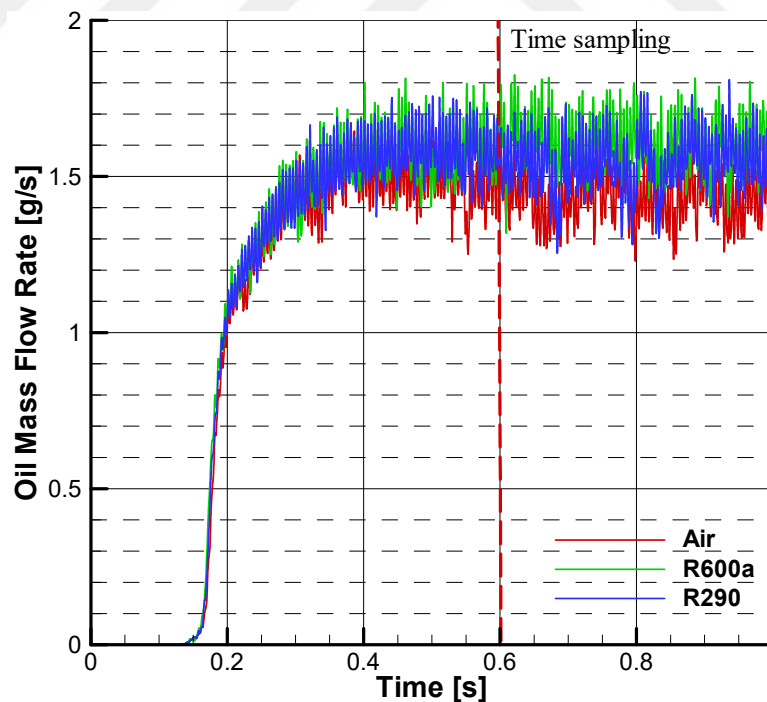


Figure 3.10 : Effect of refrigerant on the oil mass flow rate.

3.3 Moving Reference Frame Method

In the MRF method, the relative motion of a moving zone with respect to adjacent zones is not taken into account, in other words, the mesh is fixed. This means

freezing the motion of the crankshaft of a hermetic compressor in a fixed position and computing the instantaneous flow field with the crankshaft in the corresponding position. In many engineering applications, where a rotating part is present in the flow domain, MRF is widely preferred as the numerical approach. Some examples for this include turbomachinery applications with weak rotor-stator interaction, wind turbines and mixing tanks.

3.3.1 Computational model

Figure 3.11 shows the fixed domain used in MRF where the red part represents the crankshaft, the grey part is the outer wall around the crankshaft and the blue part is the oil sump.

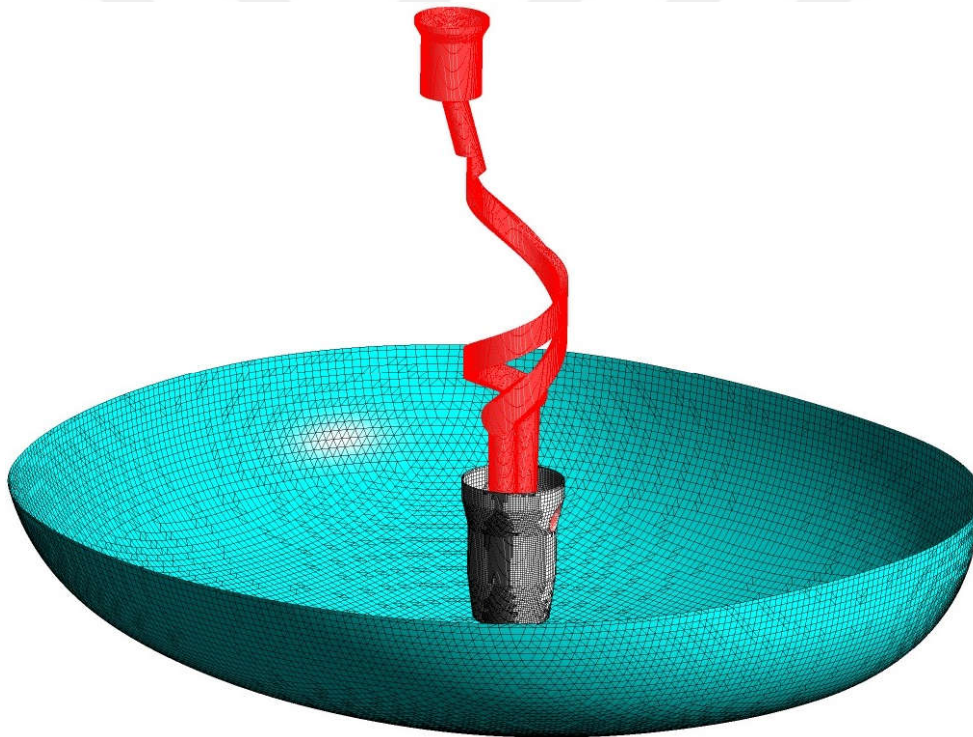


Figure 3.11 : Computational model of the MRF method.

The boundary conditions for the MRF method were defined as follows:

- Same pressure was imposed at the top of the free surface in the oil sump and crankshaft outlet.
- Angular velocity was defined on the walls of the crankshaft.
- All remaining walls and interfaces between domains were stationary.

- The thermophysical properties of all fluids were constant.

The two-phase flow in the oil lubrication system is simulated using the Volume of Fluid Method (VoF) under transient, laminar and incompressible flow conditions by using the finite volume based ANSYS-Fluent package.

Parallel computations have been performed on a 28-core processor computer using a second-order upwind scheme with appropriately selected underrelaxation factors for discretizing the continuity and momentum equations. The PISO (Pressure-Implicit with Splitting Operators) algorithm is used for pressure-velocity coupling since it is suitable for small time steps.

3.3.2 Governing equations

The absolute velocity formulation is used in the MRF method. In the below equations, \vec{v}_r is the relative velocity, \vec{v} is the absolute velocity, \vec{v}_t is the translational frame velocity and $\vec{\omega}$ corresponds the angular velocity. The velocity field was obtained from the discretization of the mass and momentum equations in MRF method given in Equation 3.7 and 3.8, respectively.

$$\frac{\partial \rho}{\partial t} + \nabla \cdot \rho \vec{v}_r = 0 \quad (3.7)$$

$$\frac{\partial}{\partial t}(\rho \vec{v}) + \nabla \cdot (\rho \vec{v}_r \vec{v}) + \rho [\omega \otimes (\vec{v} - \vec{v}_t)] = -\nabla p + \nabla \cdot \vec{\tau} + \vec{F} \quad (3.8)$$

3.3.3 Convergence tests

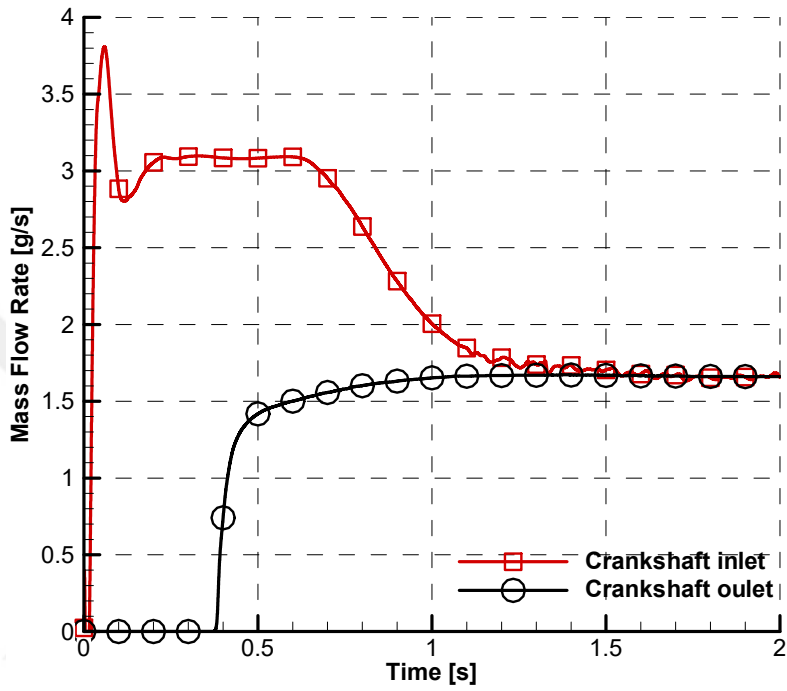
Table 3.3 indicates the mesh independency tests for MRF method. Relative errors in the averaged oil mass flow rates with respect to the solution from 1.3 million mesh are calculated for the determination of the resulting mesh for that method.

Table 3.3 : Mesh independence tests for MRF method.

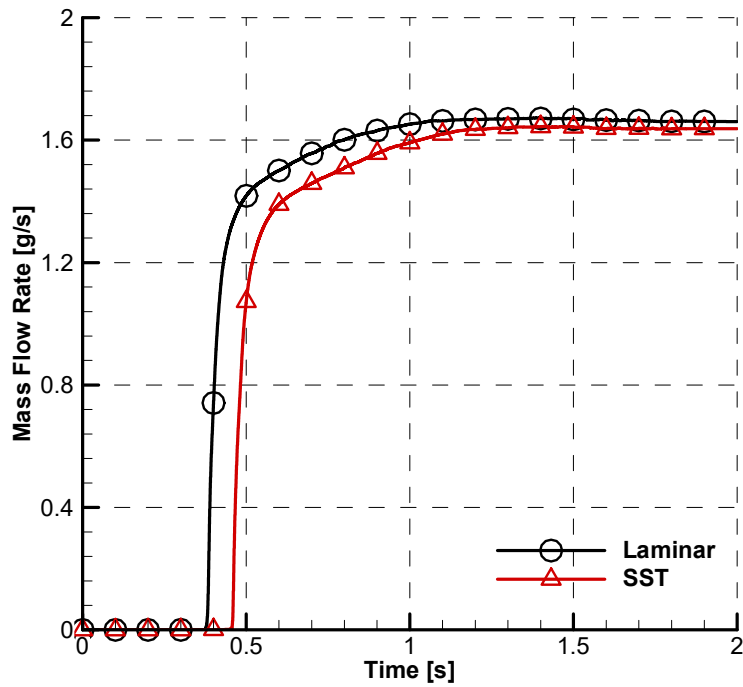
Case ID	Averaged Oil Mass Flow Rate [gs^{-1}]	Relative Error [%]
CutCell, 986 K	1.61	22
CutCell, 1.3 M	1.32	-
CutCell, 2.7 M	1.3	-1.5

The flow is assumed to be laminar but the effect of another flow solver is tested using the SST (Shear Stress Transport) model which is capable of both modeling laminar and

transitional regimes. It is shown in Figure 3.12 (a) that there is no evident difference between the numerical results obtained from laminar flow solver and SST model, hence there is no need to use transitional SST model. Moreover, the inlet and outlet oil mass flow rates of the crankshaft are plotted in the Figure 3.12 (b). The oil mass flow rate of the inlet and outlet of the crankshaft is equalized at approximately 1.5 seconds.



(a)



(b)

Figure 3.12 : a) Effect of flow solver b) Mass flow rate variations with respect to time.

3.3.4 Effect of rotational speed

To compare the performance of oil mass flow rate predictions of the MRF method, rotational speed tests are applied with the same test condition with the SM method. The effect of the rotational speed on the oil mass flow rate is shown in Figure 3.13. The time-dependent change of the oil mass flow rate is shown for eight different rotational speeds. Although the calculation time in the SM method is 1 second, this time is extended to 2 seconds due to the slow convergence of the oil mass flow rate with the MRF method.

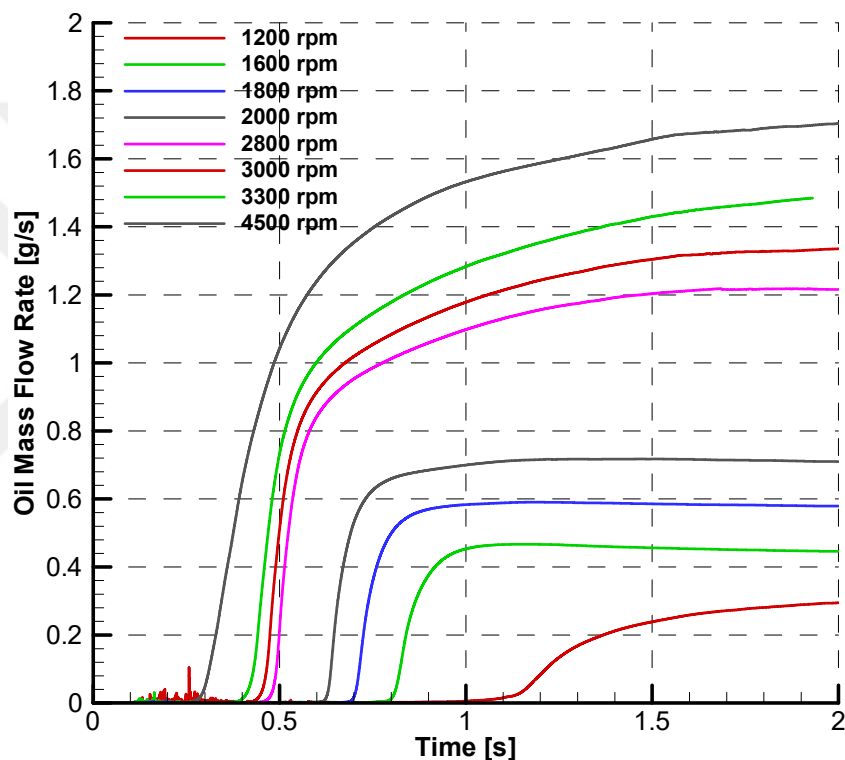


Figure 3.13 : Effect of rotational speed on the oil mass flow rate.

As shown in Figure 3.13, the oil mass flow rate is increasing with increments of the rotational speed as expected. When the oil mass flow rate results of the MRF method and the SM method are compared, it is seen that the MRF method produces higher oil mass flow rate results at rotational speeds below 2600 rpm. In addition, MRF yields lower mass flow rate estimations than SM method at speeds above 2800 rpm. Moreover, the MRF method predicts oil mass flow rate to 0.33 g/s at 1200 rpm whereas no oil mass flow rate is observed with the SM method. In addition the oil climbing time is found approximately 1 second at 1200 rpm. The increase in the oil mass flow rate is almost linear between 1500 and 2600 rpm.

The comparison with experimental results given in Figure 2.37 shows that the MRF method produces better estimates for crankshaft speeds less than 2600 rpm. On the other hand, there are large differences between the predictions and experiments above 3600 rpm. Another finding is that the MRF method underestimates the oil mass flow rate for the operating range of CIC.

3.3.5 Effect of viscosity

To investigate the effect of viscosity, various oil viscosities such as 3, 5, 10 and 15 cSt are examined at 4500 rpm. As shown in Figure 3.14, with increasing oil viscosity the oil mass flow rate is also decreasing. Moreover, oil climbing time is decreasing with decrements of the viscosity.

It is revealed that both CFD methods show similar trends with respect to the change of viscosity. The flow zone between the first and main journal bearing is numerically modeled as a closing channel whereas, in reality, there is a small gap between the surface of the body and the crankshaft. Therefore, it is considered that increasing viscosity has a greater negative impact on numerical solutions relative to the experimental results.

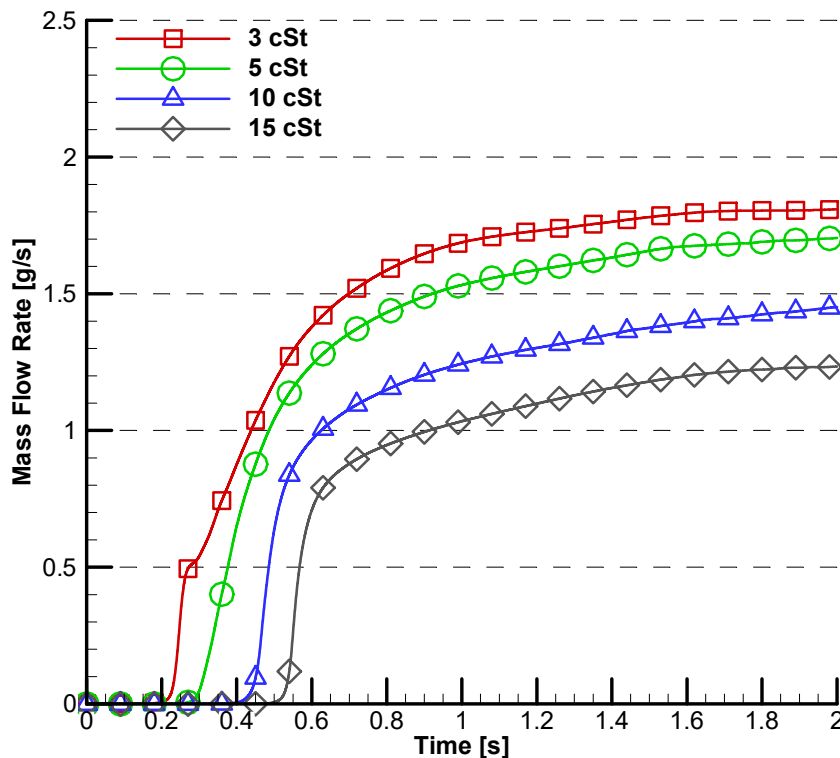


Figure 3.14 : Effect of viscosity on the oil mass flow rate.

Table 3.4 : Properties of RENISO WF10 A.

Characteristic	Mineral oil
Density at 15 °C kg/m^3	833
Kinematic viscosity at 40 °C mm^2/s	9.6
Kinematic viscosity at 100 °C mm^2/s	2.6

3.3.6 Effect of refrigerant dissolving in the oil

Refrigerant dissolving in the oil is causing viscosity change depending on the mass fraction of the oil as mentioned in Chapter 2.1.4. Kinematic viscosity of RENISO WF10 A/R600a mixture is obtained from Figure 2.30 for 100%, 95%, 90% and 85% oil concentration (mass fraction) which correspond to 9.6, 6.2, 4.3 and 3 cSt, respectively. The properties of the RENISO WF10 A is given in Table 3.4.

The computations are carried out at 1500, 2000 and 2600 rpm with the MRF method. It is seen that the oil mass flow rate increases almost linearly with the rotational speed in all cases. The difference in the oil mass flow rate is increasing with increments of the rotational speed. It is concluded that the refrigerant dissolving in the oil decreases the mixture viscosity and increases the oil mass flow rate of the lubrication system in the MRF method.

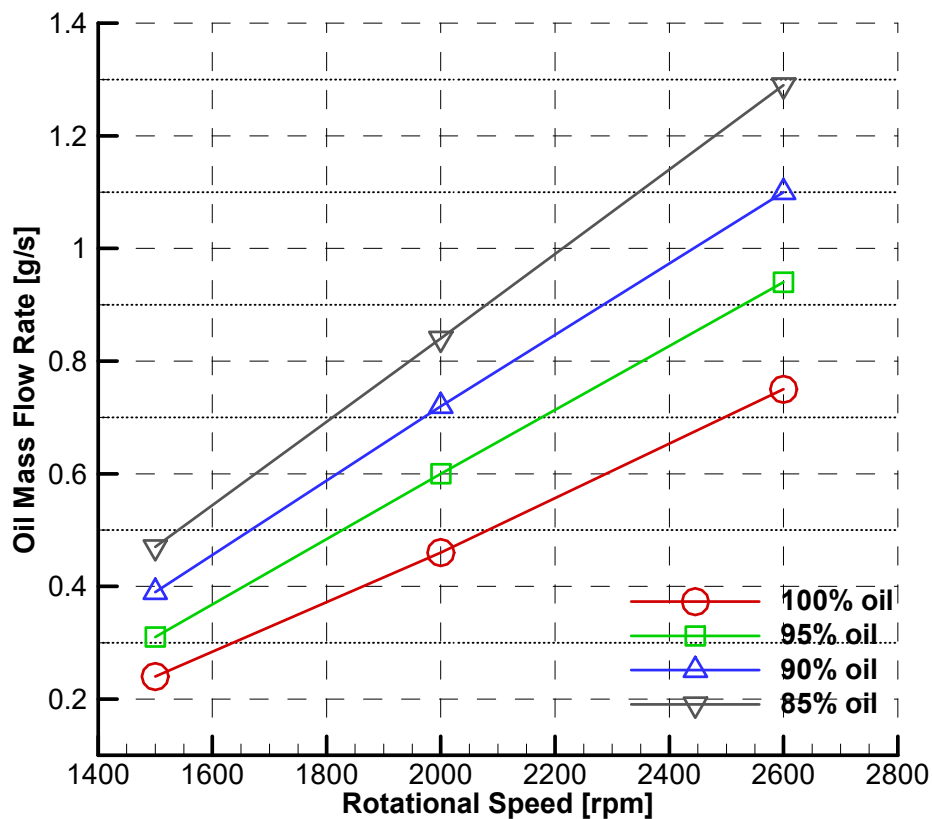


Figure 3.15 : Effect of refrigerant dissolving in the oil on the oil mass flow rate.

3.3.7 Instantaneous flow fields

Figure 3.16 shows the instantaneous oil phase fields carried out with the MRF method. As stated before, the crankshaft is fixed in a specified position and the instantaneous oil phase is visualized at 0.05, 0.1, 0.2, 0.3, 0.4 and 2 seconds. Oil climbing time is calculated at approximately 0.45 seconds. Analyses are carried out at 3000 rpm with 5 cSt oil. It is shown that the SM method fills the flow area much faster than the MRF method with infinite acceleration.

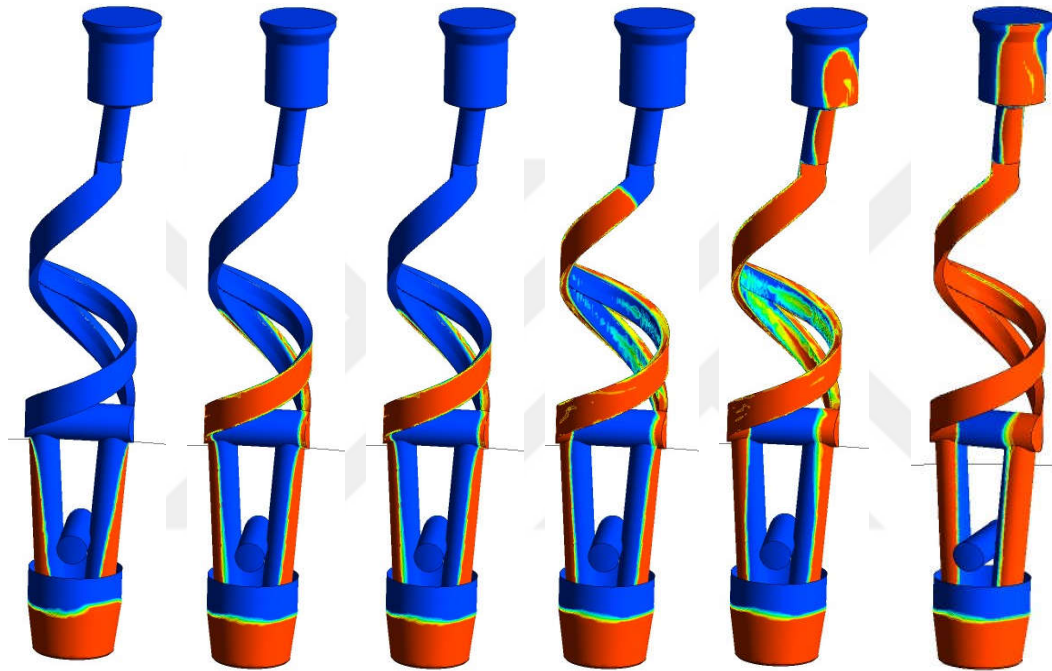


Figure 3.16 : Instantaneous oil phase fields with MRF model at $t=0.05, 0.1, 0.2, 0.3, 0.4$ and 2 s. Oil volume fractions are colored from 0 (blue) to 1 (red).

3.3.8 Effect of electrical motor acceleration

The effect of motor acceleration is investigated with the MRF method implemented via UDF in the program. Thanks to the rapid solution of the MRF method, the computational run time is selected as 27.5 seconds in the simulation. The y- axis on the right-hand side shows the rotational speed of the CIC, while the left axis shows the oil mass flow rate for the inlet and outlet of the crankshaft in Figure 3.17 . The rotational speed of the crankshaft increases to 3000 rpm in 25 seconds. Transient velocity function implemented by the UDF derived from the flow visualization tests which are indicated by the circle symbol. The mass flow of oil entering and exiting the crankshaft is equalized after 12 seconds. Although the oil climbing time appears to be

around 3 seconds, the significant increase in the oil flow rate is around 8 seconds. In this context, it is seen that numerical methods and flow visualization tests give similar results related to oil climbing at the transient acceleration of the CIC. The oil mass flow rate changes almost linearly with the rotational speed after 10 seconds.

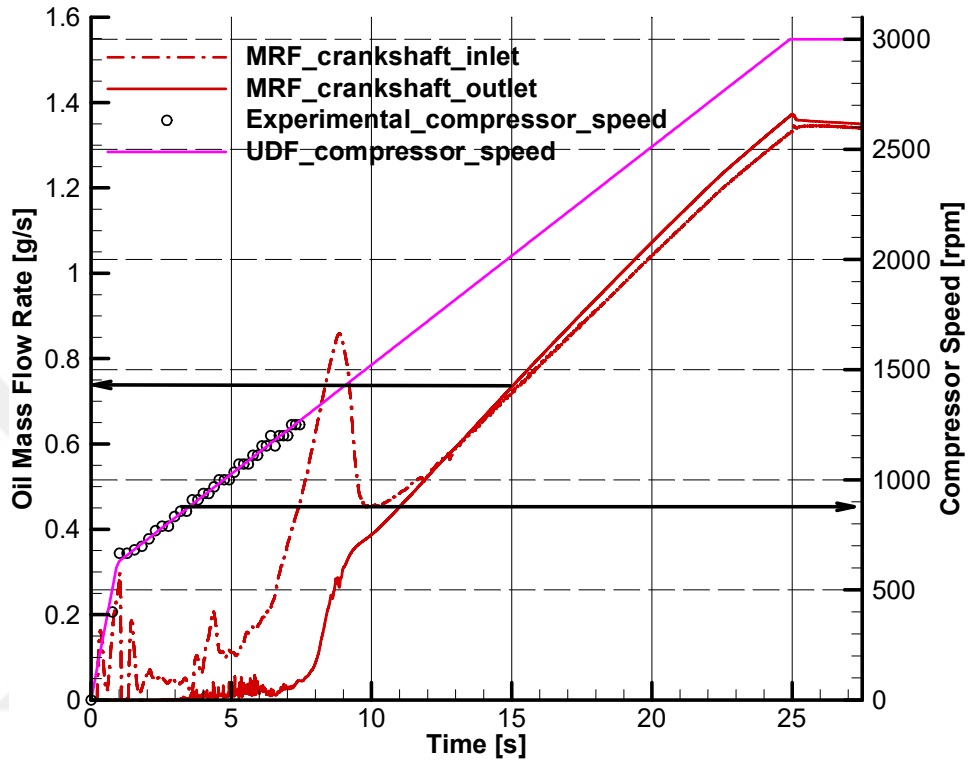


Figure 3.17 : Oil mass flow rate variation during CIC start-up with the MRF method.

3.4 Concluding Remarks

The lubrication system of the hermetic compressor is investigated numerically in this chapter. Two different methods namely SM and MRF are performed in the numerical calculations. In this context, mesh independence tests are carried out for both methods. The time step tests are carried out for various time step sizes. The effect of rotational speed, viscosity and electrical motor acceleration on the oil mass flow rate are investigated for both CFD methods. Figure 3.18 presents the predictions of oil mass flow rate of the SM and MRF methods are compared with experimental results. Besides, instantaneous oil flow fields are visualized for both CFD methods and oil climbing time is derived for both real and infinite acceleration. The main conclusions are summarized as follows:

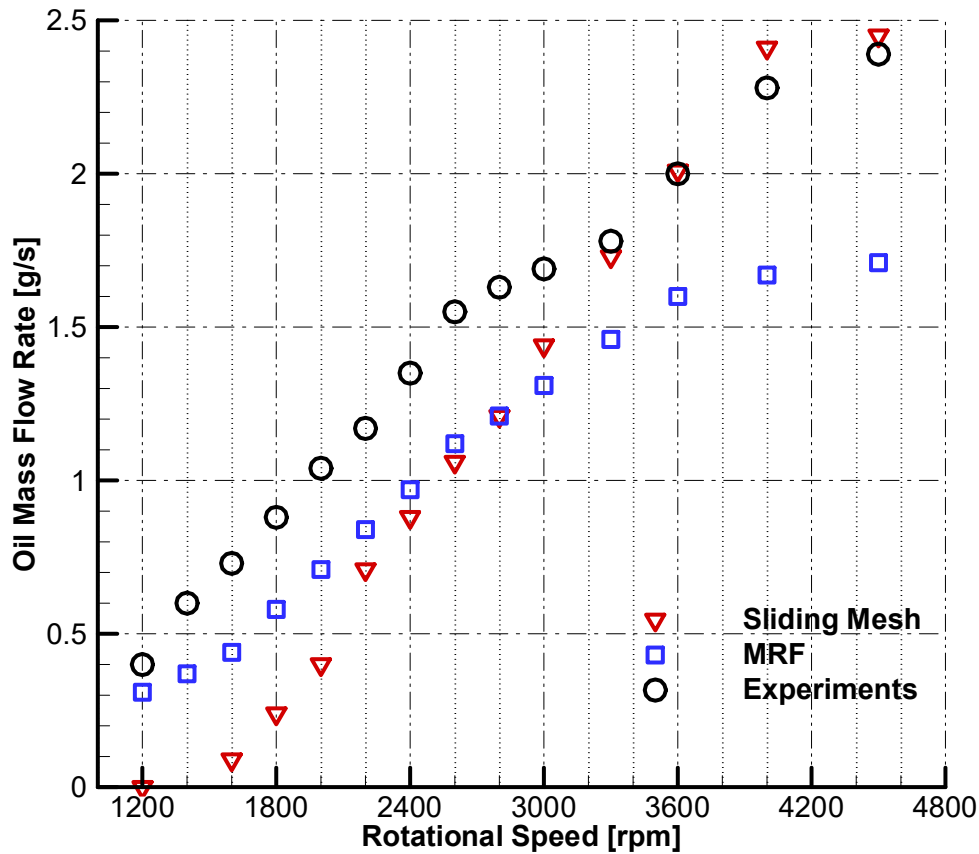


Figure 3.18 : Comparison of CFD results with experiments.

- The measurements are carried out in an environment subjected to the same boundary conditions as in simulations revealing that both CFD methods could have different tendencies at various crankshaft speeds.
- Figure 3.18 shows the comparison of the predicted averaged mass flow rates at all crankshaft speeds with the measurements for 5 cSt oil at an immersion depth of 11.5 mm. As Figure 3.18 indicates, in the range between 1200 and 2600 rpm, the measurements showed a monotone increase. In this range, all the CFD results are lower than the experimental results and the MRF predictions were relatively closer to the measurements than the SM predictions.
- Figure 3.18 presents, in the range between 3000 and 4500 rpm, SM predictions agreed better with the measurements than the MRF predictions. It should be noted that, the increase in the oil mass flow rates converged to a value indicating that, there was only a slight change after a critical crankshaft speed. It is shown that, after 3300 rpm, the discrepancies between the MRF results and the measurements were considerably high.

- The SM solutions were fluctuating during time sampling which is not the case in the MRF solutions. No oil was observed from the crankshaft outlet in the SM method at 1200 rpm and the rate of change of the oil mass flow rates was steeper compared to MRF method.
- The numerical results obtained from MRF were closer to the measurements up to 2600 rpm. The SM method became favorable as a CFD method due to better agreement with measurements between 3000 and 4500 rpm.
- The MRF method is cost-effective in terms of simulation time.
- Although the number of mesh has insignificant impact on the oil mass flow rate, the choice of time step size is very important in predicting the mass flow rate.
- As the viscosity increases, the oil mass flow rate estimates decrease for both solution methods.
- The maximum oil mass flow rate is converging to 2.5 g/s in SM method, which is very close to the experimental result.
- Oil climbing time is faster in the SM method for the infinite acceleration of the crankshaft. To test the effect of the crankshaft acceleration on the oil mass flow rates during start-up, linear acceleration data is derived from the flow visualization snapshots and two linear functions are introduced in the CFD code. These results present although the MRF method predicts lower oil climbing time, the linear increase in the oil mass oil flow rate is observed for approximately 7.5 s in both CFD methods. At that time, the corresponding compressor speed is around 1300 rpm, and this speed is very close to the compressor lower operating limit of 1200 rpm. In the flow visualization experiments, transition from oil droplets to an oil film is captured around 6.8 s, which is called, required time for sufficient lubrication.



4. CONCLUSIONS

In this study, the effects of zeotropic refrigerant mixtures are investigated to increase the energy efficiency of the refrigeration system by using new refrigerant blends with appropriate lubricants and additives which are less harmless and more environment-friendly compared to conventional refrigerants. In order to do so, brief investigations are conducted on the household refrigeration systems mainly focused on hermetic reciprocating compressor and evaporator.

In Chapter 2, the experimental investigations are presented in detail. This chapter divided into two sections, namely the Effect of Refrigerant Mixtures on the Household Refrigeration System and the Lubrication System of the Compact Inverter Compressor and . In this context, in house refrigerant mixtures test stand is constructed to test the effect of different refrigerant mixtures on the compressor performance. First, R600a is tested as a base refrigerant in the system. Then the refrigerant mixtures R600a/R290(30%/70% by weight), R600a/R290 (40%/60% by weight) and R600a/R290 (60%/40% by weight) are tested. The relative increase in COP of R600a/R290 (40%/60% by weight) is calculated as 6.15%, 12.15%, 16.47% and 23.29% for 1500, 2100, 3000 and 4500 rpm, respectively. Moreover, the effect of condensation and evaporation temperature on the COP is studied. It is found that with increasing evaporation and decreasing condensation temperature, the COP is increased. The results of the refrigerant mixtures test stand are compared with the results of the calorimeter test stand at ASHRAE conditions for four different compressor speeds. It is reported that the relative increase in COP is observed between 7.4% and 29.7%, with an increment towards higher compressor speeds, in the calorimeter test stand. It is determined that the use of R600a/R290 refrigerant mixture in household refrigeration compressors is more beneficial in terms of energy efficiency. In the second section, in house lubrication test stand is designed for the measuring oil flow rate of the compressor. The lubrication experiments are carried out between 1200 to 4500 rpm. The results reveal that the oil mass flow rate of the lubrication system is

increasing with the rotational speed. Besides, the effect of oil viscosity is investigated. The flow field of the lubrication system is identified as two different zones. It is found that there is a trade-off in the oil mass flow rate depending on the viscous and centrifugal forces in the lubrication system. It is pointed that centrifugal forces are found dominant especially in the range after 1800 rpm. Moreover, flow visualizations are carried out with a high-speed camera. The start-up and steady-state lubrication pattern inside of the compressor are visualized. The oil climbing time is seen at 0.75 s, and the transition of oil from droplets to the film is captured at 6.8 s, which is defined as the required time for sufficient lubrication. Moreover, the corresponding compressor speed at 6.8 s is near 1200 rpm, and lubrication tests revealed that it is unsafe to run compressor below this speed. The experimental results of the oil tests are used to validate CFD predictions.

In Chapter 3, numerical investigations are presented in detail. This chapter is divided into two sections. Firstly, the numerical modeling of the lubrication system of a compact inverter compressor (CIC) is presented. In the numerical modeling, a finite volume-based ANSYS-Fluent package is used to model two-phase (air-oil) flow inside the compressor using the Volume of Fluid Method (VoF) method. Transient behavior of the oil flow under laminar flow conditions is both simulated by imposing Sliding Mesh (SM) and the Moving Reference Frame (MRF) methods at various crankshaft speeds varying between 1200 and 4500 rpm. The measurements are used to compare/validate CFD results obtained from SM and MRF methods. It is reported that in the range between 1200 and 2600 rpm, the measurements showed a monotone increase. In this range, the CFD methods underestimate the oil mass flow rate and the MRF predictions are relatively close to the measurements than the SM predictions. In addition, in the range between 3000 and 4500 rpm, SM predictions agreed better with the measurements than the MRF predictions. It should be noted that the increase in the mass flow rates converged to a value indicating that, there was only a slight change after a critical crankshaft speed. It is shown that, after 3300 rpm, the discrepancies between the MRF results and the measurements are considerably high. The SM predictions are fluctuating during time sampling which is not the case in the MRF predictions. No oil is observed at the crankshaft outlet in the SM method at 1200 rpm and the rate of change of the oil mass flow rates is steeper compared to the MRF method.

In addition, the effect of viscosity is investigated with SM and MRF methods. It is shown that with increasing viscosity, the oil mass flow rate estimates decrease for both solution methods. It is shown that although the number of mesh has an insignificant impact on the oil mass flow rate, the choice of time step size is very important in predicting the mass flow rate. It is noted that the MRF method is cost-effective in terms of simulation time. Oil climbing time is faster in the SM method for the infinite acceleration of the crankshaft. Moreover, the acceleration of the crankshaft determined via a high-speed camera employed as a user-defined function to model the start-up period of the compressor. These results present although the MRF method predicts lower oil climbing time, the linear increase in the oil mass oil flow rate is observed for approximately 7.5 s in both CFD methods. At that time the corresponding compressor speed is around 1300 rpm, and this speed is very close to the compressor's lower operating limit of 1200 rpm. In the flow visualization experiments, the transition from oil droplets to an oil film is captured around 6.8 s, which is called, the required time for sufficient lubrication.



REFERENCES

- [1] **Coulomb, D., Dupont, J. and A., P.** (2015). The Role of Refrigeration in the Global Economy, 29th Informatory Note on refrigeration technologies, *International Institute of Refrigeration*.
- [2] **Coulomb, D., Dupont, J. and M., V.** (2017). The Impact of the Refrigeration Sector on Climate Change, *International Institute of Refrigeration*.
- [3] **Cengel, Y.A. and Boles, M.A.** (2004). *Thermodynamics: An Engineering Approach Seventh Edition*, McGraw-Hill Companies.
- [4] **Dinçer, I. and Kanoğlu, M.** (2010). *Refrigeration Systems and Applications, Second Edition*.
- [5] **Gaspar, P. and Da Silva, P.** (2015). *Handbook of research on advances and applications in refrigeration systems and technologies*.
- [6] **Calm, J.** (2008). The next generation of refrigerants - Historical review, considerations, and outlook, *International Journal of Refrigeration*, 31(7), 1123–1133.
- [7] **Hundy, G., Trott, A. and Welch, T.** (2008). *Refrigeration and Air-Conditioning*.
- [8] **UNEP** (2011). *HFCs: A Critical Link in Protecting Climate and the Ozone Layer*, United Nations Environment Programme (UNEP).
- [9] **Velders, G.J.M., Fahey, D.W., Daniel, J.S., McFarland, M. and Andersen, S.O.** (2009). The large contribution of projected HFC emissions to future climate forcing, *Proceedings of the National Academy of Sciences*, 106(27), 10949–10954.
- [10] **WMO** (2018). *Scientific Assessment of Ozone Depletion: 2018*, WMO (World Meteorological Organization).
- [11] **Velders, G.J., Fahey, D.W., Daniel, J.S., Andersen, S.O. and McFarland, M.** (2015). Future atmospheric abundances and climate forcings from scenarios of global and regional hydrofluorocarbon (HFC) emissions, *Atmospheric Environment*, 123, 200 – 209.
- [12] **Hanlon, P.** (2001). *Compressor handbook*, McGraw-Hill Handbooks Series, McGraw-Hill.
- [13] **Dossat, R.** (1961). *Principles of refrigeration*, Wiley.
- [14] **Fuchs Schmierstoffe GmbH** (2018). *Refrigeration Oils 2018/2019*.

- [15] **Mulroy, W., Domanski, P. and Didion, D.** (1994). Glide matching with binary and ternary zeotropic refrigerant mixtures Part 1. An experimental study, *International Journal of Refrigeration*, 17(4), 220 – 225.
- [16] **Domanski, P., Mulroy, W. and Didion, D.** (1994). Glide matching with binary and ternary zeotropic refrigerant mixtures Part 2. A computer simulation, *International Journal of Refrigeration*, 17(4), 226 – 230.
- [17] **Hansen, P., Snitkjaer, L., Skovgaard, M. and Riemer, A.** (1994). Development of Small Hermetic Compressors for R600a, *International Compressor Engineering Conference*.
- [18] **Camporese, R., Bobbo, S. and Rozza, F.** (1994). Hydrocarbons as Substitutes for Halogenated Refrigerants in Refrigerating Systems, *International Refrigeration and Air Conditioning Conference*.
- [19] **Uchida, M., Itoh, M., Shikazono, N. and Kudoh, M.** (1996). Experimental Study on the Heat Transfer Performance of a Zeotropic Refrigerant Mixture in Horizontal Tubes, *International Refrigeration and Air Conditioning Conference*.
- [20] **Yilmaz, M.** (2003). Performance analysis of a vapor compression heat pump using zeotropic refrigerant mixtures, *Energy Conversion and Management*, 44(2), 267 – 282.
- [21] **Navarro, E., Urchueguía, J., González, J. and Corberán, J.** (2005). Test results of performance and oil circulation rate of commercial reciprocating compressors of different capacities working with propane (R290) as refrigerant, *International Journal of Refrigeration*, 28(6), 881 – 888.
- [22] **Park, K.J. and Jung, D.** (2007). Thermodynamic performance of HCFC22 alternative refrigerants for residential air-conditioning applications, *Energy and Buildings*, 39(6), 675 – 680.
- [23] **Greco, A.** (2008). Convective boiling of pure and mixed refrigerants: An experimental study of the major parameters affecting heat transfer, *International Journal of Heat and Mass Transfer*, 51(3), 896 – 909.
- [24] **Mani, K. and Selladurai, V.** (2008). Experimental analysis of a new refrigerant mixture as drop-in replacement for CFC12 and HFC134a, *International Journal of Thermal Sciences*, 47(11), 1490 – 1495.
- [25] **Lee, M.Y., Lee, D.Y. and Kim, Y.** (2008). Performance characteristics of a small-capacity directly cooled refrigerator using R290/R600a (55/45), *International journal of Refrigeration*, 31(4), 734–741.
- [26] **Calm, J.M.** (2008). The next generation of refrigerants – Historical review, considerations, and outlook, *International Journal of Refrigeration*, 31(7), 1123 – 1133.
- [27] **Leighton, D.T.** (2011). *Investigation of household refrigerator with alternative low global warming potential refrigerants*. (Master's thesis). University of Maryland, College Park.

- [28] **Jin, X. and Zhang, X.** (2011). A new evaluation method for zeotropic refrigerant mixtures based on the variance of the temperature difference between the refrigerant and heat transfer fluid, *Energy Conversion and Management*, 52(1), 243 – 249.
- [29] **Navarro-Esbrí, J., Mendoza-Miranda, J., Mota-Babiloni, A., Barragán-Cervera, A. and Belman-Flores, J.** (2013). Experimental analysis of R1234yf as a drop-in replacement for R134a in a vapor compression system, *International Journal of Refrigeration*, 36(3), 870 – 880.
- [30] **Lee, Y., gyu Kang, D. and Jung, D.** (2013). Performance of virtually non-flammable azeotropic HFO1234yf/HFC134a mixture for HFC134a applications, *International Journal of Refrigeration*, 36(4), 1203 – 1207.
- [31] **Mota-Babiloni, A., Navarro-Esbrí, J., Ángel Barragán, Molés, F. and Peris, B.** (2014). Theoretical comparison of low GWP alternatives for different refrigeration configurations taking R404A as baseline, *International Journal of Refrigeration*, 44, 81 – 90.
- [32] **McLinden, M.O., Kazakov, A.F., Brown, J.S. and Domanski, P.A.** (2014). A thermodynamic analysis of refrigerants: Possibilities and tradeoffs for Low-GWP refrigerants, *International Journal of Refrigeration*, 38, 80 – 92.
- [33] **Mota-Babiloni, A., Navarro-Esbrí, J., Ángel Barragán-Cervera, Molés, F. and Peris, B.** (2015). Experimental study of an R1234ze(E)/R134a mixture (R450A) as R134a replacement, *International Journal of Refrigeration*, 51, 52 – 58.
- [34] **Mota-Babiloni, A., Navarro-Esbrí, J., Ángel Barragán-Cervera, Molés, F. and Peris, B.** (2015). Analysis based on EU Regulation No 517/2014 of new HFC/HFO mixtures as alternatives of high GWP refrigerants in refrigeration and HVAC systems, *International Journal of Refrigeration*, 52, 21 – 31.
- [35] **Bohdal, T., Charun, H. and Sikora, M.** (2015). Empirical study of heterogeneous refrigerant condensation in pipe minichannels, *International Journal of Refrigeration*, 59, 210 – 223.
- [36] **Deng, H., Fernandino, M. and Dorao, C.A.** (2015). Numerical Study of the Condensation Length of Binary Zeotropic Mixtures, *Energy Procedia*, 64, 43 – 52, 3rd Trondheim Gas Technology Conference, 4-5 June, 2014.
- [37] **Tian, Q., Cai, D., Ren, L., Tang, W., Xie, Y., He, G. and Liu, F.** (2015). An experimental investigation of refrigerant mixture R32/R290 as drop-in replacement for HFC410A in household air conditioners, *International Journal of Refrigeration*, 57, 216 – 228.
- [38] **Yan, G., Cui, C. and Yu, J.** (2015). Energy and exergy analysis of zeotropic mixture R290/R600a vapor-compression refrigeration cycle with separation condensation, *International journal of refrigeration*, 53, 155–162.

- [39] **d'Angelo, J.V.H., Aute, V. and Radermacher, R.** (2016). Performance evaluation of a vapor injection refrigeration system using mixture refrigerant R290/R600a, *International journal of refrigeration*, 65, 194–208.
- [40] **Antunes, A.H.P. and Filho, E.P.B.** (2016). Experimental investigation on the performance and global environmental impact of a refrigeration system retrofitted with alternative refrigerants, *International Journal of Refrigeration*, 70, 119 – 127.
- [41] **Chen, Q., Yu, J. and Yan, G.** (2016). Performance analysis of a modified zeotropic mixture (R290/R600) refrigeration cycle with internal subcooler for freezer applications, *Applied Thermal Engineering*, 108, 172 – 180.
- [42] **Popovic, P.** (1999). *Investigation and analysis of lubricant effects on the performance of an HFC-134a refrigeration system.* (Ph.D. dissertation). Iowa State University, Iowa.
- [43] **Lottin, O., Guillemet, P. and Lebreton, J.M.** (2003). Effects of synthetic oil in a compression refrigeration system using R410A. Part I: modelling of the whole system and analysis of its response to an increase in the amount of circulating oil, *International Journal of Refrigeration*, 26(7), 772 – 782.
- [44] **Wei, W., Ding, G., Hu, H. and Wang, K.** (2007). Influence of lubricant oil on heat transfer performance of refrigerant flow boiling inside small diameter tubes. Part I: Experimental study, *Experimental Thermal and Fluid Science*, 32(1), 67 – 76.
- [45] **Wei, W., Ding, G., Hu, H. and Wang, K.** (2007). Influence of lubricant oil on heat transfer performance of refrigerant flow boiling inside small diameter tubes. Part II: Correlations, *Experimental Thermal and Fluid Science*, 32(1), 77 – 84.
- [46] **Hu, H., Ding, G., Wei, W., Wang, Z. and Wang, K.** (2008). Heat transfer characteristics of R410A-oil mixture flow boiling inside a 7mm straight smooth tube, *Experimental Thermal and Fluid Science*, 32(3), 857 – 869.
- [47] **Youbi-Idrissi, M. and Bonjour, J.** (2008). The effect of oil in refrigeration: Current research issues and critical review of thermodynamic aspects, *International Journal of Refrigeration*, 31(2), 165 – 179.
- [48] **Prata, A.T. and Barbosa Jr, J.R.** (2009). Role of the thermodynamics, heat transfer, and fluid mechanics of lubricant oil in hermetic reciprocating compressors, *Heat Transfer Engineering*, 30(7), 533–548.
- [49] **Tas, S., S., C., Gunes, H., Sarioglu, K. and Kerpicci, H.** (2014). Experimental investigation of oil flowrate in a hermetic reciprocating compressor, *Engineering Systems Design and Analysis*.
- [50] **Tas, S.** (2014). *Experimental investigation of in a hermetic reciprocating compressor.* (Master's thesis). Istanbul Technical University, Istanbul.

- [51] **Kim, H.S., Yoon, P.H., Sa, Y.C., Chung, B.Y. and Kim, M.S.** (2014). A study on the flow characteristics of refrigerant and oil mixture in compressor suction line, *International Journal of Refrigeration*, 48, 48–59.
- [52] **Górny, K., Stachowiak, A., Tyczewski, P. and Zwierzycki, W.** (2016). Lubricity evaluation of oil–refrigerant mixtures with R134a and R290, *international Journal of Refrigeration*, 69, 261–271.
- [53] **Pizarro-Recabarren, R.A. and Barbosa, J.R.** (2016). The effect of the lubricating oil on heat transfer in a hermetic reciprocating compressor, *Journal of the Brazilian Society of Mechanical Sciences and Engineering*, 38(1), 189–208.
- [54] **Ido, S., Sasaki, T., Mizuno, K. and Koyama, S.** (2018). Tribological Properties of Sliding Elements in Refrigerant Compressors Lubricated by Low-GWP Refrigerant/Oil mixtures, *International Compressor Engineering Conference*.
- [55] **Ozsipahi, M., Cadirci, S., Gunes, H., Sarioglu, K. and Kerpicii, H.** (2014). A numerical study on the lubrication system for a hermetic reciprocating compressor used in household refrigerators, *International journal of refrigeration*, 48, 210–220.
- [56] **Ozsipahi, M., Cadirci, S., Gunes, H. and Sarioglu, K.** (2016). A COMPARISON OF AN ANALYTICAL AND NUMERICAL FLOW MODEL FOR THE LUBRICATION SYSTEM OF A VARIABLE SPEED HERMETIC, *Journal of Thermal Science and Technology*, 36.
- [57] **Lückmann, A.J., Alves, M.V.C. and Barbosa Jr, J.R.** (2009). Analysis of oil pumping in a reciprocating compressor, *Applied Thermal Engineering*, 29(14-15), 3118–3123.
- [58] **Tada, M., Hoffmann, T., Couto, P., Manke, A. and Bortoli, M.** (2014). Numerical and Experimental Examination for Oil Pump System Using a Simplified Uncoupled Simulation Model, *International Compressor Engineering Conference*.
- [59] **Kerpicii, H., Yagci, A. and Onbasioglu, S.U.** (2013). Investigation of oil flow in a hermetic reciprocating compressor, *International Journal of Refrigeration*, 36(1), 215–221.
- [60] **Alves, M.V., Barbosa, J.R., Prata, A.T. and Ribas, F.A.** (2011). Fluid flow in a screw pump oil supply system for reciprocating compressors, *International Journal of Refrigeration*, 34(1), 74 – 83.
- [61] **Zhu, Y., He, G., Sun, W., Shimoji, M. and Chen, X.** (2019). Effect of oil stirrer on the performance of oil supply system for a variable speed rotary compressor, *International Journal of Refrigeration*.
- [62] **Kovacevic, A., Stosic, N. and Smith, I.K.** (2003). Three dimensional numerical analysis of screw compressor performance, *Journal of Computational Methods in Sciences and Engineering*, 3(2), 259–284.

- [63] **Liu, Z. and Hill, D.** (2000). Issues Surrounding Multiple Frames of Reference Models for Turbo Compressor Applications, *International Compressor Engineering Conference*.
- [64] **Deng, L., Liang, S., Xu, J. and Yusheng, H.** (2016). CFD Analysis and Experiment Study of the Rotary Two-Stage Inverter Compressor with Vapor Injection, *International Compressor Engineering Conference*.
- [65] **Ozsipahi, M., Gunes, H. and Kerpicci, H.** (2018). On the CFD Modeling Approach of Lubrication System for a Hermetic Reciprocating Compressor: Sliding Mesh vs Moving Reference Frame, *International Compressor Engineering Conference*.
- [66] **Ozsipahi, M., Kose, H.A., Cadirci, S., Kerpicci, H. and Gunes, H.** (2019). Experimental and numerical investigation of lubrication system for reciprocating compressor, *International Journal of Refrigeration*, 108, 224–233.
- [67] **Cavallini, A., Doretto, L., Longo, G.A. Rossetto, L. and Bella, B.** (1996). Thermal Analysis of a Hermetic Reciprocating Compressor, *International Compressor Engineering Conference*.
- [68] **Raja, B., Sekhar, S.J., Lal, D.M. and Kalanidhi, A.** (2003). A numerical model for thermal mapping in a hermetically sealed reciprocating refrigerant compressor, *International Journal of refrigeration*, 26(6), 652–658.
- [69] **Ooi, K.T.** (2003). Heat transfer study of a hermetic refrigeration compressor, *Applied thermal engineering*, 23(15), 1931–1945.
- [70] **Rigola, J., Pérez-Segarra, C. and Oliva, A.** (2003). Modeling and Numerical Simulation of the Thermal and Fluid Dynamic Behavior of Hermetic Reciprocating Compressors—Part 2: Experimental Investigation, *HVAC&R Research*, 9(2), 237–249.
- [71] **Rigola, J., Perez-Segarra, C. and Oliva, A.** (2004). Parametric studies on hermetic reciprocating compressors, *International Journal of Refrigeration*, 28(2), 253–266.
- [72] **Ribas, F., Deschamps, C., Fagotti, F. Morriesen, A. and Dutra, T.** (2008). Thermal Analysis of Reciprocating Compressors - A Critical Review, *International Compressor Engineering Conference*.
- [73] **Dutra, T. and Deschamps, C.** (2010). Experimental Investigation of Heat Transfer in Components of a Hermetic Reciprocating Compressor, *International Compressor Engineering Conference*.
- [74] **Kara, S. and Oguz, E.** (2010). Thermal Analysis of a Small Hermetic Reciprocating Compressor, *International Compressor Engineering Conference*.
- [75] **Dincer, M.O.** (2013). *Hermetik pistonlu bir kompresörde birleşik (konjuge) ısı geçişinin sayısal olarak incelenmesi.* (Master's thesis). Istanbul Technical University, Istanbul.

- [76] **Yesilaydin, I., Erbay, L. and Inan, C.** (2014). Investigation of Flow Losses Through Discharge Line of Household Type Refrigerator Compressors, *International Compressor Engineering Conference*.
- [77] **Hopfgartner, J., Heimel, M., Berger, E. Posch, S. and Almbauer, R.** (2016). Experimental Study on the Thermal Behavior of a Domestic Refrigeration Compressor during Transient Operation in a Small Capacity Cooling System, *International Compressor Engineering Conference*.
- [78] **Posch, S., Hopfgartner, J., Heimel, M., Berger, E. and Almbauer, R.** (2016). Thermal Analysis of a Hermetic Reciprocating Compressor Using Numerical Methods, *International Compressor Engineering Conference*.
- [79] **Air-Conditioning, Heating, and Refrigeration Institute** (2011). *2015 Standard for Performance Rating Of Positive Displacement Refrigerant Compressors and Compressor Units*, United Nations Environment Programme (UNEP).
- [80] **Url-1**, <http://www.re-gent.nl/>, alındığı tarih: 25.12.2019.
- [81] **Beetz, J.** (2017). *Inbetriebnahme eines Leistungsprüfstandes für Kältemittelverdichter an Kleinkälteanlagen*. Technische Universität Dresden, Dresden.
- [82] **Fluent, A.** (2013). *15.0 Theory Guide*.



APPENDICES

APPENDIX A.1 : Calibration of pressure sensors and RTD probes

APPENDIX A.2 : Pressure-enthalpy diagrams of R600a and R600a/R290 refrigerant mixture





APPENDIX A.1

In this part, the calibration of measurement devices are given. The calibration of the RTD probes are conducted using calibration bath. Figure A.1 shows the equipments of the temperature calibration stand. RTD probes are divided into two groups according to the operating temperature. Suction and discharge line RTD probes are calibrated in the range between -30°C to 10°C and 20°C to 80°C , respectively.

Table A.1 and Table A.2 show the measured temperature values. The maximum and average reading error of the sensors are found 16.55% and 5.37%, respectively. The second order polynomials are fitted into each equipment readings and the maximum and average reading error reduced to 0.5% and 3.5%, respectively.

The pressure sensors are calibrated with a Dead-weight Tester. A dead-weight tester is a calibration standard that employs the principle of a pressure balance to calibrate pressure measuring instruments. Dead-weight testers use calibrated weights to use known pressures to a device under test for a simple and cost-effective solution that satisfies a wide range of pressure calibrations. The calibration devices of the Dead-weight pressure tester are given in Figure A.2.

Table A.3 presents the pressure readings of the sensors. It is shown that the devices are pretty accurate and the maximum error for the low and high side pressures are less than 1% and 2%, respectively. The reading results are further reduced by fitting second order polynomials for each device.



Figure A.1 : Temperature calibration with calibration bath.

Table A.1 : Measured temperature values of RTD probes.

Temperature (°C)	-30	-20	-10	0	10
RTD.1	-28.35	-18.41	-8.35	1.30	11.53
RTD.2	-28.46	-18.48	-8.58	1.23	11.51
RTD.3	-28.44	-18.51	-8.34	1.21	11.46
RTD.4	-28.46	-18.51	-8.55	1.21	11.43
RTD.5	-28.50	-18.53	-8.60	1.17	11.49

Table A.2 : Measured temperature values of RTD probes.

Temperature (°C)	20	30	40	50	60	70	80
RTD.6	21.45	30.83	40.29	51.12	61.11	71.06	81.12
RTD.7	21.61	31.39	41.25	51.38	61.36	71.33	81.64
RTD.8	21.76	30.31	38.52	50.64	60.46	70.20	81.04



Figure A.2 : Pressure calibration with dead-weight pressure tester.

Table A.3 : Pressure readings of the pressure sensors.

Bar/Equip.	1	2	3
1	1.01	1.00	1.00
3	3.00	2.99	3.00
5	5.00	4.98	4.97
7	6.98	6.99	6.98
9	8.97	8.98	8.96
2	2.00	2.04	2.03
6	6.02	6.04	6.02
10	10.00	10.01	10.02
14	14.07	13.97	14.03
18	17.98	18.06	18.05

APPENDIX A.2

Pressure-enthalpy diagrams of the refrigerant R600a and refrigerant mixture R600a/R290 (60%/40% by weight) are given in this section. Figure A.3 shows the effect of rotational speed at ASHRAE standards for R600a and R600a/R290, respectively. In the Figures, green, cyan, red and black lines represents 4500, 3000, 2100 and 1500 rpm, respectively.

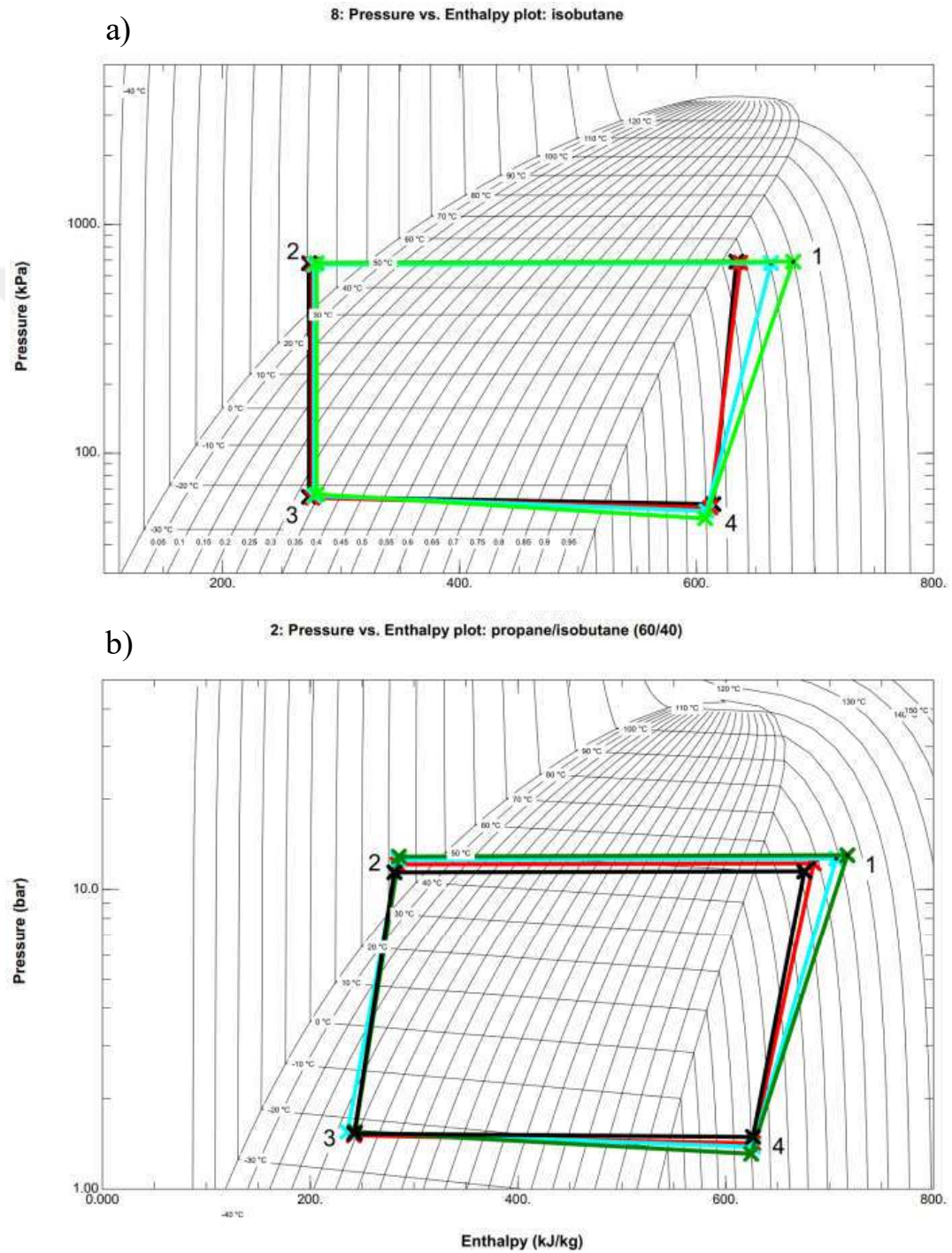


Figure A.3 : Effect of compressor speed a) R600a b) R600a/R290 mixture

Figure A.4 and Figure A.5 shows the pressure-enthalpy diagrams for three different evaporation pressure at 1500, 2100, 3000 and 4500 rpm. Cyan represents the lowest pressure hence the temperature, black and red corresponds the medium and highest evaporation pressure. Corresponding temperatures of the evaporation pressures are plotted on the Figure A.4 and Figure A.5.

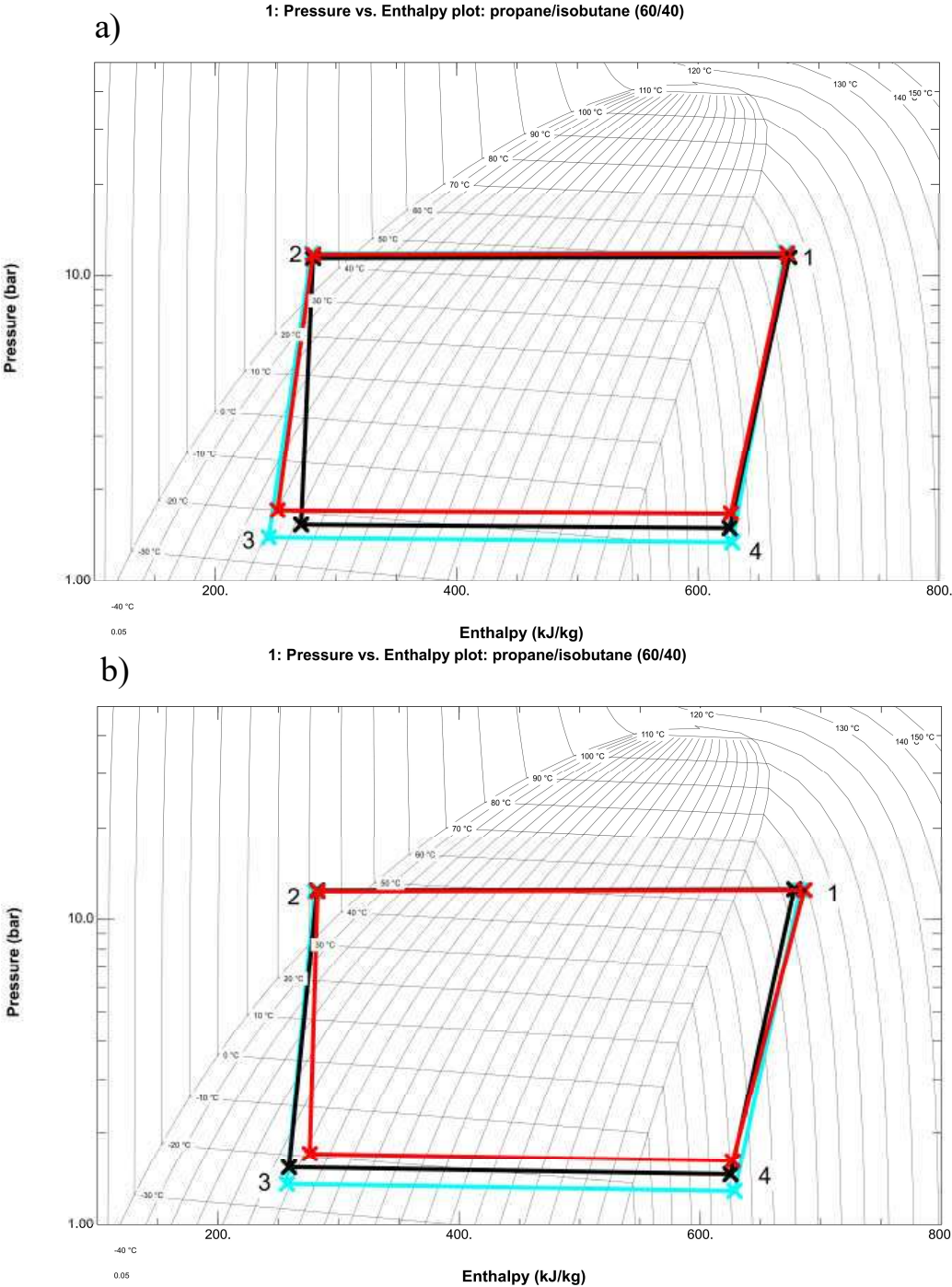
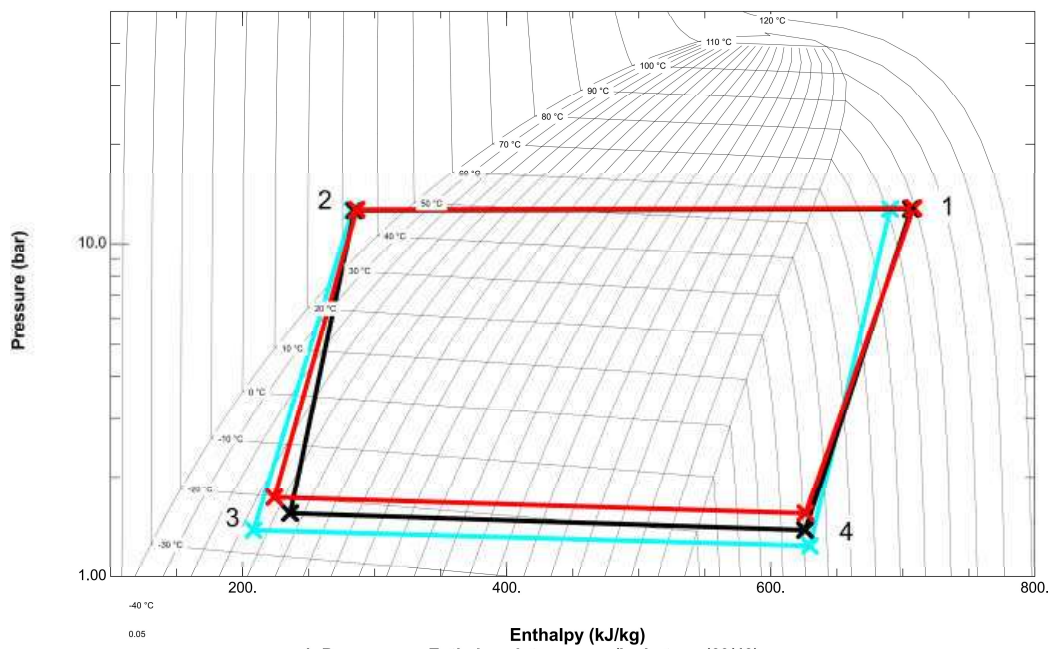


Figure A.4 : Effect of evaporation pressure a) 1500 rpm b) 2100 rpm

a)

4: Pressure vs. Enthalpy plot: propane/isobutane (60/40)



b)

4: Pressure vs. Enthalpy plot: propane/isobutane (60/40)

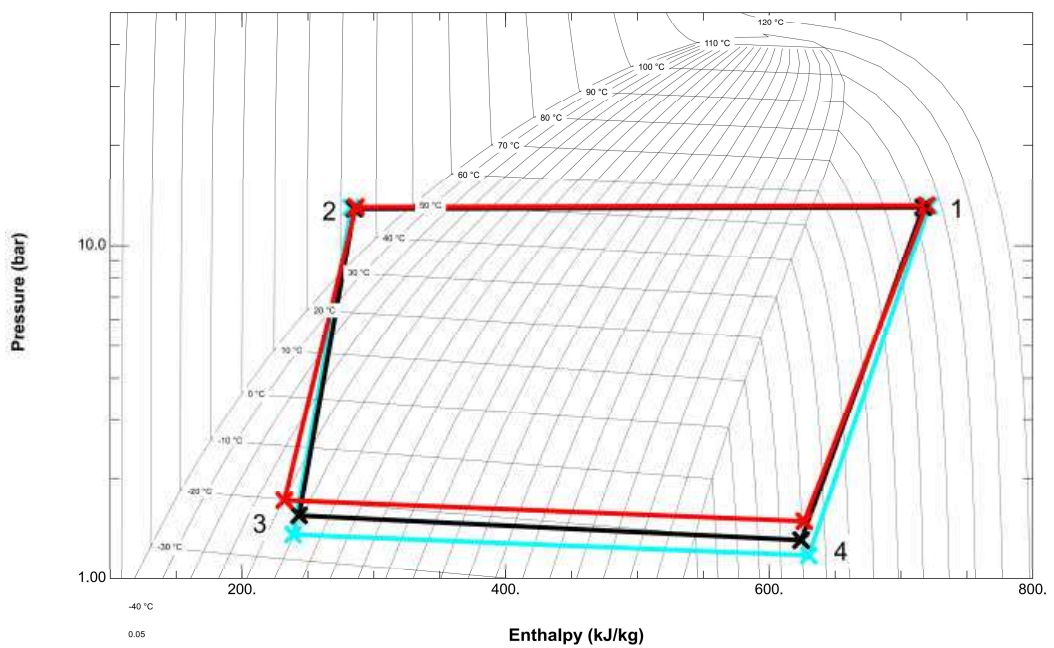


Figure A.5 : Effect of evaporation pressure a) 3000 rpm b) 4500 rpm



CURRICULUM VITAE

Name & Surname : Mustafa ÖZSİPAHI
Place and Date of Birth : Bursa - 1989
E-Mail : mustafaozsipahi@hotmail.com

EDUCATION

- **Ph.D., Mechanical Engineering** 2020
Istanbul Technical University, Istanbul/Turkey
Graduate School of Science Engineering and Technology
- **M.Sc., Mechanical Engineering** 2014
Istanbul Technical University, Istanbul/Turkey
Faculty of Mechanical Engineering
- **B.Sc., Mechanical Engineering** 2011
Yildiz Technical University, Istanbul/Turkey
Faculty of Mechanical Engineering

PROFESSIONAL EXPERIENCE AND REWARDS

- **Research and Teaching Assistant** 2013-Present
Istanbul Technical University, Turkey
Department of Mechanical Engineering
- **Visiting Researcher** 2019-2020
Technische Universität Dresden, Dresden
BITZER-Chair of Refrigeration, Cryogenics and Compressor Technology
- **Visiting Researcher** 2018-2019
Technische Universität Dresden, Dresden
BITZER-Chair of Refrigeration, Cryogenics and Compressor Technology
- **Reviewer** 2016-Present
International Journal of Refrigeration (ISSN: 0140-7007)
Applied Energy (ISSN: 0306-2619)
Engineering, Technology & Applied Science Research (ISSN: 1792-8036)

PUBLICATIONS, PRESENTATIONS AND PATENTS ON THE THESIS

- **Özsipahi, M.**, Kose, H.A., Cadirci, S., Kerpici H., Gunes H., 2019: Experimental and numerical investigation of lubrication system for reciprocating compressor. *International Journal of Refrigeration*, 108, 224-233.
- **Özsipahi, M.**, Kerpici H., Gunes H., 2018: On the cfd modeling approach of lubrication system for a hermetic reciprocating compressor:sliding mesh vs moving reference frame. *24th International Compressor Engineering Conference*, July 09-12, 2018 Purdue, USA.

OTHER PUBLICATIONS, PRESENTATIONS AND PATENTS

- Gunpinar, E., Coskun U.C., **Özsipahi, M.**, Gunpinar, S., 2019: A generative design and drag coefficient prediction system for sedan car side silhouettes based on computational fluid dynamics , *CAD Computer Aided Design*, 111, 65-79.
- **Özsipahi, M.**, Subaşı, A., Şahin, B., Güneş, H., 2018: Numerical investigation of hydraulic and thermal performance of a honeycomb heat sink, *International Journal of Thermal Sciences*, 134, 500-506.
- Subaşı, A., **Özsipahi, M.**, Şahin, B., Güneş, H., 2017: Performance evaluation of RANS-based turbulence models in simulating a honeycomb heat sink, *Heat and Mass Transfer*, 53(7), 2435-2443.
- **Özsipahi, M.**, Cadirci, S., Gunes, H., 2016: A comparison of an analytical and numerical flow model for the lubrication system of a variable speed hermetic compressor. *Isi bilimi ve tekniği dergisi/Journal of Thermal Science and Technology*, 36(2), 41-49.
- Cadirci, S., **Özsipahi, M.**, Güneş, H., 2016: POD analysis of jet and vortex flows induced by oscillating backward facing step, *Springer Proceedings in Physics*, 185, 249-257.
- **Özsipahi, M.**, Cadirci, S., Güneş, H., 2016: Numerical and analytical investigation of viscous fluids in a screw extruder, *International Mechanical Engineering Congress and Exposition*, 7, November 11-17, 2016, Arizona, USA.
- Cadirci, S., **Özsipahi, M.**, Coskun, U.C., Ak, S.E., Güneş, H., Selenbas, B., 2016: Numerical investigation of turbulent flow over a windscreen wiper blade, *International Mechanical Engineering Congress and Exposition*, 7, November 11-17, 2016, Arizona, USA.
- **Özsipahi, M.**, Cadirci, Gunes, H., Sarioglu, K., Kerpici, H., 2014: Numerical simulation of a lubrication system in a hermetic reciprocating compressor. *12th Biennial conference on engineering systems design and analysis*, 2, July 25-27, 2014, Copenhagen, Denmark.
- **Özsipahi, M.**, Cadirci, Gunes, H., Sarioglu, K., Kerpici, H., 2014: A numerical study on the lubrication system for a hermetic reciprocating compressor used in a household refrigerators. *International Journal of Refrigeration*, 48, 210-220.

